School of Electrical Engineering, Computing and Mathematical Sciences

Study of Various Fluid Flow and Heat Transfer Problems in the Slip Regime

Amani Ahmed Otaif

This thesis is presented for the Degree of
Doctor of Philosophy
of
Curtin University

December 2022

Declaration

To the best of my knowledge and belief, this thesis contains no material previously published by any other person except where due acknowledgment has been made. This thesis contains no material which has been accepted for the award of any other degree or diploma in any university.

Amani Otaif

December 2022

Abstract

Microdevices such as microelectromechanical system(MEMS) have been used in many science and technology applications. These devices and systems often involve fluid flow and heat transfer processes in microchannles. Hence, the study of fluid flow in microchannels and the associated heat transfer process is important for the design and application of microdevices and systems. This project will focus on the study of various microflow and heat transfer problems in the slip regime, including heat transfer in fluids flowing through microchannels, velocity and temperature fields in mixed electroosmotic and pressure-driven flow of fluids, and unsteady flow of fluids in rectangular microchannels in the slip regime.

A mathematical model has been constructed to study the transient temperature field in fluids flowing through microchannels driven by pressure gradient in the slip regime. Based on the finite difference method, a computation scheme is then developed to obtain the solution of the temperature field. A subsequent numerical analysis, based on the established computation scheme, is then conducted to investigate the influence of boundary slip and heat convection due to fluid flow on the temperature field.

Heat transfer in a mixed electroosmotic and pressure-driven flow is examined in the slip system. Exact solutions have been obtained analytically for the fluid flow and heat transfer problems. The influence of the axial dependence of both the dimensionless bulk temperature θ_b and the dimensionless wall temperature

θ_w for various Péclet number Pe and wall flux functions under slip condition are examined.

The slip flow of an incompressible fluid flow through a rectangular microchannel has also been studied. A mathematical model, including the governing differential equation and boundary conditions, has been constructed for the problem. A new exact solution has been deduced analytically by using Fourier series expansion in the time domain and the separation of variable method in the spatial domain. Numerical analysis has also been carried out for some special cases to examine the influence of slip parameters on the velocity field.

Acknowledgements

Contents

List of Tables

List of Figures

1

Chapter 1

Introduction

1.1   Background

Various applications in advanced technologies involve heat transfer and fluid flow, for example, cooling and heating, thermal sources, transportation of fluids, and development of microelectromechanical systems. Micro-scale transport processes have been explored by the research community in order to perform efficient design for microfluidic systems. The efficiency of such devices can be improved by altering the physical properties of the fluids, geometry of the flow channel and modification of boundary conditions [1]. Slip-flow and heat transfer in microchannels have been investigated by several researchers [2–6]. The slip-flow and heat transfer processes are governed by the Navier-Stokes and energy equations supplemented by boundary conditions. It is found that the temperature-jump effect plays a significant role in the modeling of the slip-flow and heat transfer problems, and over prediction of heat transfer rate may occur if such effect is neglected [7].

Convective heat transfer in an isoflux rectangular microchannel has been examined analytically for a fully developed flow field both thermally and hydrodynamically [8]. Shojaeian investigated the convective heat transfer of non-Newtonian

fluid flow in the circular channel [9]. They realized from their investigation that the heat transfer properties and the entropy generation are affected by neglecting the property variation. Considerable studies have been focused on the behavior of flow and heat transfer in the channels and microchannels. In particular, the research examined the effect of Reynolds number, layout of channels cross-sections, and geometric properties. The forced convection of a non-Newtonian nanofluid in a microchannel has been investigated [10]. It was under the fixed temperature and heat flux boundary conditions. It was found that as Nusselt number increased, the convection in the tube is slowed down by higher slip of particles. It was also demonstrated that the impact of slip coefficient under fixed heat flux was more significant than under fixed temperature boundary condition. Laminar flow in a microchannel has been investigated numerically under the slip and no-slip boundary conditions [11]. The effects of Reynolds number, volume fraction, and slip velocity on heat transfer rate of forced convection flow were investigated. The numerical solution for the three-dimensional Navier-Stokes and energy equations has been achieved by the control volume method [7]. It was done under velocity-slip and temperature-jump boundary conditions and included the investigation of the axial molecular diffusion of heat.

Several theoretical studies have considered the description of the hydrodynamics of electroosmotic flow through microchannels with various different cross-sections, but little work has been done on convective heat transfer in electroosmotic flows. Essentially, the Knudsen number is the ratio of the mean free path to the macroscopic length scale of the flow and can be used to classify flow regimes if the boundary conditions are properly modified. Electroosmosis has been utilized fundamentally in Biochip technology to transport liquid samples of nanovolumes applications used for chemical and biological analysis and medical diagnosis [12]. The electroosmotic flow in fluid dynamics differs from traditional pressure-driven flow, and hence the thermal transport dynamics are also expected to be quite different. Numerous recent works have examined the electroosmotic velocity distribution, and the associated momentum transport of electroosmotic

velocity and capillary momentum as a function of channel diameter-to-Debye length ratio [13, 14]. The influences of electrokinetics on pressure-driven flow and heat transfer properties have been explored for both round and rectangular microchannels [15, 16].

1.2 Objectives

Study of fluid flow and heat transfer has great significance in science, engineering, and industry. However, although a lot of results have been obtained, there are still many issues and problems which need to be considered particularly in the slip system.

This work focuses on fluid flow and heat transfer in microchannels of various types of cross-sections in the slip regime. The aim is to derive solutions for the fluid flow and heat transfer problems and investigate the fluid flow and heat transfer characteristics under different conditions as well as the influence of boundary slip. The specific objectives are as follows:

(i) Construct a mathematical model for the transient temperature field in the fluid flowing through a circular microchannel under slip boundary conditions, then construct a numerical scheme to investigate the influence of boundary slip and convection heat transfer due to fluid flow on the temperature field in the microchannel.

(ii) Investigate the electroosmotic flow under slip condition. This includes the construction of the governing field equations for the velocity field and the temperature field, derivation of analytical solutions, and investigation of the slip parameter on the temperature distribution.

(iii) Study the transient fluid flow in a rectangular microchannel under slip condition. This includes the derivation of a new exact solution and investi-

gation of the boundary slip parameter on the velocity distribution and flow rate.

1.3   Outline of the thesis

This thesis develops various analytical and numerical results for fluid flow and heat transfer in microchannels in the slip regime. The thesis consists of 6 chapters.

Chapter 1 introduces the background of this research and presents the objectives of this study.

Chapter 2 reviews previous research relevant to the field of study, including a review of existing models and results relevant to this research.

Chapter 3 studies the transfer of heat in the fluid flowing through a circular microchannel. A numerical scheme is constructed to determine the transient temperature field, and the influences of the convection term and boundary slip are investigated.

Chapter 4 investigates the electroosmotic flow in the slip regime. Analytical solutions are derived in the slip regime. The features of such flow are demonstrated, and the influences of boundary slip on flow velocity and temperature fields are investigated.

Chapter 5 studies the flow of an incompressible Newtonian fluid through a rectangular microchannel. New exact solutions for the velocity field and flow rate are derived, and the influences of boundary slip on the axial velocity are investigated in the chapter.

Chapter 2

Literature Review

Over the last couple of decades, many biological and engineering devices and systems at microscale have been developed. These devices and systems often involve fluid flow and heat transfer in microchannels. Hence, a great deal of research work has been carried out in recent years to study the behaviour of fluid flow and heat transfer in microchannels of various types of cross-sections. The Navier-Stokes equations and energy equations are employed by many researchers for such investigations. These equations are often supplemented by a variety of boundary conditions including velocity slip or temperature jump on the walls of the ducts. Many results have been obtained, including numerical and analytical results.

This chapter will give a review of previous work relevant to the research. Section 2.1 will review previous research on fluid flows, including steady flow and unsteady flow, through microchannels of various types of cross-sections. Section 2.2 will review previous work on heat transfer and temperature distribution in fluids flowing through microchannles of various types of cross-sections in the slip regime.

2.1 Slip flow of fluids in microchannels

2.1.1 Flow of fluids through circular microchannels

Heterogeneous boundary was considered priority by investigating configurations of surface heterogeneity. These configurations were examined transversely and longitudinally. In 2003, Ericlauga and Stone [17] investigated a steady pressure-driven Stokes flow in a circular tube. The model for transverse flow was presented by dimensionless Stokes and continuity equations

$$\nabla^2 u = \nabla p,$$

$$\nabla \cdot u = 0,$$

subject to the boundary conditions: $u = 0$ for $r = 1$, $\frac{1}{2}l < |z| \leq \frac{1}{2}L$, $0 \leq \theta < 2\pi$, $u_r = 0$, $\sigma_{rz} = \sigma_{r\theta} = 0$ for $r = 1$, $|z| \leq \frac{1}{2}l$, $0 \leq \theta < 2\pi$. The longitudinal flow where the slip regions were formed parallel to the flow direction satisfies the slip equation:

$$u = \lambda n \cdot ((\nabla u) + (\nabla u)^T),$$

where λ is the slip length and the dimensionless velocity profile in this situation was given by

$$u(r) = \frac{1}{4}(1 - r^2) + \frac{1}{2}\frac{\lambda}{R}.$$

The effective slip length of the parallel flow was defined by

$$\frac{\lambda_{eff}}{R} = \frac{1}{4}(\frac{8Q}{\pi} - 1),$$

where Q is the total dimensionless flow rate.

The influence of partial slip condition on the velocity and resistance of the flow has been examined through a curved tube by Wang (2003) [18]. The flow in a circular channel of tiny curvature was investigated by the perturbation method. The effect of Knudsen number has been investigated for slip flow in

hydrodynamic entrance region [19]. The studies considered circular ducts and parallel plates under the assumptions of steady state laminar flow, and body forces were neglected. Wang (2016) [20] investigated slip flow in a curved circular channel. Zero Reynolds number was considered in small curvature via circular channel and the flow was perturbed. An analytical result, for zero Reynolds number, was derived

$$V = \frac{1}{8}\left[1 + 4\lambda + \frac{1}{c^2}\left(\frac{1 + 7\lambda - 288\lambda^2}{48(1+\lambda)}\right) + O(c^{-4})\right].$$

It has been found that the maximum velocity was located off-centered at low slip whereas it went off the symmetry line at high slip. The comparison results were tabulated [20].

In 2008, the pressure field with a pressure gradient $\bar{q}(t)$ is employed for a derivation of the transient velocity flow, that is

$$\frac{\partial p}{\partial z} = \bar{q}(t) = a_0 + \sum_{n=1}^{\infty}[a_n\cos(nwt) + b_n\sin(nwt)].$$

The influence of the slip condition on velocity and flow rate behavior has been investigated. This is based on the derivation of the exact solution for the transient flow of an incompressible Newtonian fluid in microchannels with a supplemented slip condition on the boundary [21]. In addition, an explicit formula for the flow rate was derived, namely

$$Q^*(t) = -\frac{2\mu}{a_0\pi R^3}Q = (l + \frac{R}{4}),$$

which can be useful to define the slip length in a simple experiment. Moreover, the normalized velocity depends on the dimensionless parameter $\bar{\beta}$ as well as the slip parameter l^*.

Pressure gradient driven transient flow has been investigated in 2009 [22]. The flow was an incompressible Newtonian in micro-annulus of inner radius a and

outer radius R with the z-axis being in the axial direction. The flow was formulated via the continuity equation and Navier-Stokes equations as follows

$$\frac{\mu}{\rho}\left(\frac{\partial^2 u}{\partial r^2} + \frac{1}{r}\frac{\partial u}{\partial r}\right) - \frac{\partial u}{\partial t} = \frac{1}{\rho}\frac{\partial p}{\partial z}.$$

The fluid flow is driven by the pressure gradient which can be represented by the Fourier series

$$\frac{\partial p}{\partial z} = \bar{q}(t) = a_0 + \sum_{n=1}^{\infty}[a_n\cos(nwt) + b_n\sin(nwt)].$$

This problem was supplemented by the Navier slip boundary condition, namely

$$u(a,t) = \pm L_1\frac{\partial u}{\partial r}(a,t) \qquad u(R,t) = \pm L_2\frac{\partial u}{\partial r}(R,t)$$

where L_1,L_2 indicate the slip parameters of the inner and outer surface respectively. The exact solution of such problem was achieved by using analytical approach. The effect of the slip parameter and the geometry of the cross-section on the flow rate was also examined in [22].

2.1.2 Flow of fluids through microchannels with elliptic cross-section

Duan and Muzychka performed in 2007 a theoretical analysis for slip flow in elliptic micro channels [23]. They examined the prediction of the Poiseuille number for slip flow which relies on the geometry of the cross-section. An elliptic cylinder coordinate system was used to derive the analytical solution of Poiseulle number. The momentum equation was written in elliptic coordinates by

$$\frac{\partial^2 u}{\partial \eta^2} + \frac{\partial^2 u}{\partial \xi^2} = \frac{c^2}{\mu}\frac{dp}{dz}(\cosh^2\eta - \cos^2\xi),$$

which is subject to the first-order slip boundary condition assumed in one quarter basic cell

9

$$\frac{1}{\sqrt{g_2}}\frac{\partial u}{\partial \xi} = 0 \quad \text{at} \quad \xi = 0$$

$$\frac{1}{\sqrt{g_2}}\frac{\partial u}{\partial \xi} = 0 \quad \text{at} \quad \xi = \frac{\pi}{2}$$

$$\frac{1}{\sqrt{g_1}}\frac{\partial u}{\partial \eta} = 0 \quad \text{at} \quad \eta = 0$$

$$u = -\frac{\lambda\frac{2-\sigma}{\sigma}}{\sqrt{g_1}}\frac{\partial u}{\partial \eta} \quad \text{at} \quad \eta = \eta_0$$

where $g_1 = g_2 = c^2(\cosh^2 \eta - \cos^2 \xi)$ is the metric coefficients for the elliptic coordinates, λ represents the molecular mean free path and σ indicates the tangential momentum. They obtained a comparison of the achieved Poiseuille number

$$P_0 D_h = \frac{\bar{\tau} D_h}{\mu \bar{u}} = \frac{-\frac{A}{P}\frac{dp}{dz}D_h}{\mu \bar{u}} = \frac{-\frac{dp}{dz}\left(\frac{\pi b}{E(e)}\right)^2}{4\mu \bar{u}},$$

where $D_h = 4A/P$ is the hydraulic diameter, $E(e)$ is the complete elliptical integral of the second kind, $Kn = \lambda/D_h$, P is the perimeter of ellipse, p is the pressure. Different values for the obtained Poiseuille number, P_0, have been investigated by using one to four terms of binomial series. Poiseuille number was also compared with respect to different ratios ε and Knudsen number. They have found that the increase of Kn for the same aspect ratio will lead to the drop of the values of P_0.

The constitutive equation which was expressed as

$$\sigma = -pI + 2\mu d,$$

describes the relationship between the stress field and the velocity field where d is the rate of deformation tensor defined by

$$d = \frac{1}{2}(\nabla v + (\nabla v)^T).$$

In 2008, an analytical solution for the pulsatile velocity field in a straight annulus of elliptic cross section was deduced [24]. This was under the assumption of viscous laminar flow of an incompressible Newtonian fluid, driven by an oscillatory

10

pressure gradient. The flow was formulated mathematically by the Navier-Stokes equations. It assumed that the flow is fully developed in an unlimited length and constant form of elliptic annulus. The transverse components of the velocity were neglected. This gets to the Navier-Stokes equations as follows

$$\frac{\partial^2 u_z}{\partial x^2}(x,y,t) + \frac{\partial^2 u_z}{\partial y^2}(x,y,t) - \frac{\rho}{\mu}\frac{\partial u_z}{\partial t}(x,y,t) = \frac{1}{\mu}\frac{\partial p}{\partial z}(z,t),$$

which is then converted by coordinate transformation from the rectangular coordinate system (x,y) to the elliptic coordinate system (ξ,η), namely

$$\frac{2}{h^2(\cosh 2\xi - \cos 2\eta)}\left[\frac{\partial^2 u_z(\xi,\eta,t)}{\partial \xi^2} + \frac{\partial^2 u_z(\xi,\eta,t)}{\partial \eta^2}\right] - \frac{\rho}{\mu}\frac{\partial u_z(\xi,\eta)}{\partial t} = \frac{1}{\mu}\frac{\partial p}{\partial z}(z,t).$$

The exact solution of the steady state flow was studied. By integrating it over the annulus area, the steady flow rate $\dot{Q}_s$ as a function of pressure gradient was obtained. The steady velocity solution after some work was given by

$$u_{z,s}(\xi,\eta) = \frac{\dot{Q}_s}{\pi h^2}\left(\frac{N_s(\xi,\eta)}{D_s}\right),$$

where

$$N_s(\xi,\eta) = \left(\frac{(\xi_0 - \xi)}{(\xi_0 - \xi_i)}\cosh 2\xi_i + \frac{(\xi - \xi_i)}{(\xi_0 - \xi_i)}\cosh 2\xi_0 + \right.$$

$$\left.\frac{\cosh(2\xi - \xi_i - \xi_0)}{\cosh(\xi_0 - \xi_i)}\cos 2\eta - (\cosh 2\xi + \cos 2\eta)\right),$$

and D_s was represented as

$$D_s = \left(\frac{(\sinh 4\xi_0 - \sinh 4\xi_i)}{8} - \frac{(\cosh 2\xi_0 - \cosh 2\xi_i)^2}{4(\xi_0 - \xi_i)} - \frac{\cosh 2(\xi_0 - \xi_i) - 1}{2\sinh 2(\xi_0 - \xi_i)}\right).$$

Gupta [24] also obtained the solution for the oscillatory velocity component of the flow which requires the computation of the Mathieu and modified Mathieu functions of the first and second kinds. This was done over three steps. In addition, the total velocity solution in the straight elliptic annulus was derived. This model minimizes the cost and develops numerical and experimental models.

11

Slip flow in straight ducts has emerged significantly in research in microchannels. On the other hand, scarce research was focused on slip flow in curved ducts. The Ritz variational method has been used to approximate the solution for viscous flow in a curved channel. Wang (2016) considered the fluid characteristics for Stokes flow in a curved channel as well as the Ritz method for elliptic cross section [20]. The flow rate was found to be larger in a curved duct than those in a straight duct. The reduced Stokes equation in cylindrical coordinates (r, θ, z) for the problem was given by

$$\frac{\partial^2 v}{\partial r^2} + \frac{1}{r}\frac{\partial v}{\partial r} - \frac{v}{r^2} + \frac{\partial^2 v}{\partial z^2} = -\frac{c}{r},$$

where the azimuthal velocity directed in θ was represented by $v(r,z)$, and the normalized radial distance from the symmetry axis was represented by r. The normalized length was produced as

$$\Delta v\Big|_{wall} + \lambda \, \tau_{n\theta} = 0.$$

The directional derivative of velocity in the normal direction of the surface was given by

$$\frac{\partial v}{\partial n} = \overrightarrow{n} \cdot \nabla v = n_r \frac{\partial v}{\partial r} + n_z \frac{\partial v}{\partial z},$$

while the stress components were given by

$$\tau_{r\theta} = \frac{\partial v}{\partial r} - \frac{v}{r}, \quad \tau_{z\theta} = \frac{\partial v}{\partial z},$$

$$\tau_{n\theta} = n_r \tau_{r\theta} + n_z \tau_{rz} = \frac{\partial v}{\partial n} - \frac{n_r}{r}v.$$

The Navier slip boundary condition in cylindrical coordinates was expressed as

$$v + \lambda \left(\frac{\partial v}{\partial n} - \frac{n_r}{r}v \right) = 0.$$

Based on the Ritz method,

$$v = \Sigma a_i \phi_i,$$

where $\{\phi_i\} = \{1, x, x^2, z^2, ...\}$ is a set of Ritz functions appropriate to the symmetry in z. Wang(2016) accomplished the average velocity after some algebraic attempts which evaluate the flow, that is

$$V = \frac{1}{A} = \int \int v \, dr \, dz = \frac{1}{A} \sum_1^N c_i B_i.$$

The author realized that the Poiseuille number and friction factor Reynolds number product were unsuitable quantities in the case of curved ducts. The Ritz method was applied to the curved elliptic duct of any constant cross-section by assuming

$$r = c + x,$$

with the boundary

$$H(x,z) = 1 - x^2 - (\frac{z}{b})^2 = 0.$$

The convergence of the average velocity V was shown and compared with the known outcomes. The results for curved elliptic ducts were tabulated. The average velocity was found to be increased if slip represented by the slip factor λ or the aspect ratio b increase. For elliptic curved ducts, the flow rate for a straight duct was found to be larger than a curved duct in the case of a large slip factor. However, in the case of a small slip factor, the flow rate is seen to be larger for a curved duct than a straight duct.

Gaseous slip flow in elliptic cross-section was investigated in 2016. An analytical solution of velocity was established by Das and Tahmouresi [25]. The non-dimensional form of the governing equation (momentum equation) and the boundary conditions were given as follows

$$\frac{\partial^2 u}{\partial x^2} + \frac{\partial^2 u}{\partial y^2} = P,$$

$$u = \beta_s = -\beta_v kn \frac{\partial u}{\partial n} \mid_\Gamma,$$

where

$$P = \frac{(\sqrt{A_c})^2}{\mu u_m^*} \frac{dp}{dz},$$

13

$$\beta_s = \frac{u_s^*}{u_m^*},$$

where Γ denotes the boundary of the non-dimensional elliptic micro channel $\Omega : \frac{x^2}{a^2} + \frac{y^2}{b^2} = 1$. The integral transform approach was used by transforming the rectangular coordinate system to elliptic cylindrical coordinates (ξ, η). The governing equation and boundary conditions then can be written as

$$\frac{\partial^2 \tilde{u}}{\partial \xi^2} + \frac{\partial^2 \tilde{u}}{\partial \eta^2} = c^2(\cosh^2 \xi - \cos^2 \eta)P,$$

$$\frac{\partial \tilde{u}}{\partial \eta} = 0 \quad \text{at} \quad \eta = 0,$$

$$\frac{\partial \tilde{u}}{\partial \eta} = 0 \quad \text{at} \quad \eta = \frac{\pi}{2},$$

$$\frac{\partial \tilde{u}}{\partial \xi} = 0 \quad \text{at} \quad \xi = 0,$$

$$\tilde{u} = 0 \quad \text{at} \quad \xi = \xi_0.$$

The final form of the velocity profile was achieved analytically for various ratios $\varepsilon = \frac{b}{a}$, namely

$$u(\xi, \eta) = \sum_{n=1}^{\infty} \frac{[c^2 A_n(\cos(2\eta) - \cosh(2\xi_0))p]\cos(\mu_n \xi)}{N_n^{\frac{1}{2}}} + \beta_s.$$

Applying different characteristic lengths for elliptic cross-section, the friction factor Reynolds number was given by

$$fR_e D_h = \frac{2(-\frac{A_c}{P_c}\frac{dp}{dz})D_h}{\mu u_m},$$

and the simple expression of the Poiseuille number was

$$Po_{L_c} = \frac{fR_{e_{L_c}}}{2}.$$

Das and Tahmouresi [25] showed consistent data of friction factor and Reynolds number product and normalized Poiseuille number for elliptic micro channels in [23] and [26].

By assuming that the velocity of the fluid on the surface of the channel is proportional to the shear stress, in 2018, Wilmott et.al [27] investigated the slip flow considering a variation of the elliptic cross-section. The model is described by the incompressible Stokes equations:

$$\mu \nabla^2 u = \nabla p, \quad \nabla \cdot u = 0,$$

subject to the boundary condition

$$\mu + \beta \frac{\partial u}{\partial n} = 0,$$

with the central axis of the channel lying along the straight z-axis as well as an angle $\phi(z)$ being assumed between the semi-major axis and the x-axis in the (x, y) plane. After introducing the non-dimensionalize variables, the boundary conditions of the problem were simplified by using the elliptic coordinates (η, ξ, z) by the following change of variables:

$$x = a(z)\cosh \eta \cos \xi \cos \phi - a(z)\sinh \eta \sin \xi \sin \phi \qquad 0 \le \eta \le \eta_0$$

$$y = a(z)\cosh \eta \cos \xi \sin \phi + a(z)\sinh \eta \sin \xi \cos \phi \qquad 0 \le \xi \le 2\pi$$

Then, the incompressible Stokes equations with boundary conditions were expressed as

$$\frac{\partial^2 w}{\partial \eta^2} + \frac{\partial^2 w}{\partial \xi^2} = a^2 h^2 \frac{\partial p}{\partial z}, \quad \frac{\partial p}{\partial \eta} = 0, \quad \frac{\partial p}{\partial \xi} = 0,$$

$$\frac{1}{a^2 h^2}\left[\frac{\partial}{\partial \eta}(ahu) + \frac{\partial}{\partial \xi}(ahv) \right] + \frac{1}{a^2}\frac{\partial}{\partial z}(a^2 w) = 0,$$

subject to

$$\begin{cases} \text{p=1} & \text{at} \quad \text{z=0} \\ \text{p=0} & \text{at} \quad \text{z=1,} \end{cases}$$

15

$$w = \frac{-\varepsilon_2}{ah} \frac{\partial w}{\partial \eta}, \quad \text{at} \quad \eta = \eta_0,$$

$$ah\frac{dN}{dz}w - u = 0, \quad \text{at} \quad \eta = \eta_0,$$

where

$$h = \sqrt{\tfrac{1}{2}(\cosh 2\eta - \cos 2\xi)}.$$

The solution was required to be subject to

$$\frac{\partial w}{\partial \eta} = 0 \quad \text{at} \quad \eta = 0,$$

because the problem is symmetric under a rotation of π. The flux through the channel was obtained. The flux with the variation of the cross-section was given by the harmonic mean of the equivalent flux via a uniform channel. Furthermore, the flux through three elliptic channels was evaluated. The flux computed by two existing methods was compared. In addition, they found that the flux through a pore threat extracted from a micro-CT image of a Berea sandstone was approximated by the most adequate method.

In 2018, the solution of unsteady slip flow with constant pressure gradient in the elliptic micro tube was achieved analytically [28]. This derivation is based on the method of separation of variables. The flow was formulated by transforming the Navier-Stokes equations from rectangular coordinates to elliptic cylindrical coordinates.

Micro-flow behavior can be obtained factually through the velocity slip condition. This was prevalent in the literature. A micro-fluidic examination and pulsating pressure gradient were treated together to make the problem appropriate in many reports. In 2017, the solution for such a problem was obtained [29]. An elliptic cylindrical microchannel supplemented by Navier slip condition was used to formulate the problem. The problem for an incompressible Newtonian fluid was introduced via the fundamental equations as follows

16

$$\nabla \cdot v = 0,$$

$$\rho \left(\frac{\partial v}{\partial t} + (v \cdot \nabla)v \right) = -\nabla p + \mu \nabla^2 v + F_{ek}.$$

The above equations govern the transient electroosmotic flow through an elliptical duct. The Poisson equation which describes the distributions of electric potential was given by

$$\nabla^2 \psi(\xi, \eta) = -\frac{\rho_e}{\varepsilon}.$$

The pressure gradient $\frac{\partial p}{\partial z}$ was approximated by

$$\frac{\partial p}{\partial z}(t) = a_0 + \sum_{n=1}^{\infty} [a_n \cos(n\omega t) + b_n \sin(n\omega t)].$$

By assuming $U = u - (\varepsilon E \mu^{-1})\psi$ and making some simplifying assumptions, the incompressible Navier-Stokes equation in the axial direction in elliptic coordinate can be written as

$$\frac{1}{c^2(\cos h^2 \xi - \cos^2 \eta)} \left(\frac{\partial^2 U}{\partial \xi^2} + \frac{\partial^2 U}{\partial \eta^2} \right) - \frac{\rho}{\mu} \frac{\partial U}{\partial t} = \frac{1}{\mu} \frac{\partial p}{\partial z}.$$

The corresponding boundary conditions in elliptic cylindrical coordinates were given by

$$\frac{\partial U}{\partial \eta}(\xi, 0, t) = 0,$$

$$\frac{\partial U}{\partial \eta}\left(\xi, \frac{\pi}{2}, t \right) = 0,$$

$$\frac{\partial U}{\partial \xi}(0, \eta, t) = 0,$$

$$U(\xi_0, \eta, t) + \frac{l}{c\sqrt{\cosh^2 \xi_0 - \cos^2 \eta}} \frac{\partial U}{\partial \xi}(\xi_0, \eta, t) = 0,$$

$$\psi(\xi_0, \eta) = \zeta.$$

Numerical and analytical solutions have been derived for the velocity profile. These derivations were under the oscillating pressure gradient and at different

times. The Mathieu and modified Mathieu equations were employed to analyze the influence of pulsatile pressure gradients. It has been distinguished that the oscillatory of pulsatile pressure behaves critically. Moreover, the volumetric rate became more adequate when a higher number of terms in the Fourier expansion is used.

2.1.3 Flow of fluids through channels of triangular cross-section

Flow of fluids through equilateral triangular ducts has been studied in terms of local and global fluid dynamic properties [30]. The no-slip velocity is expressed as

$$w_0 = -\frac{x^2 + y^2}{4} - \frac{x^2 - 3xy^2}{12} + \frac{1}{3},$$

and the slip flow is given by

$$w = w_0 + w_s,$$

based on the constant slip assumption, where w_s is the slip velocity which is equal to $w_s = \frac{\lambda}{2}$ by using Navier's slip condition. Constant velocity lines were compared for the equilateral triangular duct between exact solution and using constant velocity assumption. This leads to that local properties were not predicted by the constant slip approximation. A comparison of the Poiseuille number was illustrated as well in [30] which has shown growth in the error.

2.1.4 Flow of fluids through channels of rectangular cross-section

The Lattice Boltzmann equation method was employed to examine gaseous slip flow in rectangular tubes [31]. The influences of the outlet Knudsen number on slip velocity, flow rate, nonlinear pressure, and the proportion of the channel

were considered. This consideration was found to be consistent with parallel plate microchannel limiting cases.

In 2011 [32], the transient flow of an incompressible Newtonian fluid through a rectangular microchannel was investigated for Reynolds number between 2000-2500. The flow is symmetric about the xz and yz planes and horizontally. These simplify the Navier-Stokes equations and the continuity equation to

$$\rho(\frac{\partial v}{\partial t}) = \mu(\frac{\partial^2 v}{\partial x^2} + \frac{\partial^2 v}{\partial y^2}) - \frac{\partial p}{\partial z},$$

$$\frac{\partial v}{\partial z} = 0.$$

Fourier series expansion was employed to approximate the pressure gradient $q(t)$, that is

$$\frac{\partial p}{\partial z} = q(t) = a_0 + \sum_{n=1}^{\infty} [a_n \cos(nwt) + b_n \sin(nwt)].$$

Navier slip conditions were applied on the boundary. Then, the exact solution for the transient velocity field was achieved, namely

$$v(x,y,z) = \sum_{n=1}^{\infty} Re[e^{inwt}(A_n \cosh(\gamma_n x)\cos(k_n y) + B_n \cos(\alpha_n x).\cosh(\beta_n y) - \frac{c_n}{inw\rho})].$$

2.1.5 Flow of fluids in super-elliptic duct

Since rolled rectangular ducts have rounded corners that shrink the frictional perimeter, Wang [33] in 2009 studied the effect of corner rounding on flow and heat transfer. The author obtained that both flow and heat transfer decreased depending on the aspect ratio, while wall shear stress increased. The author assumed that the length of the major axis is $2L$ and the length of the minor axis is $2CL$. Super-ellipse was written as

$$x^{2n} + (\frac{y_1}{c})^{2n} = 1,$$

19

and the Navier-Stokes equations became the Poisson equation

$$\nabla^2 w = -1,$$

where w is the normalized axial velocity. The Ritz method was used to solve the flow and heat transfer problems by first approximating the axial velocity by

$$w = [1 - x^{2n} - (\frac{y}{c})^{2n}]Q(x,y) = \sum_{i=1}^{N} a_i \phi_i(x,y),$$

where Q is defined by

$$Q = a_1 + a_2 x^2 + a_3 y^2 + a_4 x^4 + a_5 x^2 y^2 + a_6 y^4 + a_7 x^6 + \dots..$$

The heat transfer problem was also examined by the Ritz method by assuming:

$$\tau = [1 - x^{2n} - (\frac{y}{c})^{2n}]R(x,y) = \sum_{i=1}^{N} b_i \phi_i(x,y),$$

where R is a polynomial. Constant lines of both velocity and temperature were illustrated. It was found that the velocity has its maximum at the center whereas the temperature has its minimum at the center. Rounded corner has an impact on the area, perimeter, flow rate, and heat transfer. Shear stress on the boundary is also influenced by rounded corner. However, shear stress is zero in rectangular duct at the sharp corner whilst the shear stress for super-elliptic duct normalized by $\frac{\mu V_0}{L}$ is

$$\sigma = \hat{n}.\nabla w = -\frac{\frac{x^{2n-1}w_x + y^{2n-1}w_y}{c^{2n}}}{\sqrt{\frac{x^{4n-2}+y^{4n-2}}{c^{4n}}}}.$$

The computation results show that the rounded corners lead to the drops in both flow rate and heat transfer but an increase in the minimum wall shear stress. A numerical approach has been used to derive solutions for problems in fluid dynamics such as slip flow in ducts as well as no-slip fluid flow in tubes. In 2014, the Ritz method was employed originally to study the slip flow in supanelliptic ducts [34].

The average velocity and the friction factor-Reynolds number were given by $V = \frac{Q}{A}$, $fRe = \frac{8A^2}{VP^2}$, where Q is the flow rate, A and P represent the normalized area and the normalized perimeter length of the cross-section respectively. In addition, the exact solution for slip flow in a circular duct was established in [17]. The Ritz method was powerful for slip flow. But since $\lambda \neq 0$, the Ritz method is not useful for no-slip flow.

2.1.6   Studies on other flow problems

Shale gas flow has been developed in nanoporous reservoirs. This was in 2014 [35] by using the classical Kn scale which primarily was obtained from the physics of rarefied gas flow. The classical Hagen-Poiseuille equation with slip correction has been utilized to explore slip flow in natural gas through nanoporous. Such equation was expressed as

$$Q = \frac{\pi R^4}{16\mu L}(P_1^2 - P_2^2)\left[1 + 4(\frac{2}{f} - 1)\frac{\lambda m}{R}\right],$$

where the term $1 + 4(\frac{2}{f} - 1)\frac{\lambda m}{R}$ represents the slip correction. The results were accomplished without time consuming molecular dynamics and lab experiments by employing PVT(Pressure–Volume–Temperatures). It was realized that slip flow is anticipated when the temperature is higher and the pressure is lower for exact tight shale (R=1nm). However, there was no slip flow corresponding for large pore size (R=1000nm) whatever the temperature and the pressure. This agrees with the results by Roy and Raju [36] when they have examined the flow rate via $(R = 10nm)$. They have shown that the flow velocity is higher for slip flow than no-slip flow with identical pressure ratio. The mean free path varies at low temperatures slightly and slip flow varies trivially. Natural gas flow system is almost independent of the classical Kn scale at all temperatures and pressures.

In 2007, Hayat, Khan and Ayub studied the oldroyd 6-constant flow and slip flow on three non-linear boundary problems [37]. Their study investigated

21

the effects of slip and non-Newtonian parameters. It focused on three steady flows (Couette, Poiseuille and generalized couette). They found that velocity is reduced near the moving plate when the slip coefficient increased for couette and generalized couette flows whereas near the fixed plate the velocity is increased. In poiseuille flow, the velocity is symmetric and increased with the slip coefficient. Moreover, the Homotoby analysis method was used to obtain analytical solutions for the governing non-linear equations. The entry length of a laminar Newtonian steady Poiseuille flow has been investigated [38]. Oldroyd-B and PPT-linear mechanisms were considered to develop the entry region. These developments have focused on the characteristics of the flow such as velocity, axial stress and pressure. It is based on the collocated grid arrangement which includes five different meshes. It has been shown that the velocities in the oldryd-B model converged to the same value and rose slightly when the Weissenberg number (We) reaches 0.3. However, the velocity of PPT-linear fluid became smaller when (We) increased. Moreover, the effect of maximum stress in the case of Oldroyd-B fluid appears to be close to each other with the variation of (We) whilst stress relaxation imposes longer distances at higher (We). The maximum stress values on the other hand for the PPT-linear fluid declined with the growth of (We). The influence of pressure quantity in entry region showed an increase in the pressure with respect to (We) where PTT-linear fluid effects were lower than those in the Oldroyd-B model at specific (We).

The pressure drop of fully-developed flow has been investigated for the slip-flow regime [39]. It was an extension work for Bahrami's model. It was suggested that pressure drop is modeled by a function of geometrical variables of the channel: cross-sectional area, perimeter, polar moment of inertia and the Knudsen number. Based on the first order Maxwell boundary condition for slip-velocity and neglecting the thermal creep effects term, pressure drop under some assumptions was found to be governed by the momentum equation:

$$\frac{dp}{dx} = \mu \left(\frac{\partial^2 u}{\partial y^2} + \frac{\partial^2 u}{\partial z^2} \right),$$

subject to the boundary condition:

$$u_s = \frac{\sigma - 2}{\sigma} \lambda \frac{\tau_w}{\mu}, \quad \tau_w = \mu \frac{\partial u}{\partial n}\bigg|_{wall}.$$

It was noticed that the momentum equation and boundary condition form a Poisson's equation with slip boundary condition. The pressure drop was predicted by analytical solution for circular micro-channel, rectangular microchannel, trapezoidal micro-channel, double-trapezoidal microchannel. It was found that the analytical model supports the numerical and experimental data in the literature with a difference of around 8%. The Poiseuille number can be evaluated by determining only the nondimensional parameter $I_p^* \frac{\sqrt{A}}{\Gamma}$. However, the velocity field and the mean velocity can be found by solving Poisson's equation with slip boundary that leads to evaluating $fRe_{\sqrt{A}}$ after calculating wall shear stress.

Microfluidic mechanisms have been developed recently by comprehensive studies. These studies concern time periodic electroosmotic flow under slip boundary condition. The flow of an incompressible ionized fluid is governed by the Navier-Stokes equations:

$$\rho_f(\frac{\partial \overrightarrow{V}}{\partial t} + (\overrightarrow{V} \cdot \nabla)\overrightarrow{V}) = -\nabla P + \mu \nabla^2 \overrightarrow{V} + \rho_e \overrightarrow{E},$$

which is reduced under some assumptions [40] to

$$\rho_f \frac{\partial u}{\partial t} = \mu \frac{\partial^2 u}{\partial^2 y} + \rho_e E_x \sin(\Omega t).$$

The superposition principle was used to solve the problem. The exact solution for the fluid flow is accomplished by solving the differential equation subject to the following boundary and initial conditions

$$u(0,t) + l\frac{\partial u}{\partial y}(0,t) = 0,$$

$$\frac{\partial u}{\partial y}(h,t) = 0, \quad u(y,0) = u_0(y).$$

The general solution for this boundary value problem has been obtained. The authors also investigated the influence of the slip parameters on the flow behavior. The velocity was found to drop to zero in the centre when the normalized parameter $k = (\frac{\Omega \lambda^2}{\mu})^{\frac{1}{2}}$ increases.

The influence of oscillatory motion was examined on the Stokes and Couette flows [41]. It was studied in terms of sinusoidal behavior. The exact solutions for both Stokes and Couette flows were obtained under slip condition for both small and large times. In this case, the Stokes flow was governed by

$$\frac{\partial u}{\partial t} = v \frac{\partial^2 u}{\partial y^2},$$

subject to the boundary and initial conditions

$$u(0,t) - \beta \frac{\partial u(0,t)}{\partial y} = u_w,$$

$$u(y,0) = 0,$$

$$u(y \to \infty, t) = 0,$$

where β represents the slip coefficient, and the speed of the wall u_w is expressed by either

$$u_w = u_0 \cos(\omega t) \quad \text{or}$$

$$u_w = u_0 \sin(\omega t).$$

The steady periodic velocity and the transient velocity were achieved by utilizing the Laplace transform approach. They are respectively,

$$\frac{u_{sp}(\eta,\tau)}{u_0} = \left[\frac{(1+\lambda)\cos(\tau - \frac{\eta}{\sqrt{2}}) + \lambda \sin(\tau - \frac{\eta}{\sqrt{2}})}{2\lambda^2 + 2\lambda + 1} \right] e^{\frac{-\eta}{\sqrt{2}}},$$

$$\frac{u_t(\eta,\tau)}{u_0} = -\frac{1}{\pi} \int_0^\infty \frac{re^{-r\tau}}{(r^2+1)} \left[\frac{\sin(\sqrt{r}\eta) + \lambda\sqrt{2r}\cos(\sqrt{r}\eta)}{1 + 2\lambda^2 r} \right] dr,$$

which describe a motion in cosine form. This velocity became zero asymptotically when the dimensionless coordinate η and the oscillating slip parameter reach their asymptote lower values:

$$\frac{u_t(\eta,\tau)}{u_0} \approx -\frac{3}{4\sqrt{\pi}} \frac{(\eta+\sqrt{2}\lambda)}{\tau^{\frac{5}{2}}} \quad \text{as} \quad \tau \to \infty.$$

In addition, for the case when the motion of the flow takes sine form, the results can be described in a similar way. It was observed that the effects of the motion in cosine form have less transient than the motion in sine form. The normalized equation for the Couette flow was given by

$$\frac{\partial U}{\partial \tau} = \frac{1}{R}\frac{\partial^2 U}{\partial Y^2},$$

subject to the following normalized wall slip conditions and initial condition

$$U(0,\tau) - \frac{\beta}{h}\frac{\partial U(0,\tau)}{\partial Y} = R_0\sin(\tau),$$

$$U(1,\tau) + \frac{\beta}{h}\frac{\partial U(1,\tau)}{\partial Y} = 0,$$

$$U(Y,0) = 0.$$

It was noticed that a reduction in the transient velocity occurs for Stokes flow with wall slip, whereas a reduction for transient effects for the Couette flow occurs only for large and small values of the wall slip coefficient.

2.2 Heat transfer in slip flow of fluids

2.2.1 Heat transfer in fluids in channels of circular cross-section

In 2008, annular microchannels were selected to investigate heat transfer in slip flow of fluids [42]. The velocity problem has been examined at first due to the

dependence of heat transfer analysis on the velocity distributions. Then, the velocity was determined by the reduced momentum equation

$$\mu\left(\frac{d^2u}{dr^2}+\frac{1}{r}\frac{du}{dr}\right)=\frac{dp}{dx},$$

since the micro channels were long enough $(L/D_h \gg 1)$ and the Reynolds number was relatively low. The supplementing slip boundary conditions on the walls were expressed as

$$u=\lambda\frac{2-\sigma}{\sigma}\frac{du}{dr}\quad\text{at}\quad r=b,$$

$$u=-\lambda\frac{2-\sigma}{\sigma}\frac{du}{dr}\quad\text{at}\quad r=a.$$

The Knudsen number was defined as the ratio between the molecular mean free path λ and the hydraulic diameter, that is

$$Kn=\frac{\lambda}{D_h}=\frac{\lambda}{2(a-b)},$$

and the authors in [42] have obtained the solution for this problem. The heat flux was analyzed under hydrodynamically and thermally fully developed condition through the following energy equation

$$\rho c_p u\frac{\partial T}{\partial x}=\frac{k}{r}\frac{\partial}{\partial r}\left(r\frac{\partial T}{\partial r}\right).$$

The temperature distribution was then computed with the following boundary conditions:

$$\frac{dT}{dr}=0\quad\text{at}\quad r=a,$$

$$T-T_w=\frac{2-\sigma_T}{\sigma_T}\frac{2\gamma}{\gamma+1}\frac{\lambda}{P_r}\frac{dT}{dr}\quad\text{at}\quad r=b.$$

On the other hand, the energy equation together with the boundary condition for uniform wall heat flux on the outer wall can be given by

$$\frac{2qa}{(a^2-b^2)}\frac{u}{\bar{u}}=\frac{k}{r}\frac{\partial}{\partial r}\left(r\frac{\partial T}{\partial r}\right),$$

$$\frac{dT}{dr} = 0 \quad \text{at} \quad r = b,$$

$$T - T_w = -\frac{2-\sigma_T}{\sigma_T}\frac{2\gamma}{\gamma+1}\frac{\lambda}{P_r}\frac{dT}{dr} \quad \text{at} \quad r = a.$$

In addition, uniform wall heat flux on both walls was also considered. The consequence of this analysis has shown that the Nusselt numbers for the slip flow are lower than those for no-slip flow. An increase in Knudsen's number has led to a drop in the Nusselt number for useful applications. Heat transfer characteristics were found to be influenced by the Knudsen number, radius rational heat flux ratio as indicated.

Heat transfer in slip flow was reviewed in 2012 [43] . Pressure-driven flows of gases with heat transfer in microchannels of circular cross-sections were investigated. Their review includes the analytical solution of hydrodynamic and thermal fully developed flow with uniform wall heat flux achieved by Sparrow and Lin [44]. The classic first-order boundary conditions were used to get an exact expression of the Nusselt Number, namely

$$U - u_w = \frac{2-\sigma_u}{\sigma_u}\lambda\frac{\partial u}{\partial n}|_\Gamma, \tag{2.1}$$

$$T - T_w = \frac{2-\sigma_T}{\sigma_T}\frac{2\gamma}{\gamma+1}\frac{\lambda}{Pr}\frac{\partial T}{\partial n}|_\Gamma. \tag{2.2}$$

2.2.2 Heat transfer in fluids in channels of rectangular cross-section

In 2001, an examination of heat transfer in slip flow of fluids in rectangular microchannels was conducted [45]. Velocity slip and temperature jump boundary conditions on the gas-surface interface in the y-direction were given by

$$u(x,b) = \left[-\beta_v \lambda \frac{\partial u}{\partial y} + 3\left(\frac{\Re T}{8\pi}\right)^{\frac{1}{2}}\frac{\lambda}{T}\frac{\partial T}{\partial z} \right]_{y=b},$$

$$T(x,b,z) - T_w = \left[-\beta_t \lambda \frac{\partial T}{\partial y} + \frac{1}{4\Re} u^2 \right]_{y=b},$$

where β_v and β_t were determined by

$$\beta_v = \frac{2-F_v}{F_v},$$

$$\beta_t = \frac{2-F_t}{F_t} \frac{2\gamma}{\gamma+1} \frac{1}{Pr},$$

in which F_v and F_t are the tangential momentum accommodation coefficient and thermal accommodation coefficient respectively. The slip-flow boundary conditions in the x-direction have the same form as that in the y-direction. Velocity slip in the y-direction transverse velocity gradient yields the first term in the first equation, whereas the thermal creep due to temperature gradient in the flow direction forms the second term of the first equation. The second term in the first equation was ignored because $\frac{\partial}{\partial y} >> \frac{\partial}{\partial z}$. Based on the typical low Eckert number assumption, the second term of the second equation was ignored. Under the assumption of Newtonian fluid, negligible body forces, constant properties and steady-state flow, the velocity profile for slip-flow can be determined from the z-momentum equation, namely

$$\frac{\partial^2 U}{\partial X^2} + \frac{\partial^2 U}{\partial Y^2} = \frac{1}{Pr} \frac{dP}{dZ}.$$

For the rectangular channel of sides $2a$ and $2b$ with the origin of the coordinate system being located at the centreline of the rectangular channel, the supplemented boundary conditions were given by

$$\left. \frac{\partial U}{\partial X} \right|_{X=0} = 0,$$

$$\left[U + (\beta_v Kn) \frac{\partial U}{\partial X} \right]_{X=\hat{a}} = 0,$$

$$\left. \frac{\partial U}{\partial Y} \right|_{Y=0} = 0,$$

$$\left[U + (\beta_v Kn)\frac{\partial U}{\partial Y}\right]_{Y=b} = 0.$$

The dimensionless energy equation and thermal boundary conditions and initial condition under the assumption of hydrodynamically fully developed flow, high Péclet number, negligible energy dissipation and constant properties, were given by

$$\frac{\partial^2 \theta}{\partial X^2} + \frac{\partial^2 \theta}{\partial Y^2} = U(X,Y)\frac{\partial \theta}{\partial Z},$$

$$\left.\frac{\partial \theta}{\partial X}\right|_{X=0} = 0,$$

$$\left[\theta + \beta(\beta_v Kn)\frac{\partial \theta}{\partial X}\right]_{X=\hat{a}} = 0,$$

$$\left.\frac{\partial \theta}{\partial Y}\right|_{Y=0} = 0,$$

$$\left[\theta + \beta(\beta_v Kn)\frac{\partial \theta}{\partial Y}\right]_{Y=b} = 0,$$

$$\left.\theta\right|_{Z=0} = 1.$$

The modified generalized integral transform method has been used to solve the problem of thermally fully developed laminar flow in a rectangular channel. Such method is computationally efficient.

The heat transfer problem in rectangular microchannels was considered in 2002 [46]. An analytical model in a such microchannel in the slip flow regime was examined for hydrodynamics of gases with second-order boundary conditions. Heat transfer in slip flow in a rectangular microchannel was investigated in recent years under some assumptions [43].

A control-Volume based numerical method was employed to solve the initial-value problem for incompressible gas flows and heat transfer in rectangular

microchannels. The problem was formulated in 2006 [7] by the three-dimensional Navier-Stokes equations, continuity equation and energy equations

$$\nabla \cdot \overrightarrow{V} = 0,$$

$$\rho \frac{D\overrightarrow{V}}{Dt} = -\nabla p + \mu \nabla^2 \overrightarrow{V},$$

$$\rho c_p \frac{DT}{Dt} = k \nabla^2 T,$$

where body forces and viscous dissipation were neglected. Profiles for the inflow boundary conditions were uniform, namely

$$u = U_i = U_m,$$

$$v = w = 0,$$

$$T = T_i,$$

and zero-gradients along the axial flow direction were considered outflow, that is $\frac{\partial f}{\partial x} = 0$, where $f = u, v, w, T$. The complementary slip/jump boundary conditions were given respectively by

$$u - u_w = \alpha \left(\frac{2 - \sigma_v}{\sigma_v} \right) \lambda \left(\frac{\partial u}{\partial n} \right)_w + \frac{3}{4} \frac{\mu}{\rho T_w} \left(\frac{\partial T}{\partial s} \right)_w,$$

$$T - T_w = \beta \left(\frac{2 - \sigma_T}{\sigma_T} \right) \left(\frac{2\gamma}{\gamma + 1} \right) \frac{\lambda}{Pr} \left(\frac{\partial T}{\partial n} \right)_w + \frac{u^2}{4\Re},$$

where only the first terms were considered for simplicity. The influence on the slip-flow and heat transfer by varying Reynolds number $(0.1 \leq Re \leq 10)$ and channel aspect ratio $(0 \leq \alpha^* \leq 1)$ was investigated in the slip-flow regime. In the entrance region, the velocity and pressure fields were examined depending on the axial variations to achieve the flow characteristics. The results on pressure

distributions show that the local maxima appears near the walls with validity of the no-slip boundary condition. Reduction in pressure gradients occurred due to slip on the wall. The flow was pushed toward the core as well as the fluid near the wall due to strong pressure gradients, in the axial direction. The slip velocity on the wall was dictated. When the flow approaches the fully developed region, at $Kn = 0.1$ the amount of slip drooped because the velocity gradients on the wall are reduced. In addition, lower velocities resulted in higher slip as illustrated for all four axial locations. The temperature profile illustrated that the central region was independent of the wall temperature whereas strong gradients emerged near the walls, for the $Kn = 0.05$ and 0.1 cases. For a square channel, the variations in the heat transfer rate were demonstrated for different values of Knudsen number.

Microelectromechanical systems technology have motivated micro scale fluid dynamics. Velocity slip and temperature jump have activated at the duct walls when the mean free path of the gas was comparable to the channel's characteristic dimension.

2.2.3 Heat transfer in fluids in channels of elliptic cross-section

Spiga and Vocale considered the dynamic and thermal representation of rarefied flow in 2012 [47]. They studied the flow in a microchannel with elliptical cross-section under the assumption of slip flow, laminar, steady state, fully developed forced convection, and the range of Knudsen number between 0.001-0.1, as well as H1 boundary condition. The fluid and wall temperatures under their proposed hypotheses on the gas flow and the walls were modeled via the Navier Stokes and energy equations

$$-\frac{\partial p}{\partial z} + \mu \left(\frac{\partial^2 u}{\partial x^2} + \frac{\partial^2 u}{\partial y^2} \right) = 0, \tag{2.3}$$

$$\frac{q}{A} \frac{u}{W} = \lambda \left(\frac{\partial^2 T}{\partial x^2} + \frac{\partial^2 T}{\partial y^2} \right) = 0. \tag{2.4}$$

The dimensionless independent variables were given by

$$\eta = \frac{x}{a}, \quad \xi = \frac{y}{a}, \quad z = \frac{z}{a}, \tag{2.5}$$

and the dimensionless dependent functions were given by

$$p^* = -\frac{a^2}{\mu W}\frac{\partial p}{\partial z}, \quad U = \frac{u}{W}, \quad \theta = \frac{\lambda(T - T_w)}{q}. \tag{2.6}$$

Then, the dimensionless Navier Stokes and energy equations became

$$p^* + \frac{\partial^2 U}{\partial \eta^2} + \frac{\partial^2 U}{\partial \xi^2} = 0, \tag{2.7}$$

$$\frac{\partial^2 \theta}{\partial \eta^2} + \frac{\partial^2 \theta}{\partial \xi^2} = \frac{1}{\pi \gamma}U. \tag{2.8}$$

The supplemented dimensionless first-order slip flow boundary conditions for velocity and temperature on the wall were

$$U_s = \frac{2 - \sigma_v}{\sigma_v}Kn\frac{D_h}{a}(\frac{\partial U}{\partial n})_w = \beta_v Kn\frac{D_h}{a}(\frac{\partial U}{\partial n}), \tag{2.9}$$

$$\theta_j = \frac{2 - \sigma_T}{\sigma_T}\frac{2k}{k+1}\frac{Kn}{Pr}\frac{D_h}{a}(\frac{\partial \theta}{\partial n}) = \beta_t Kn\frac{D_h}{a}(\frac{\partial \theta}{\partial n}). \tag{2.10}$$

A numerical solution for such problem was obtained and compared to the analytical solution in the literature. The effects of friction factors and convective heat transfer coefficients were also examined in [47].

2.2.4 Heat transfer in Transient and Starting flows

In 2010, the unsteady flow and heat transfer was examined by Makinde and Chinyoka [48]. These examinations considered electrically conducting, incompressible dusty fluids together with temperature dependant viscosity and thermal conductivity. The fluid flow was between two isolated infinite plates where their temperatures sustained constant but different with the Navier wall slip condition. The dusty-fluid equations were used. The governing momentum and energy equations and boundary conditions for the flow of fluid and dust particles were expressed as follows

$$\frac{\partial u}{\partial t} = \alpha + \frac{1}{Re}\frac{\partial}{\partial y}\left(\mu(T)\frac{\partial u}{\partial y}\right) - \frac{Ha^2}{Re}u - \frac{R}{Re}(u - u_p),$$

$$\frac{\partial u_p}{\partial t} = \frac{1}{ReG}(u - u_p),$$

$$\frac{\partial T}{\partial t} = \frac{1}{RePr}\frac{\partial}{\partial y}\left(k(T)\frac{\partial T}{\partial y}\right) + \frac{Ec}{Re}\mu(T)\left(\frac{\partial u}{\partial y}\right)^2 + \frac{Ec}{Re}Ha^2u^2 + \frac{2R}{3RePr}Re(T_p - T),$$

$$\frac{\partial T_p}{\partial t} = -L(T_p - T), \text{with}$$

$$u(y,t) = u_p(y,t) = T(y,t) = T_p(y,t) = 0, \text{for} \quad t \leq 0,$$

$$u_p(0,t) = u_p(1,t) = T_p(0,t) = T(0,t) = 0, \text{for} \quad t > 0,$$

$$\beta\frac{\partial u}{\partial y} = u, \text{for} \quad y = 0,1, t > 0,$$

$$T_p(1,t) = T(1,t) = 1, \text{for} \quad t > 0,$$

where the viscosity and thermal conductivity depending on the temperature as given below

$$\mu(T) = exp(-aT), \quad k(T) = exp(bT).$$

These equations were simplified by using dimensionless parameters, and were then solved numerically by using the semi-implicit finite difference method. The investigation of this problem illustrated that the velocity and temperature increase until the appearance of a steady state. Fluid velocity increases with decreasing in the viscosity value. Under the Navier slip conditions, there is no effect on the temperature distribution, whereas an increase occurs in the velocity.

Chapter 3

Temperature field in fluids in circular microchannels in the slip regime

3.1 General

In recent years, with the advancement of nano-science and technologies, many biological and engineering devices in microscale have been developed [49, 50]. These include, for example, drug delivery systems [51] and micro-electro-mechanical systems (MEMS) [52] etc. These systems usually involve fluid flow and heat transfer processes, and the behaviour of these processes determines the functional characteristics of the devices/systems. Hence, the study of fluid flow in micro-channels and the associated heat transfer process is extremely important in order to get a better understanding and consequently better characteristics or performance of the associated devices or systems.

The fluid and heat transfer processes are governed by the continuity equation, the Navier-Stokes equations, and the energy equation. Conventionally the field equations for fluid flows are supplemented by the so-called no-slip boundary condition for the velocity field. However, many recent experimental results

show evidence of slip of a fluid on a solid boundary [53]. Through intensive investigations and simulation studies in micrometerscale (see for example [54], [55], [4]), it has now been established that the flow of fluids in microchannels is granular and slip on the solid surface may occur [6, 56–58]. Hence, slip boundary conditions have been used for fluid flows in micro-systems.

Although closed form exact solutions for many fluid flow problems are available in literature, only a few closed form solutions for the slip boundary case have been obtained in recent years. Various steady state solutions have been derived for flows through channels of various types of cross-sections in the slip regime [59, 60]. Various exact solutions of the velocity field for the transient flows of fluids through microtubes have also been developed in [61]. However, the associated temperature field in the microflow has not been investigated. In this work, a mathematical model is constructed and applied to investigate the heat transfer processes and temperature field in microflows in the slip regime. The rest of this chapter is organized as follows. The mathematical model is formulated in section 3.2. Then, a computation scheme based on the finite difference method is derived in section 3.3 for the determination of the transient temperature field. In section 3.4, the computation scheme is applied to investigate the influences of boundary slip and convection heat transfer due to fluid flow on the temperature field. A conducting remark is given in section 3.5.

3.2   Mathematical model

In this work, we consider the heat transfer of an incompressible Newtonian fluid flowing through a circular microchannel with the *z*-axis being in the axial direction. The problem involves both fluid flow and heat transfer and the interaction between the two processes. From the principle of continuum mechanics, the heat transfer process is governed by the convection-diffusion equation as follows

$$\rho c_p (\frac{\partial T}{\partial t} + \mathbf{v} \cdot \nabla T) = \nabla \cdot (k \nabla T) + \mu \Phi, \tag{3.1}$$

where T denotes the temperature in the fluid, $\mathbf{v}$ is the velocity vector of the fluid, ρ, c_p, k, μ, and Φ are respectively the fluid density, specific heat, thermal conductivity, fluid viscosity, and dissipation function. Based on the material assumption, from the principle of fluid dynamics, the equations governing the velocity field include the standard continuity equation and the Navier-Stokes equations, namely

$$\nabla \cdot \mathbf{v} = 0, \tag{3.2}$$

$$\frac{\partial \mathbf{v}}{\partial t} + (\mathbf{v} \cdot \nabla)\mathbf{v} = \frac{\mu}{\rho}\nabla^2\mathbf{v} - \frac{1}{\rho}\nabla p - f, \tag{3.3}$$

where p denotes the fluid pressure, and f represents the body force acting in the fluid. As the problem is axially symmetric, it is more convenient to formulate the equations in cylindrical coordinates. In cylindrical polar coordinates,

$$\mathbf{v} = \mathbf{e}_r \mathbf{v}_r + \mathbf{e}_\theta \mathbf{v}_\theta + \mathbf{e}_z \mathbf{v}_z, \tag{3.4}$$

$$\nabla = \mathbf{e}_r \frac{\partial}{\partial r} + \mathbf{e}_\theta \frac{\partial}{r \partial r} + \mathbf{e}_z \frac{\partial}{\partial z}, \tag{3.5}$$

where $\mathbf{e_r}, \mathbf{e_\theta}$ and $\mathbf{e_z}$ are unit vectors in the radial, transverse and axial directions respectively. Thus, the energy equation becomes

$$\rho c_p \left(\frac{\partial T}{\partial t} + v_r \frac{\partial T}{\partial r} + \frac{v_\theta}{r}\frac{\partial T}{\partial \theta} + v_z \frac{\partial T}{\partial z}\right) = k\left[\frac{1}{r}\frac{\partial}{\partial r}\left(r\frac{\partial T}{\partial r}\right) + \frac{1}{r^2}\frac{\partial^2 T}{\partial \theta^2} + \frac{\partial^2 T}{\partial z^2}\right] + \mu\Phi. \tag{3.6}$$

As the flow is axially symmetric in the axial direction, we have $v_\theta = 0$, and the flow in the radial direction is negligible. The temperature field is also independent of the angle θ for axial symmetric flows. Moreover, the dissipation function Φ is to be neglected. Hence, the energy equation simplifies to

$$\rho c_p \left(\frac{\partial T}{\partial t} + v_z \frac{\partial T}{\partial z}\right) = k\left(\frac{\partial^2 T}{\partial z^2} + \frac{\partial^2 T}{\partial r^2} + \frac{1}{r}\frac{\partial T}{\partial r}\right). \tag{3.7}$$

As derived in [21], the velocity v_z can be shown to be governed by

$$\frac{\partial v_z}{\partial t} = -\frac{1}{p} + \frac{\partial p}{\partial v_z} + \frac{\mu}{p}\left(\frac{\partial^2 v_z}{\partial r^2} + \frac{1}{r}\frac{\partial v_z}{\partial r}\right). \tag{3.8}$$

36

Without lose of generality, Wu et al [21] consider the fluid flow driven by the pressure gradient which can be approximated by

$$\frac{\partial p}{\partial z} = a_0 + \sum_{n=1}^{\infty} a_n \cos(n\omega t) + b_n \sin(n\omega t), \tag{3.9}$$

and study the fluid flow field in the slip regime. Under the Navier boundary slip assumption, solutions for the velocity field and stress field have been derived. However, no closed-form exact work has been done on the associated energy equation and the temperature field. The previous study on the velocity field has laid a solid foundation for the study of the temperature field, and the results will be used in solving the associated heat transfer problem.

To solve the energy equation (3.7), we need to construct proper boundary conditions and initial condition since the flow is unsteady. In general, there are three types of boundary conditions, including Dirichlet type in which the temperature (T) is prescribed on the boundary, Neumann type in which the heat flux $(\frac{\partial T}{\partial n})$ is prescribed on the boundary, and Robin type in which the mixture of temperature and heat flux is prescribed. For the problem investigated in cylindrical coordinates (r, θ, z), the boundary conditions based on Robin type may be written as

$$\alpha_1 \frac{\partial T}{\partial r} + k_1 T = f_1 \quad \text{on} \quad r = R,$$

$$-\alpha_2 \frac{\partial T}{\partial z} + k_2 T = f_2 \quad on \quad z = 0,$$

$$\alpha_2 \frac{\partial T}{\partial z} + k_2 T = f_2 \quad on \quad z = L,$$

$$\left. \frac{\partial T}{\partial r} \right|_{r=0} = 0,$$

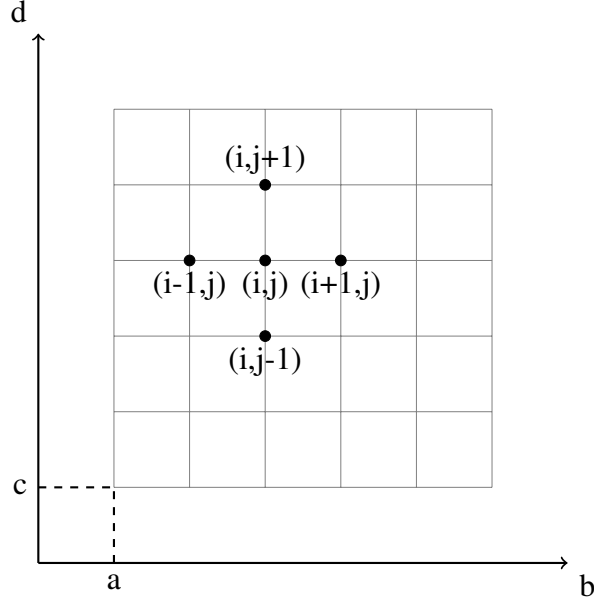where R is the radius of the circular micorchannel.

Figure 3.1: Diagram showing the 5-point finite difference scheme

3.3 Computational Scheme

Firstly, we subdivide the domain in the (r, z)-plane as shown in Fig.3.1, i.e the domain $(a, b) \times (c, d)$ in the rz-plane, into a set of equal rectangles, since the flow is axially symmetric. The lengths of the sides of these rectangles are:

$$\delta r = h = \frac{b-a}{n_r}, \delta z = \frac{d-c}{n_z}.$$

In the selected coordinate system, we have

$$(r_i, z_j) = (a + ih, c + jk), (i = 0, n_r; j = 1, n_z).$$

We also use (i, j) to represent position (r_i, z_j) and $T_{i,j}^n$ to indicate $T(r_i, z_j, t_n)$. The differential equation (3.7) is a field equation defined in the domain $(a, b) \times (c, d)$. To find a numerical solution by the finite difference method, we consider the differential equation at a finite number of points in the domain $(a, b) \times (c, d)$, and hence get

$$\rho \frac{c_p}{k} \left[\frac{\partial T_{i,j}^n}{\partial t} + \upsilon_z \frac{\partial T_{i,j}^n}{\partial z} \right] = \left[\frac{\partial^2 T_{i,j}^n}{\partial z^2} + \frac{\partial^2 T_{i,j}^n}{\partial r^2} + \frac{1}{r} \frac{\partial T_{i,j}^n}{\partial r} \right], \qquad (3.10)$$

38

where $i = 0, \cdots, n_r,$ $j = 1, \cdots, n_z,$ $n = 0, \cdots, n_t$. Then, based on Taylor's Theorem, we have

$$T(r_i + h, z_j) = T_{i+1,j} = T_{i,j} + hT_r + \frac{h^2}{2}T_{rr} + \cdots$$

$$T(r_i - h, z_j) = T_{i-1,j} = T_{i,j} - hT_r + \frac{h^2}{2}T_{rr} - \cdots$$

where T_r and T_{rr} are all evaluated at (r_i, z_j). The central finite-difference formulae based on Taylor's Theorem can then be applied to calculate the derivatives in (3.10), namely,

$$\frac{\partial T_{i,j}^n}{\partial r} = \frac{T_{i+1,j}^n - T_{i-1,j}^n}{2h} + O(h^2), \tag{3.11}$$

$$\frac{\partial^2 T_{i,j}^n}{\partial r^2} = \frac{T_{i-1,j}^n - 2T_{i,j}^n + T_{i+1,j}^n}{h^2} + O(h^2), \tag{3.12}$$

$$\frac{\partial T_{i,j}^n}{\partial z} = \frac{T_{i,j+1}^n - T_{i,j-1}^n}{2g} + O(g^2), \tag{3.13}$$

$$\frac{\partial^2 T_{i,j}^n}{\partial z^2} = \frac{T_{i,j-1}^n - 2T_{i,j}^n + T_{i,j+1}^n}{g^2} + O(g^2). \tag{3.14}$$

For $h = g$, we have the five points of the central difference scheme,

$$\nabla^2 T_{i,j}^n = \frac{1}{h^2}\left[T_{i-1,j}^n + T_{i+1,j}^n + T_{i,j-1}^n + T_{i,j+1}^n - 4T_{i,j}^n\right] + O(h^2). \tag{3.15}$$

Equation (3.10) can be written as

$$\rho\frac{c_p}{k}[\frac{\partial T_{i,j}^n}{\partial t} + \upsilon_z\frac{\partial T_{i,j}^n}{\partial z}] - \frac{1}{r}\frac{\partial T_{i,j}^n}{\partial r} = \nabla^2 T_{i,j}^n. \tag{3.16}$$

To derive a computational scheme for the problem investigated, at first, as an example, we discretize the domain into a mesh with 6×6 grid points, as shown in Fig.3.2. These points (i, j) are called nodes with $i = 0, 1, 2, 3, 4, 5$ and $j = 1, 2, 3, 4, 5, 6$.
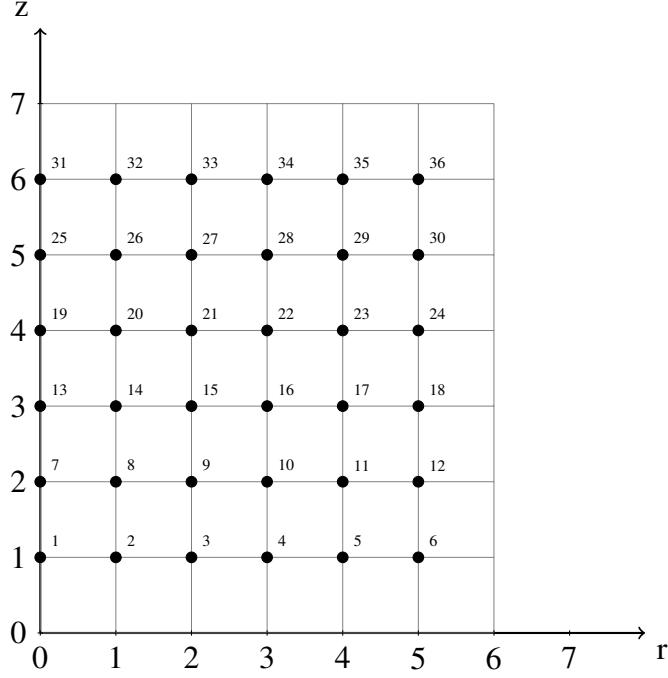
Figure 3.2: The finite difference mesh

Then, we can set up an equation at each of these nodes. Therefore, the total number of equations equals to the number of unknown, i.e., 36. These equations define $T_{i,j}^n (i = 0, 5, j = 1, 6)$.

To construct such equations we substitute equations (3.11)-(3.14) into equation (3.10) and obtain:

$$T_{i,j-1}^n + T_{i-1,j}^n - 4T_{i,j}^n + T_{i+1,j}^n + T_{i,j+1}^n =$$
$$\frac{\rho h^2 c_p}{k} \left[\frac{\partial T_{i,j}^n}{\partial t} + \frac{T_{i,j+1}^n - T_{i,j-1}^n}{2h} v_z(r_i, t) \right] - \frac{h^2}{r_i} \frac{T_{i+1,j}^n - T_{i-1,j}^n}{2h}, \quad (i = 0, 5, j = 1, 6) \tag{3.17}$$

Let $\frac{\rho h^2 c_p}{k} = \alpha$, $\quad \frac{v_z(r_i,t)}{2h} = \beta_i$, $\quad \frac{h}{2r_i} = \gamma_i$, $\quad$ we get

$$(1 + \alpha\beta_i)T_{i,j-1}^n + (1 - \gamma_i)T_{i-1,j}^n - 4T_{i,j}^n + (1 + \gamma_i)T_{i+1,j}^n +$$
$$(1 - \alpha\beta_i)T_{i,j+1}^n = \alpha \frac{\partial T_{i,j}^n}{\partial t}. \tag{3.18}$$

40

These equations can be established row by row. Now, for $i = 0$, the above equation becomes:

$$(1 + \alpha\beta_0)T_{0,j-1}^n + (1 - \gamma_0)T_{-1,j}^n - 4T_{0,j}^n + (1 + \gamma_0)T_{1,j}^n +$$
$$(1 - \alpha\beta_0)T_{0,j+1}^n = \alpha \frac{\partial T_{0,j}^n}{\partial t}, \quad (3.19)$$

where the terms $T_{-1,j}^n$ are at the nodes outside the range considered. Then, we need to eliminate this term by using the symmetrical boundary condition

$$T_{-i,j}^n = T_{i,j}^n, \quad (3.20)$$

Hence, by substituting (3.20) into (3.19) we get

$$(1 + \alpha\beta_0)T_{0,j-1}^n + 2T_{1,j}^n - 4T_{0,j}^n + (1 - \alpha\beta_0)T_{0,j+1}^n = \alpha \frac{\partial T_{0,j}^n}{\partial t}. \quad (3.21)$$

For $i = 5$, Eq. (3.18) becomes

$$(1 + \alpha\beta_5)T_{5,j-1}^n + (1 - \gamma_5)T_{4,j}^n - 4T_{5,j}^n + (1 + \gamma_5)T_{6,j}^n +$$
$$(1 - \alpha\beta_5)T_{5,j+1}^n = \alpha \frac{\partial T_{5,j}^n}{\partial t}, \quad (3.22)$$

where the terms $T_{6,j}^n$ are located outside the defined region. Thus, we need to express these terms using other values via the boundary conditions on $r = R$

$$\alpha_1 \frac{\partial T}{\partial r} + k_1 T = f_1. \quad (3.23)$$

Thus, by using the finite difference scheme for the derivative in the boundary condition on $i = 5$, we get from the above

$$\alpha_1 \left[\frac{T_{6,j}^n - T_{4,j}^n}{2h} \right] + k_1 T_{5,j}^n = f_1, \quad (3.24)$$

which gives

$$T_{6,j}^n = \frac{2hf_1}{\alpha_1} + T_{4,j}^n - \frac{2k_1 h}{\alpha_1} T_{5,j}^n, \quad (3.25)$$

41

that is,

$$T_{6,j}^n = f_n + T_{4,j}^n - mT_{5,j}^n, \tag{3.26}$$

where $f_n = \frac{2hf_1}{\alpha_1}, m = \frac{2k_1h}{\alpha_1}$.

Substituting Eq. (3.26) into Eq. (3.22) we get

$$(1+\alpha\beta_5)T_{5,j-1}^n + (1-\gamma_5)T_{4,j}^n - 4T_{5,j}^n + (1+\gamma_5)(f_n + T_{4,j}^n - mT_{5,j}^n) +$$
$$(1-\alpha\beta_5)T_{5,j+1}^n = \alpha\frac{\partial T_{5,j}^n}{\partial t}, \tag{3.27}$$

which yields

$$(1+\alpha\beta_5)T_{5,j-1}^n + 2T_{4,j}^n - (m+\gamma_5 m+4)T_{5,j}^n + (1-\alpha\beta_5)T_{5,j+1}^n$$
$$+ (1+\gamma_5)f_n = \alpha\frac{\partial T_{5,j}^n}{\partial t}. \tag{3.28}$$

For $j = 1$, Eq. (3.18) becomes

$$(1+\alpha\beta_i)T_{i,0}^n + (1-\gamma_i)T_{i-1,1}^n - 4T_{i,1}^n + (1+\gamma_i)T_{i+1,1}^n + (1-\alpha\beta_i)T_{i,2}^n = \alpha\frac{\partial T_{i,1}^n}{\partial t}, \tag{3.29}$$

where $T_{i,0}^n$ are outside the region. So we use the boundary condition

$$-\alpha_2\frac{\partial T}{\partial z} + k_2 T = f_2 \quad \text{on} \quad z = 0. \tag{3.30}$$

By using the central finite difference scheme for the derivative in the boundary condition on $z = 0$, we have

$$-\alpha_2\frac{T_{i,2}^n - T_{i,0}^n}{2g} + k_2 T_{i,1}^n = f_2, \tag{3.31}$$

which gives

$$T_{i,0}^n = f_w + T_{i,2}^n - dT_{i,1}^n, \tag{3.32}$$

where $f_w = \frac{2gf_2}{\alpha_2}, d = \frac{2gk_2}{\alpha_2}$.

Substituting (3.32) into (3.29), we get

$$(1-\gamma_i)T_{i-1,1}^n - (4+d+d\alpha\beta_i)T_{i,1}^n + 2T_{i,2}^n + (1+\gamma_i)T_{i+1,1}^n =$$
$$- (1+\alpha\beta_i)f_w + \alpha\frac{\partial T_{i,1}^n}{\partial t}. \tag{3.33}$$

For $j = 6$, Eq. (3.18) becomes

$$(1 + \alpha\beta_i)T_{i,5}^n + (1 - \gamma_i)T_{i-1,6}^n - 4T_{i,6}^n + (1 + \gamma_i)T_{i+1,6}^n$$
$$+ (1 - \alpha\beta_i)T_{i,7}^n = \alpha\frac{\partial T_{i,6}^n}{\partial t}, \tag{3.34}$$

where $T_{i,7}^n$ are outside the domain. Then, we use the boundary condition

$$\alpha_2\frac{\partial T}{\partial z} + k_2 T = f_2 \quad \text{on} \quad z = L, \tag{3.35}$$

to eliminate them. By using the central finite difference scheme for the derivative above on $z = L$, we have

$$\alpha_2\frac{T_{i,7}^n - T_{i,5}^n}{2g} + k_2 T_{i,6}^n = f_2, \tag{3.36}$$

which gives

$$T_{i,7}^n = f_w + T_{i,5}^n - dT_{i,6}^n. \tag{3.37}$$

Substituting (3.37) into (3.34) we get

$$2T_{i,5}^n + ((\alpha\beta_i - 1)d - 4)T_{i,6}^n + (1 - \gamma_i)T_{i-1,6}^n + (1 + \gamma_i)T_{i+1,6}^n$$
$$+ (1 - \alpha\beta_i)f_w = \alpha\frac{\partial T_{i,6}^n}{\partial t}. \tag{3.38}$$

Now we discuss the corner points. At the point $(i, j) = (0, 1)$, from (3.21) with $j = 1$ we have

$$(1 + \alpha\beta_0)T_{0,0}^n + 2T_{1,1}^n - 4T_{0,1}^n + (1 - \alpha\beta_0)T_{0,2}^n = \alpha\frac{\partial T_{0,1}^n}{\partial t}. \tag{3.39}$$

As the term $T_{0,0}^n$ is outside the domain, equation (3.32) for $i = 0$ gives

$$T_{0,0}^n = f_w - dT_{0,1}^n + T_{0,2}^n. \tag{3.40}$$

Substituting (3.40) into (3.39), we have

$$2T_{1,1}^n + (-4 - d\alpha\beta_0 - d)T_{0,1}^n + 2T_{0,2}^n = \alpha\frac{\partial T_{0,1}^n}{\partial t} - f_w - f_w\alpha\beta_0. \tag{3.41}$$

43

At the corner point $(0,6)$, from (3.21) with $j = 6$, we have

$$(1 + \alpha\beta_0)T_{0,5}^n + 2T_{1,6}^n - 4T_{0,6}^n + (1 - \alpha\beta_0)T_{0,7}^n = \alpha\frac{\partial T_{0,6}^n}{\partial t}. \tag{3.42}$$

Since the term $T_{0,7}^n$ is outside the defined domain, we use the boundary condition to eliminate it. Substituting (3.37) with $i = 0$ into (3.42) we get

$$2T_{0,5}^n + 2T_{1,6}^n + (-4 - d + d\alpha\beta_0)T_{0,6}^n + (1 - \alpha\beta_0)f_w = \alpha\frac{\partial T_{0,6}^n}{\partial t}. \tag{3.43}$$

At the corner point $(5,1)$, we use Eq. (3.28) with $j = 1$, then we have

$$(1 + \alpha\beta_5)T_{5,0}^n + 2T_{4,1}^n - (m + \gamma_5 m + 4)T_{5,1}^n + (1 - \alpha\beta_5)T_{5,2}^n$$
$$+ (1 + \gamma_5)f_n = \alpha\frac{\partial T_{5,1}^n}{\partial t}. \tag{3.44}$$

Since the term $T_{5,0}^n$ is outside the range, we reduce it using Eq. (3.32) for $i = 5$. Then, we get

$$T_{5,0}^n = f_w - dT_{5,1}^n + T_{5,2}^n, \tag{3.45}$$

and then substituting (3.45) into (3.44), we have

$$2T_{4,1}^n + (-(1 + \alpha\beta_5)d + (-(1 + \gamma_5)m - 4))T_{5,1}^n + 2T_{5,2}^n + (1 + \gamma_5)f_n$$
$$+ (1 + \alpha\beta_5)f_w = \alpha\frac{\partial T_{5,1}^n}{\partial t}. \tag{3.46}$$

For the corner point $(5,6)$, we use Eq. (3.28) with $j = 6$, we have

$$(1 + \alpha\beta_5)T_{5,5}^n + 2T_{4,6}^n - (m + \gamma_5 m + 4)T_{5,6}^n + (1 - \alpha\beta_5)T_{5,7}^n + (1 + \gamma_5)f_n = \alpha\frac{\partial T_{5,6}^n}{\partial t}. \tag{3.47}$$

As the term $T_{5,7}^n$ is outside the range, we use Eq. (3.37) with $i = 5$ to eliminate it, and hence,

$$2T_{5,5}^n + 2T_{4,6}^n + (-(1 + \gamma_5)m - 4 - (1 - \alpha\beta_5)d)T_{5,6}^n + (1 + \gamma_5)f_n$$
$$+ (1 - \alpha\beta_5)f_w = \alpha\frac{\partial T_{5,6}^n}{\partial t}. \tag{3.48}$$

These equations can be assembled together to get a system of 36 equations as follows

$$
\begin{bmatrix}
B_0 & I_b & 0 & 0 & 0 & 0 \\
I+I_c & B_1 & I-I_c & 0 & 0 & 0 \\
0 & I+I_c & B_1 & I-I_c & 0 & 0 \\
0 & 0 & I+I_c & B_1 & I-I_c & 0 \\
0 & 0 & 0 & I+I_c & B_1 & I-I_c \\
0 & 0 & 0 & 0 & 2I & B_2
\end{bmatrix}
T = \alpha I \frac{\partial T}{\partial t} +
\begin{bmatrix}
F_0 \\ F_1 \\ F_1 \\ F_1 \\ F_1 \\ F_2
\end{bmatrix},
\qquad (3.49)
$$

where

$$
B_0 =
\begin{bmatrix}
-4-d-d\alpha\beta_0 & 2 & 0 & 0 & 0 & 0 \\
1-\gamma_1 & -4-d-d\alpha\beta_1 & 1+\gamma_1 & 0 & 0 & 0 \\
0 & 1-\gamma_2 & -4-d-d\alpha\beta_2 & 1+\gamma_2 & 0 & 0 \\
0 & 0 & 1-\gamma_3 & -4-d-d\alpha\beta_3 & 1+\gamma_3 & 0 \\
0 & 0 & 0 & 1-\gamma_4 & -4-d-d\alpha\beta_4 & 1+\gamma_4 \\
0 & 0 & 0 & 0 & 2 & -d-d\alpha\beta_5-(1+\gamma_5)m-4
\end{bmatrix},
$$

$$
B_1 =
\begin{bmatrix}
-4 & 2 & 0 & 0 & 0 & 0 \\
1-\gamma_1 & -4 & 1+\gamma_1 & 0 & 0 & 0 \\
0 & 1-\gamma_2 & -4 & 1+\gamma_2 & 0 & 0 \\
0 & 0 & 1-\gamma_3 & -4 & 1+\gamma_3 & 0 \\
0 & 0 & 0 & 1-\gamma_4 & -4 & 1+\gamma_4 \\
0 & 0 & 0 & 0 & 2 & -(1+\gamma_5)m-4
\end{bmatrix},
$$

$$
I_b = 2I, \quad I_c =
\begin{bmatrix}
\alpha\beta_0 & 0 & 0 & 0 & 0 & 0 \\
0 & \alpha\beta_1 & 0 & 0 & 0 & 0 \\
0 & 0 & \alpha\beta_2 & 0 & 0 & 0 \\
0 & 0 & 0 & \alpha\beta_3 & 0 & 0 \\
0 & 0 & 0 & 0 & \alpha\beta_4 & 0 \\
0 & 0 & 0 & 0 & 0 & \alpha\beta_5
\end{bmatrix},
$$

$$
B_2 =
\begin{bmatrix}
-4-d+d\alpha\beta_0 & 2 & 0 & 0 & 0 & 0 \\
1-\gamma_1 & -4-d+d\alpha\beta_1 & 1+\gamma_1 & 0 & 0 & 0 \\
0 & 1-\gamma_2 & -4-d+d\alpha\beta_2 & 1+\gamma_2 & 0 & 0 \\
0 & 0 & 1-\gamma_3 & -4-d+d\alpha\beta_3 & 1+\gamma_3 & 0 \\
0 & 0 & 0 & 1-\gamma_4 & -4-d+d\alpha\beta_4 & 1+\gamma_4 \\
0 & 0 & 0 & 0 & 2 & -d+d\alpha\beta_5-(1+\gamma_5)m-4
\end{bmatrix},
$$

$$
F_0 =
\begin{bmatrix}
-f_w-f_w\alpha\beta_0 \\
-(1+\alpha\beta_1)f_w \\
-(1+\alpha\beta_2)f_w \\
-(1+\alpha\beta_3)f_w \\
-(1+\alpha\beta_4)f_w \\
-(1+\gamma_5)f_n-(1+\alpha\beta_5)f_w
\end{bmatrix},
$$

$$F_1 = \begin{bmatrix} 0 \\ 0 \\ 0 \\ 0 \\ 0 \\ -(1+\gamma_5)f_n \end{bmatrix}, F_2 = \begin{bmatrix} -(1-\alpha\beta_0)f_w \\ -(1-\alpha\beta_1)f_w \\ -(1-\alpha\beta_2)f_w \\ -(1-\alpha\beta_3)f_w \\ -(1-\alpha\beta_4)f_w \\ (-(1+\gamma_5)f_n-(1-\alpha\beta_5)f_w) \end{bmatrix}.$$

The system (3.49) can be written as

$$MT - \alpha I \frac{\partial T}{\partial t} = F. \tag{3.50}$$

The Crank-Nicolson Scheme can then be used to find numerical solutions. For this purpose, let

$$\frac{\partial T}{\partial t}\left(t+\frac{\Delta t}{2}\right) = \frac{T(t+\Delta t)-T(t)}{\Delta t}, \tag{3.51}$$

$$T\left(t+\frac{\Delta t}{2}\right) = \frac{1}{2}[T(t)+T(t+\Delta t)]. \tag{3.52}$$

Then, by considering Eq. (3.50) at $t+\frac{\Delta t}{2}$, we get

$$M\left[\frac{1}{2}T(t)+\frac{1}{2}T(t+\Delta t)\right] = \alpha\left[\frac{T(t+\Delta t)-T(t)}{\Delta t}\right]+F, \tag{3.53}$$

which can be rewritten as

$$\left(I-\frac{\Delta t}{2\alpha}M\right)T^{n+1} = \left(I+\frac{\Delta t}{2\alpha}M\right)T^n-\frac{\Delta t}{\alpha}F. \tag{3.54}$$

To analyse the convergence of the numerical scheme for the system of differential equations, based on the work in [62], let $e(t)$ be the error in $T(t)$ due to a small change in T, then,

$$\left(I-\frac{\Delta t}{2\alpha}M\right)(T^{n+1}+e_{n+1}) = \left(I+\frac{\Delta t}{2\alpha}M\right)(T^n+e_n)-\frac{\Delta t}{\alpha}F,$$

and hence,

$$\left(I-\frac{\Delta t}{2\alpha}M\right)e_{n+1} = \left(I+\frac{\Delta t}{2\alpha}M\right)e_n, \tag{3.55}$$

that is,

$$e_{n+1} = R_-^{-1}R_+e_n, \tag{3.56}$$

46

where $R_- = I - \frac{\Delta t}{2\alpha}M$, $R_+ = I + \frac{\Delta t}{2\alpha}M$. Further, assume that M has N linearly independent eigenvectors ω_i, and λ_i be eigenvalues. Then, we can approximate the error at $t = 0$ as

$$e_0 = \sum_{i=1}^{N} \alpha_i \omega_i.$$

Further, through some calculations, we get

$$e_{n+1} = \sum_{i=1}^{N} \rho_i^{n+1} \alpha_i \omega_i,$$

where $\rho_i = \frac{1 + \frac{\Delta t}{2\alpha}\lambda_i}{1 - \frac{\Delta t}{2\alpha}\lambda_i}$. If the eigenvalues λ_i are all negative, $|\rho_i| \leq 1$, then, the error will not grow and the scheme is stable.

Based on the above time stepping scheme, the following algorithm is used for solving the problem numerically.

Numerical algorithm:

Input: $k, \rho, c_p, \mu, \alpha_1, k_1, f_1, \alpha_2, k_2, f_2, l, \omega, R, h, g, dt, N_t$ (Number of time steps)
Set $T(1) = T_0$
Set $t = 1$
while $(t < N_t)$ do
    Calculate $v_z(r,t)$
    Calculate α, β, γ
    Calculate $B_0, B_1, B_2, I_b, I_c, F_0, F_1, F_2$
    Construct M and F
    Solve $(I - \frac{\Delta t}{2\alpha}M)T(t+1) = (I + \frac{\Delta t}{2\alpha}M)T(t) - \frac{\Delta t}{\alpha}F$
    Set $t = t+1$, then go to the next cycle of the while loop
while.

3.4 Numerical investigations

In this section, the computation method established in section 3.3 is applied to study the transient temperature field in microchannels and investigate the influence of the slip parameter l and the convection heat transfer due to fluid flow in microchannels.

For the investigation, we choose the fluid axial velocity v_z as given by Eq. (29) in [21] for the case where a pressure field has a cosine wave form pressure gradient $\frac{dp}{dz} = a_0 + a_1 \cos(\omega t)$, namely

$$v_z = -\frac{a_0 R^2}{4\mu}[1-(\frac{r}{R})^2+\frac{2l}{R}]-Re[\frac{c_1 i}{\rho\omega}(\frac{J_0(\beta_1 r)}{J_0(\beta_1 R)-l\beta_1 J_1(\beta_1 R)}-1)e^{i\omega t}],$$

where l denotes the boundary slip parameter, J_0 is the zero-order Bessel function of the first kind.

For the input parameter values for the investigation, we choose the parameters in the boundary conditions as $\alpha_1 = \alpha_2 = k, k_1 = k_2 = h_\infty, f_1 = h_\infty T_{\infty 1}, f_2 = h_\infty T_{\infty 1}$ on $z = 0$ and $f_2 = h_\infty T_{\infty 2}$ on $z = L$. The values of $k, h_\infty, T_{\infty 1}, T_{\infty 2}$ together with the input values for all other parameters are given in Table 3.1.

From the governing partial differential equation, for $v_z = 0$, the heat transfer is by diffusion only. For $v_z \neq 0$, transfer of heat by convection will occur. Hence, to investigate the influence of convection heat transfer due to fluid flow on the temperature field, the value of a_0 in v_z is varied from 0 to -0.02. Figures 3.3-3.5 show the essential features of the temperature fields obtained respectively for $a_0 = 0, -0.01$ and -0.02. By comparing the corresponding figures for different a_0 values, it can be noted that the convection heat transfer affects the temperature field significantly. As a_0 and consequently the fluid axial velocity v_z increases, the temperature in the channel decreases significantly.

For the conventional no-slip boundary condition, $l = 0$. As slip occurs at microscale, $l > 0$, and the intensity of slip on boundary is measured by the l value

Table 3.1: Input parameters values

Parameters	Their values
R	0.005 m
h	0.001 m
g	0.001 m
k	$0.5918\ Wm^{-2}K^{-1}$
μ	$0.003\ kgm^{-1}s^{-1}$
ω	$1\ s^{-1}$
ρ	$1000\ kgm^{-3}$
c_p	$4000\ Jkg^{-1}K^{-1}$
$T_{\infty 1}$	$0°C$
$T_{\infty 2}$	$20°C$
T_0	$20°C$
h_∞	$3000\ Wm^{-2}K^{-1}$
l	0.005
a_0	$-0.01\ N/m^3$
a_1	$-0.01\ N/m^3$

which consequently affects the velocity v_z. Hence, to investigate the influence of boundary slip on the temperature field, the l value is varied from $l = 0$ for the no-slip case to $l = 0.005$ and 0.02, while all other parameter values remain unchanged. Figures 3.6-3.8 show the temperature fields obtained respectively by $l = 0, 0.005$ and 0.02. It can be noted from the figures, boundary slip has a significant effect on the temperature field in the channel. As l increases, the temperature decreases.

3.5 Concluding Remarks

In this chapter, a computation scheme has been developed based on the finite difference method to solve the heat transfer problem numerically. Numerical experiments show that the developed computational method can capture the essential features of the temperature field in microchannels and the influence of the system parameters. The numerical simulation results show that boundary slip
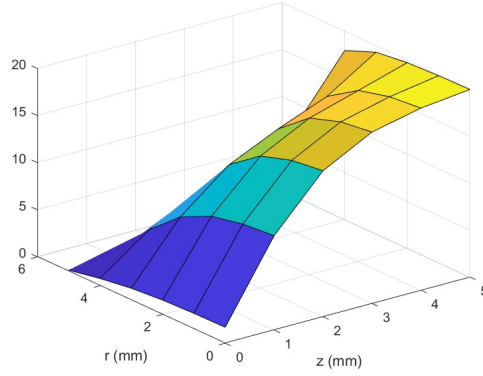
(a) Distribution of temperature in the channel at $t = T$
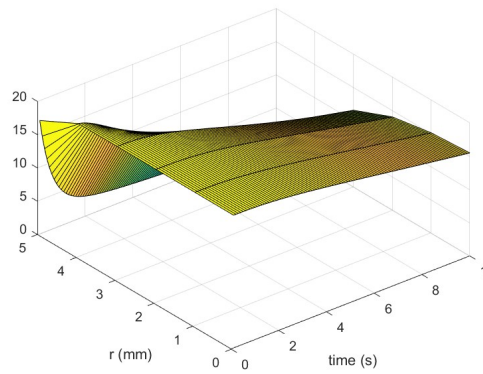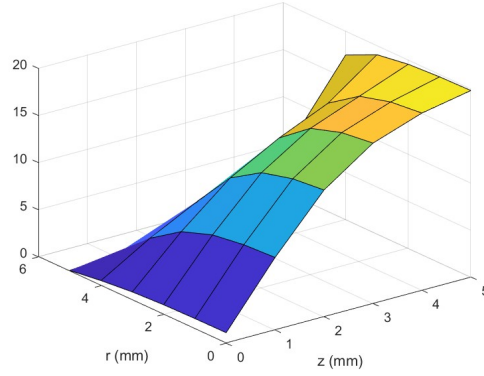

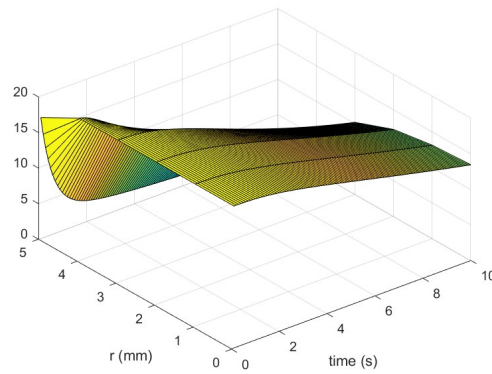(b) Evolution of Temperature at the cross-section $z = L/2$
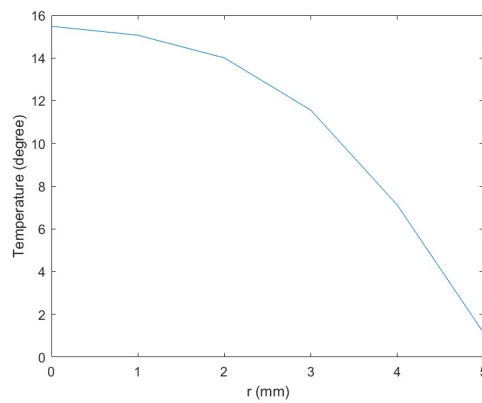
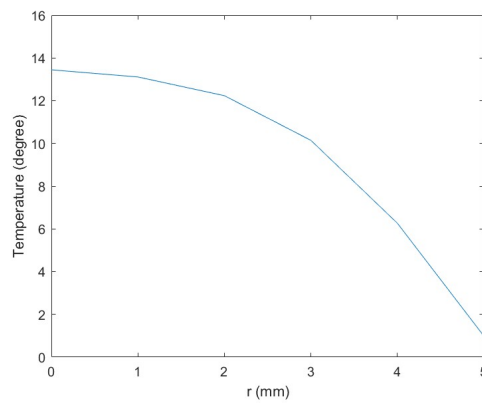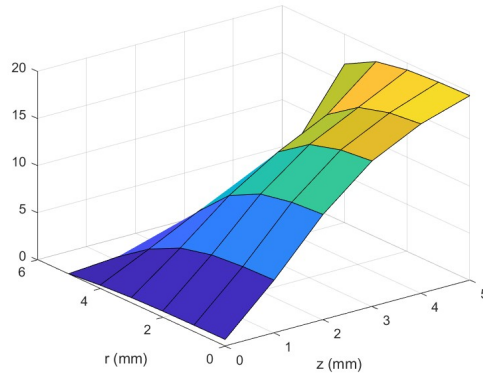(c) Distribution of temperature along r at $z = L/2, t = T$

Figure 3.3: Temperature field $T(r,z,t)$ in microchannel for $a_0 = 0$

(a) Distribution of temperature in the channel at $t = T$

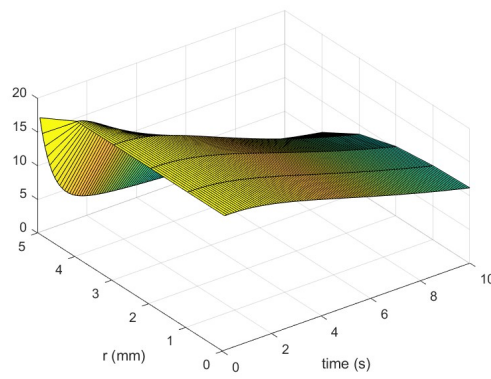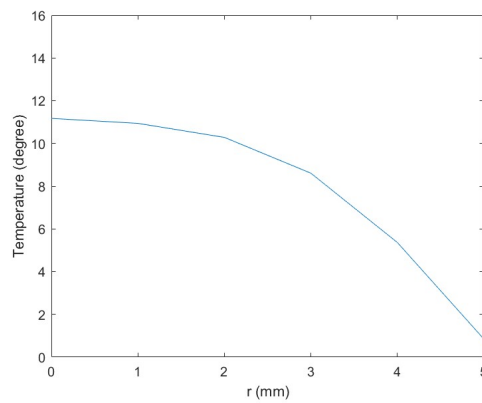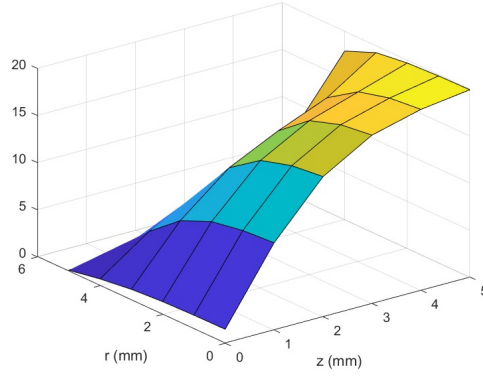(b) Evolution of temperature at the cross-section $z = L/2$

(c) Distribution of temperature along r at $z = L/2, t = T$

Figure 3.4: Temperature field $T(r,z,t)$ in microchannel for $a_0 = -0.01$

(a) Distribution of temperature in the channel at $t = T$

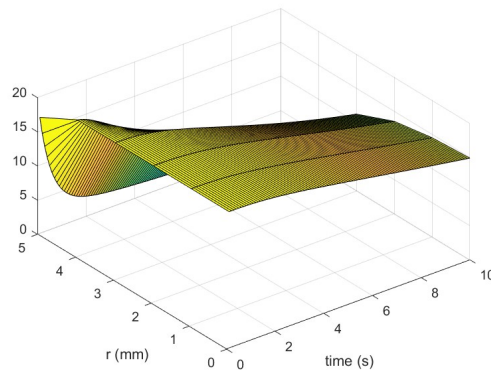(b) Evolution of temperature at the cross-section $z = L/2$

(c) Distribution of temperature along r at $z = L/2, t = T$

Figure 3.5: Temperature field $T(r,z,t)$ in microchannel for $a_0 = -0.02$

(a) Distribution of temperature in the channel at $t = T$

(b) Evolution of temperature at the cross-section $z = L/2$

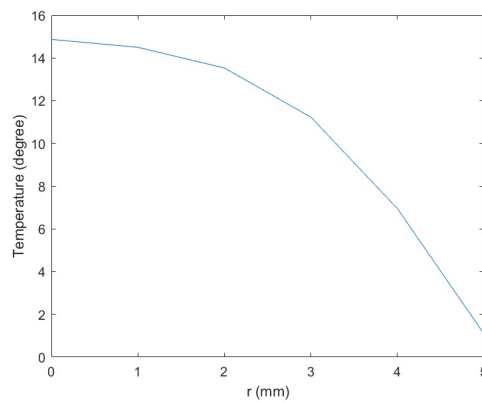(c) Distribution of temperature along r at $z = L/2, t = T$

Figure 3.6: Temperature field $T(r,z,t)$ in microchannel for $l = 0$

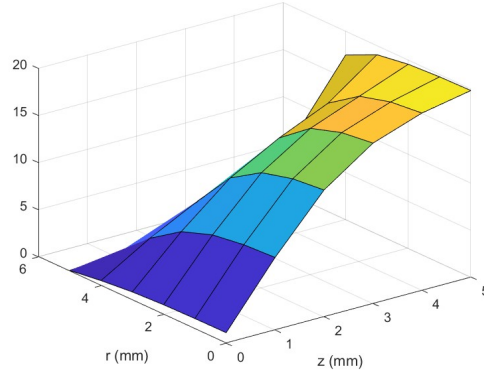(a) Distribution of temperature in the channel at $t = T$

(b) Evolution of temperature at the cross-section $z = L/2$

(c) Distribution of temperature along r at $z = L/2, t = T$

Figure 3.7: Temperature field $T(r,z,t)$ in microchannel for $l = 0.005$

(a) Distribution of temperature in the channel at $t = T$

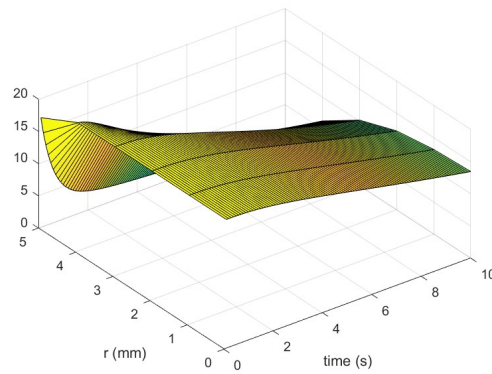(b) Evolution of temperature at the cross-section $z = L/2$

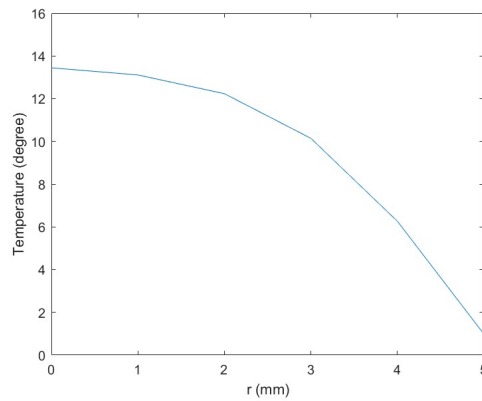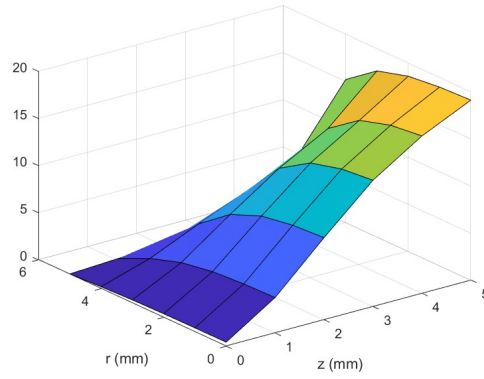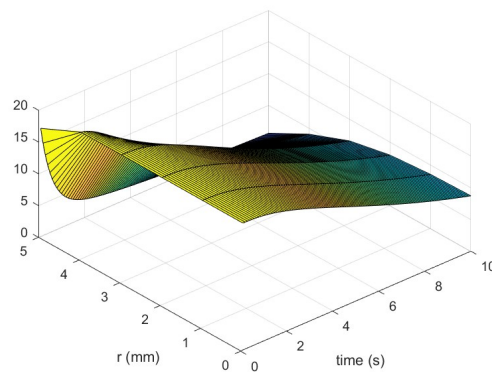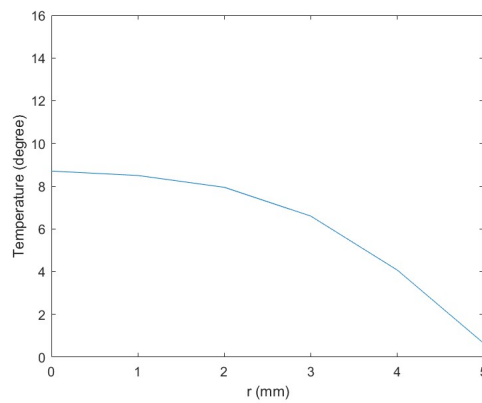(c) Distribution of temperature along r at $z = L/2, t = T$

Figure 3.8: Temperature field $T(r,z,t)$ in microchannel for $l = 0.02$

as well as convection heat transfer have significant effects on the temperature field.

Chapter 4

Velocity and temperature fields in mixed electroosmotic and pressure-driven flow of fluids in slip regime

4.1 General

The hydrodynamic characteristics of combined electroosmotic and pressure-driven flows have been studied for several micro-geometries [63–66]. A mixed flow occurs once a pressure-driven system and the electrokinetic mechanism are combined together to minimize the effect of the joule heating associated with electro-osmosis. The other way in which a mixed flow can be created is when a liquid can be carried through a micrometer channel by using a pressure gradient [67–70].

The thermal characteristics of electro-kinetic flow have been studied by Myness and Webb's research group [71–73]. They focused on exploring the features of the thermally fully developed electro-osmotic flow. Such a flow was considered at low [71] and high [73] zeta potentials. Their studies involve a mixed electro-osmotic and pressure-driven flow [74].

Electro-osmosis flows are employed in several applications due to its various advantages. For example, the operations become simpler once any moving parts of the mechanisms are loosed, for example, de-watering of waste sludges and removing of contaminants from soils [75]. An analytical solution was derived for Electro-osmosis flow in cylindrical annulus model in 2000 [75].

Research communities focused recently on micro-scale transport processes in the applications of biomedical and biotechnological [76]. The electro-osmotic flow in comparison to the conventional pressure-driven has many features. On the other hand, electro-osmotic flow mechanisms have side effects of Joule heating. The effects have been shown by research studies in low column separation efficiency, and reducing the resolution of research. In addition, the electro-osmotic flow may have certain benefits by using mechanical pressure pumping. Namely, mechanical pumping on its own may not be a chosen mechanism to drive the flow through micro applications. Mixed electro-osmotic and pressure-driven transport mechanisms are thus suggested by many researchers for pumping the flow of liquids via microchannels, in particular for biotechnological implementations.

Solutions for temperature distributions were obtained in the thermally developing systems of electro-osmotic flows Dutta [77]. However, only a few results have been obtained in solving the Graetz problem identified on an acceptable physical basis for electro-osmotic derived flow in microchannels. The Graetz problem concerns the laminar forced convective heat transfer in a circular channel that was initially solved by Graetz using analytical method [78]. It was under certain assumptions such as hydro-dynamically fully developed flow whereas both stream-wise heat conduction and viscous dissipation were neglected. The original Graetz problem was extended by Sellars et al [5]. They used effective techniques to solve the eigenvalues problem. The solution of the Graetz problem was also expanded to involve the effects of stream-wise conduction by Lahjomri et al. [79]. In the recent past, some researchers obtained analytical solutions of the Graetz problem for gas flows in microchannels, that is associated with wall-slip boundary conditions [2, 80].

Several recent technologies have an interest in utilising microfluidic transport to generate micropower, separate chemical processes and other biomedical mechanisms [71]. Since considerable pressures are demanded in pressure-driven flow, they are complicated to manufacture and maintain [81]. Elctroosmotic flow might produce an applicable alternative to pressure-driven liquid flow in microchannel. Electroosmosis has been first notified and observed by Reuss approximately two centuries ago [82]. The electroosmotic character of the flow results in a strong velocity profile function that affects the temperature distribution and resulting heat transfer. Joule heating in the fluid is established by the applied voltage gradient, and its electric conduction and volumetric energy then emerge therein.

The aim of this chapter is to study the velocity field and temperature field for mixed electroosmotic and pressure-driven flow in the slip regime. This study focuses on analytical solution for heat transfer equation and fluid flow by constructing the mathematical model under the Navier slip boundary condition. The rest of the chapter is organised as follows. A brief description of the problem, together with the mathematical model, is presented in section 4.2. Then based on previous work for the case with no-slip boundary conditions, analytical solutions for the case with slip boundary conditions are derived in section 4.3. Then numerical investigation of the temperature field under slip condition as well as the influence of the slip parameter are given in section 4.4, followed by a concluding remark in section 4.5.

4.2   Problem Description and Mathematical Model

The aim is to investigate the heat transfer in a mixed electroosmotic and pressure-driven flow of a Newtonian fluid through a circular microchannel. The diameter of this channel is denoted D. The length of the heating section is finite and is denoted by L. The geometry of the microchannel, together with the coordinates, the applied electric field and other details, are shown in Fig.4.1. Throughout this
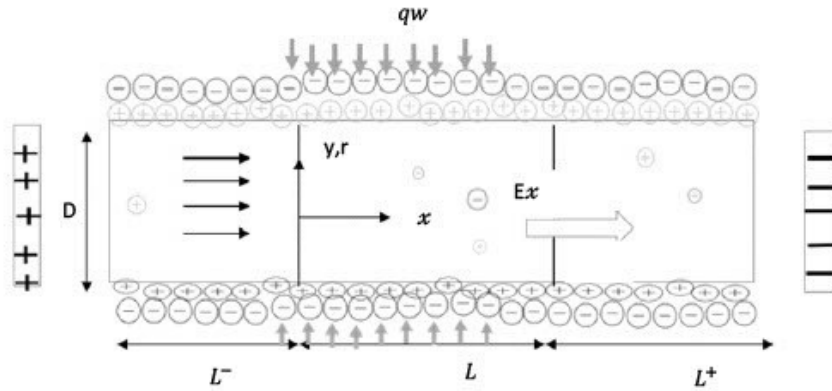
Figure 4.1: Schematic of the physical problem

investigation, the following assumptions are made as in [83]:

- The start point for the fluid to flow through the channel is $x = -L^-$. The velocity profile is fully developed with a uniform temperature of T_0.

- Fluid is assumed to be heated by Joule heat.

- The heating section has a length L starting at the point $x = 0$.

- The channel is insulated for $x \in [L, L+L_+]$.

- The net conductive heat flux at the exit is secured to be zero since L^+ is chosen to be sufficiently large.

- The characteristics of the thermo-physico-chemical are all constants.

- The employment of Debye-Hückel linearization is ensured since the zeta potential is sufficiently low.

- The Péclet number is low enough to assume that the transverse variations of the temperature are small.

The problem to be investigated involves both heat transfer and fluid flow driven by mixed pressure gradient and electroosmotic pumping mechanisms. From the principle of continuum mechanisms, the governing equations for the velocity field of the mixed electroosmotic and pressure-driven flow include the continuity equation and the Navier-Stokes equations, namely

$$\nabla \cdot v = 0, \tag{4.1}$$

$$\rho \left(\frac{\partial v}{\partial t} + (v \cdot \nabla)v \right) = -\nabla p + \mu \nabla^2 v + \rho_e E, \tag{4.2}$$

where v denotes the velocity vector, p is the pressure, μ and ρ are the viscosity and the density respectively, E denotes the externally applied electric field, ρ_e is the net electrical chase density, and in cylindrical polar coordinates

$$v = v_r e_r + v_\theta e_\theta + u e_x, \tag{4.3}$$

$$\nabla = e_r \frac{\partial}{\partial r} + e_\theta \frac{\partial}{r \partial r} + e_x \frac{\partial}{\partial x}. \tag{4.4}$$

For steady-state fully developed axially symmetric flows through micro-channels of circular cross-section, the velocity components in the transverse and radial directions vanish, that is

$$v_r = 0, \quad v_\theta = 0. \tag{4.5}$$

Hence, the continuity equation becomes

$$\frac{\partial u}{\partial x} = 0, \tag{4.6}$$

which requires $u = u(r, \theta)$, and further as the problem is axially symmetric, $u = u(r)$. Therefore, by substituting Eqs.(4.5),(4.6) into Eq.(4.2), the governing equation for $u(r)$ is as given in [84] as follows

$$\frac{1}{r} \frac{d}{dr} \left(\mu r \frac{du}{dr} \right) = \frac{dp}{dx} - \rho_e E_x. \tag{4.7}$$

By introducing the dimensionless parameters $\Gamma = u_{PD}/u_{HS}$ where $u_{HS} = -\varepsilon \zeta E_x/\mu$ is the Helmholtz-Smoluchowski velocity and $u_{PD} = -R^2(dp/dx)/4\mu$ represents

61

the pressure-driven velocity, the equation for the axial velocity is given in [83] in dimensionless form as follows

$$\frac{1}{r^*}\frac{d}{dr^*}(r^*\frac{du^*}{dr^*}) = -4\Gamma - K^2\frac{I_0(Kr^*)}{I_0(K)}. \tag{4.8}$$

In previous work, Eq. (4.8) is solved subject to no-slip boundary condition. However, as microslip has been found to occur at microscale, we propose to use the Navier slip boundary condition, namely at the solid-fluid interface with $r^* = 1$, we assume

$$u^*(1) + l\frac{du^*(1)}{dr^*} = 0. \tag{4.9}$$

Due to axial symmetry, we also have

$$\frac{\partial u^*}{\partial r^*}\Big|_{r^*=0} = 0. \tag{4.10}$$

The heat transfer process is governed by the standard convection-diffusion equation with a source term due to the externally applied electric field. By using dimensionless variables, the heat transfer equation is given in [83] in dimensionless form as follows

$$\frac{Pe\alpha}{4}u^*\frac{\partial\theta}{\partial x^*} = \frac{1}{r^*}\frac{\partial}{\partial r^*}(r^*\frac{\partial\theta}{\partial r^*}) + \frac{\alpha^2}{4}\frac{\partial^2\theta}{\partial x^{*2}} + S, \tag{4.11}$$

subject to boundary conditions

$$\theta\Big|_{x^*=-\beta} = 0, \quad \frac{\partial\theta}{\partial x^*}\Big|_{x^*=1+\beta^+} = \frac{4S}{Pe\alpha u_m^*}, \quad \frac{\partial\theta}{\partial r^*}\Big|_{r^*=0} = 0,$$

$$\frac{\partial\theta}{\partial r^*}\Big|_{r^*=1} = \mathcal{Q}_w(x^*) = \begin{cases} q_w(x^*) & \text{for} \quad 0 \le x^* \le 1 \\ 0 & \text{otherwise} \end{cases} \tag{4.12}$$

where $q_{av} = \frac{1}{L}\int_0^L q_w(x)dx$ denotes the average wall heat flux, $Pe = \frac{u_{HS}D}{k/\rho c_p}$ is the Péclet number, $S = \frac{RE_x^2}{q_{av}\sigma_0}$ demonstrates the heat sources, and $\alpha = \frac{D}{L}$ represents the channel diameter-to-length ratio. $\beta^- = L^-/L, \beta^+ = L^+/L$, and $q_w(x^*) = q_w(x^*)/q_{av}$. In previous work, the heat transfer problem has been solved for the no-slip case. In this work, we will focus on solving and investigating the problem for the slip case.

62

4.3 Derivation of Analytical solutions

Firstly, we solve the velocity equation subject to the slip boundary condition to obtain the velocity $u^*(r)$. To solve Eq.(4.12), we first solve the homogeneous equation

$$\frac{1}{r^*}\frac{d}{dr^*}(r^*\frac{du^*}{dr^*}) = 0,$$ (4.13)

and get

$$u_c^* = A\ln r^* + B,$$ (4.14)

where A, B are arbitrary constants. From Eq.(4.8) the particular solution has the form

$$u_p^* = \Gamma(1-r^{*2}) - \frac{I_0(Kr^*)}{I_0(K)}.$$ (4.15)

Thus, the general solution is

$$u^* = A\ln r^* + B + \Gamma(1-r^{*2}) - \frac{I_0(Kr^*)}{I_0(K)}.$$ (4.16)

The coefficients A and B can be determined by using the symmetrical condition and the slip boundary condition. Now from Eq. (4.12), we get

$$\frac{du^*}{dr^*} = A\frac{1}{r^*} - 2r^*\Gamma - \frac{d}{dr^*}[\frac{I_0(Kr^*)}{I_0(K)}],$$

$$= A\frac{1}{r^*} - 2r^*\Gamma - \frac{K}{I_0(K)}I_1(Kr^*).$$ (4.17)

From (4.10), we get

$$A\frac{1}{r^*} - 2r^*\Gamma - \frac{K}{I_0(K)}I_1(0) = 0,$$ (4.18)

which gives $A = 0$ since the modified Bessel function of order 1 at the origin is zero. Now from Eq.(4.9) we have

$$B = l[2\Gamma + \frac{K}{I_0(K)}I_1(K)] + 1.$$ (4.19)

Then, the exact solution is

$$u^* = 1 + l[2\Gamma + \frac{K}{I_0(K)}I_1(K)] + \Gamma(1-r^{*2}) - \frac{I_0(Kr^*)}{I_0(K)}.$$ (4.20)

Further, the dimensionless mean velocity is given by

$$u_m^* = 2\int_0^1 u^* r^* dr^* = 1 + l[2\Gamma + \frac{K}{I_0(K)}I_1(K)] + \frac{\Gamma}{2} - \frac{2I_1(K)}{KI_0(K)}.$$ (4.21)

Remark 4.3.1 *In comparison with the solution in [83], the solution (4.20) derived in this work has two additional terms, that is the second or third terms above. The solution u_m^* in Eq.(4.21) also has two additional terms, the second and the third terms, in comparison with the corresponding solutions for the no-slip case.*

Now we consider solving the heat transfer equation (4.11) subject to the boundary condition (4.12). As the diameter of the channel is very small, it results in a low Péclet number flow, and hence a small variation should occur on the temperature over the radial coordinate [85]. To take advantage of these flow thermal properties, as in [83], θ is divided into two parts

$$\theta(x^*, r^*) = \theta_b(x^*) + \phi(x^*, r^*), \tag{4.22}$$

where $\theta_b(x^*) = \frac{2}{u_m^*} \int_0^1 \theta(x^*, r^*) u^* r^* dr^*$ represents the dimensionless bulk temperature, while $\phi(x^*, r^*)$ is subject to

$$\int_0^1 \phi(x^*, r^*) u^* r^* dr^* = 0. \tag{4.23}$$

Further, by assuming that $\frac{\partial \phi}{\partial x^*} \ll \frac{d\theta_b}{dx^*}$ and $\frac{\partial^2 \phi}{\partial x^{*2}} \ll \frac{d^2 \theta_b}{dx^{*2}}$, it has been shown in [83] that θ_b and ϕ satisfy the following equation

$$\frac{Pe\alpha}{4} u^* \left(\frac{d\theta_b}{dx^*} \right) = \frac{1}{r^*} \frac{\partial}{\partial r^*} \left(r^* \frac{\partial \phi}{\partial r^*} \right) + \frac{\alpha^2}{4} \frac{d^2 \theta_b}{dx^{*2}} + S, \tag{4.24}$$

subject to

$$\theta \Big|_{x^* = -\beta^-} = 0, \quad \frac{d\theta_b}{dx^*} \Big|_{x^* = 1 + \beta^+} = \frac{4S}{Pe\alpha u_m^*}$$

$$\frac{\partial \phi}{\partial r^*} \Big|_{r^* = 0} = 0, \quad \frac{\partial \phi}{\partial r^*} \Big|_{r^* = 1} = \mathcal{Q}_w(x^*). \tag{4.25}$$

The solution of the problem for the no-slip case has been derived in [83]. Here the focus is on the slip case. Through some computation, it is found that θ_b for the slip case can be expressed in the same form as that for the no-slip case except for some differences detailed in the remark below, namely

$$\theta_b = \frac{8}{Peu_m^* \alpha} \left[Int_{\mathcal{Q}_w} + f(x^*) - f(-\beta^-) + \frac{S}{2}(x^* + \beta^-) \right], \qquad (4.26)$$

where

$$f(x^*) = e^{\frac{u_m^* Pe}{\alpha} x^*} \int_{x^*}^1 \mathcal{Q}_w(x^{**}) e^{-\frac{u_m^* Pe}{\alpha} x^{**}} dx^{**},$$

$$Int_{\mathcal{Q}_w} = \int_0^{x^*} \mathcal{Q}_w(x^{**}) dx^{**}.$$

Remark 4.3.2 *The solution of θ_b in Eq.(4.26) has the same form as that for the no-slip case. However, the u_m^* in the above formula has two additional terms due to boundary slip as mentioned in Remark 4.3.1. The function $f(x^*)$, which involves u_m^*, is thus also different to that for the no-slip case.*

Now we focus on finding the solution of ϕ. From Eq.(4.26), one get

$$\frac{d\theta_b}{dx^*} = \frac{8}{\alpha^2} e^{\frac{Peu_m^*}{\alpha} x^*} \int_{x^*}^1 \mathcal{Q}_w e^{-\frac{Peu_m^*}{\alpha} x^*} dx^* + \frac{4S}{Peu_m^* \alpha}, \qquad (4.27)$$

$$\frac{d\theta_b^2}{dx^{*2}} = \frac{8}{\alpha^2} \frac{Peu_m^*}{\alpha} e^{\frac{Peu_m^*}{\alpha} x^*} \int_{x^*}^1 \mathcal{Q}_w e^{-\frac{Peu_m^*}{\alpha} x^*} dx^* - \frac{8}{\alpha^2} \mathcal{Q}_w. \qquad (4.28)$$

Substituting the above into Eq. (4.24), we get

$$\frac{2Peu^*}{\alpha} f(x^*) + \frac{Su^*}{u_m^*} = \frac{1}{r^*} \frac{\partial}{\partial r^*} (r^* \frac{\partial \phi}{\partial r^*}) + 2 \frac{Peu_m^*}{\alpha} f(x^*) - 2\mathcal{Q}_w + S. \qquad (4.29)$$

Substituting for u^* from (4.20) into (4.29), we have

$$\frac{1}{r^*} \frac{\partial}{\partial r^*} (r^* \frac{\partial \phi}{\partial r^*}) = \left[\frac{2Pe}{\alpha} f(x^*) + \frac{S}{u_m^*} \right] \left[1 + l[2\Gamma + \frac{K}{I_0(K)} I_1(K)] + \Gamma(1 - r^{*2}) - \frac{I_0(Kr^*)}{I_0(K)} \right]$$
$$- \frac{2u_m^*}{\alpha} Pe f(x^*) + 2\mathcal{Q}_w - S. \qquad (4.30)$$

By integrating with respect to r^*, we have

$$r^* \frac{\partial \phi}{\partial r^*} = \int r^* \left[\frac{2Pe}{\alpha} f(x^*) + \frac{S}{u_m^*} \right] \left[1 + l[2\Gamma + \frac{K}{I_0(K)} I_1(K)] + \Gamma(1 - r^{*2}) - \frac{I_0(Kr^*)}{I_0(K)} \right] dr^*$$

$$- \int \frac{2u_m^*}{\alpha} Pe f(x^*) r^* dr^* + \int 2\mathcal{Q}_w r^* dr^* - \int Sr^* dr^* + C_3$$

$$= \frac{r^{*2}}{2} \left[\frac{2Pe}{\alpha} f(x^*) + \frac{S}{u_m^*} \right] \left[1 + l[2\Gamma + \frac{K}{I_0(K)} I_1(K)] \right] + (\frac{2Pe}{\alpha} f(x^*) + \frac{S}{u_m^*}) \left[\frac{r^{*2}}{2} \Gamma - \frac{r^{*4}}{4} \Gamma \right]$$

$$- \frac{1}{I_0(K)} (\frac{2Pe}{\alpha} f(x^*) + \frac{S}{u_m^*}) \left[\frac{1}{K} r^* I_1(Kr^*) \right] - \frac{Peu_m^*}{\alpha} f(x^*) r^{*2} + \mathcal{Q}_w r^{*2} - \frac{S}{2} r^{*2} + C_3,$$

$$\frac{\partial \phi}{\partial r^*} = \frac{r^*}{2} \left[\frac{2Pe}{\alpha} f(x^*) + \frac{S}{u_m^*} \right] \left[1 + l[2\Gamma + \frac{K}{I_0(K)} I_1(K)] \right] + (\frac{2Pe}{\alpha} f(x^*) + \frac{S}{u_m^*}) \left[\frac{r^*}{2} \Gamma - \frac{r^{*3}}{4} \Gamma \right]$$

$$- \frac{1}{I_0(K)} (\frac{2Pe}{\alpha} f(x^*) + \frac{S}{u_m^*}) \left[\frac{1}{K} I_1(Kr^*) \right] - \frac{Peu_m^*}{\alpha} f(x^*) r^* + \mathcal{Q}_w r^* - \frac{S}{2} r^* + \frac{C_3}{r^*},$$

$$\phi = \frac{r^{*2}}{4} \left[\frac{2Pe}{\alpha} f(x^*) + \frac{S}{u_m^*} \right] \left[1 + l[2\Gamma + \frac{K}{I_0(K)} I_1(K)] \right] + (\frac{2Pe}{\alpha} f(x^*) + \frac{S}{u_m^*}) \left[\frac{r^{*2}}{4} \Gamma - \frac{r^{*4}}{16} \Gamma \right]$$

$$- \frac{1}{K^2 I_0(K)} (\frac{2Pe}{\alpha} f(x^*) + \frac{S}{u_m^*}) \left[I_0(Kr^*) \right] - \frac{Peu_m^*}{2\alpha} f(x^*) r^{*2} + \frac{1}{2} \mathcal{Q}_w r^{*2} - \frac{S}{4} r^{*2} + C_3 \ln r^* + C_4.$$

Rearranging, we have

$$\phi = \left[\frac{2Pe}{\alpha} f(x^*) + \frac{S}{u_m^*} \right] \left[\frac{r^{*2}}{4} + l \frac{r^{*2}}{4} [2\Gamma + \frac{K}{I_0(K)} I_1(K)] + \frac{r^{*2}}{4} \Gamma - \frac{r^{*4}}{16} \Gamma - \frac{I_0(Kr^*)}{K^2 I_0(K)} \right]$$

$$\text{(4.31)}$$

$$+ \frac{r^{*2}}{4} \left[2\mathcal{Q}_w(x^*) - 2\frac{Peu_m^*}{\alpha} f(x^*) - S \right] + C_3 \ln r^* + C_4,$$

which can be rewritten in the following form

$$\phi = a \cdot A(r^*) + \frac{r^{*2}}{4} \cdot d + C_3 \ln r^* + C_4, \tag{4.32}$$

where

$$A(r^*) = \frac{r^{*2}}{4} + l \frac{r^{*2}}{4} b + \frac{r^{*2}}{4} \Gamma - \frac{r^{*4}}{16} \Gamma - \frac{I_0(Kr^*)}{K^2 I_0(K)},$$

$$a = \left[\frac{2Pe}{\alpha} f(x^*) + \frac{S}{u_m^*} \right],$$

$$b = [2\Gamma + \frac{K}{I_0(K)} I_1(K)],$$

$$d = \left[2\mathcal{Q}_w(x^*) - 2\frac{Peu_m^*}{\alpha}f(x^*) - S\right].$$

Now we use the condition (4.23) to calculate the integration constants

$$\int_0^1 \left\{a\left[\frac{r^{*2}}{4} + l\frac{r^{*2}}{4}b + \frac{r^{*2}}{4}\Gamma - \frac{r^{*4}}{16}\Gamma - \frac{I_0(Kr^*)}{K^2 I_0(K)}\right] + \frac{r^{*2}}{4}d + C_3\ln r^* + C_4\right\}$$
$$\left\{1 + lb + \Gamma(1 - r^{*2}) - \frac{I_0(Kr^*)}{I_0(K)}\right\}r^* dr^* = 0. \tag{4.33}$$

We need to choose $C_3 = 0$ as $\ln r^*$ tends to $-\infty$ as $r^* \to 0$, to get a reasonable solution. Then,

$$\int_0^1 \left\{a\left[\frac{r^{*2}}{4} + l\frac{r^{*2}}{4}b + \frac{r^{*2}}{4}\Gamma - \frac{r^{*4}}{16}\Gamma - \frac{I_0(Kr^*)}{K^2 I_0(K)}\right] + \frac{r^{*2}}{4}d + C_4\right\}$$
$$\left\{1 + lb + \Gamma(1 - r^{*2}) - \frac{I_0(Kr^*)}{I_0(K)}\right\}r^* dr^* = 0, \tag{4.34}$$

which gives

$$\int_0^1 a\left[\frac{r^{*3}}{4} + l\frac{r^{*3}}{4}b + \frac{r^{*3}}{4}\Gamma - \frac{r^{*5}}{16}\Gamma - \frac{r^* I_0(Kr^*)}{K^2 I_0(K)}\right] dr^*$$
$$+ \int_0^1 bal\left[\frac{r^{*3}}{4} + l\frac{r^{*3}}{4}b + \frac{r^{*3}}{4}\Gamma - \frac{r^{*5}}{16}\Gamma - \frac{r^* I_0(Kr^*)}{K^2 I_0(K)}\right] dr^* +$$
$$\int_0^1 a\Gamma(1 - r^{*2})\left[\frac{r^{*3}}{4} + l\frac{r^{*3}}{4}b + \frac{r^{*3}}{4}\Gamma - \frac{r^{*5}}{16}\Gamma - \frac{r^* I_0(Kr^*)}{K^2 I_0(K)}\right] dr^* -$$
$$\frac{a}{I_0(K)}\left\{\int_0^1\left(I_0(Kr^*)\frac{r^{*3}}{4} + lb\frac{r^{*3}}{4}I_0(Kr^*) + \frac{r^{*3}}{4}\Gamma I_0(Kr^*) - \right.\right.$$
$$\frac{r^{*5}}{16}\Gamma I_0(Kr^*) - r^*\frac{I_0^2(Kr^*)}{K^2 I_0(K)}\bigg) dr^*\bigg\} + \int_0^1\left(\frac{r^{*3}}{4}d + \frac{r^{*3}}{4}dlb + \frac{r^{*3}}{4}d\Gamma(1 - r^{*2}) - \right.$$
$$\frac{r^{*3}}{4}d\frac{I_0(Kr^*)}{I_0(K)}\bigg) dr^* + C_4\int_0^1\left(r^* + lbr^* + r^*\Gamma(1 - r^{*2}) - \frac{r^* I_0(Kr^*)}{I_0(K)}\right) dr^* = 0. \tag{4.35}$$

67

Consequently,

$$a\left[\frac{r^{*4}}{16}+lb\frac{r^{*4}}{16}+\Gamma\frac{r^{*4}}{16}-\frac{r^{*6}}{96}\Gamma-\frac{1}{K^2 I_0(K)}\int_0^1 r^* I_0(Kr^*)dr^*\right]$$

$$+bal\left[\frac{r^{*4}}{16}+lb\frac{r^{*4}}{16}+\frac{r^{*4}}{16}\Gamma-\frac{r^{*6}}{96}\Gamma-\frac{1}{K^2 I_0(K)}\int_0^1 r^* I_0(Kr^*)dr^*\right]$$

$$+a\int_0^1\left\{\frac{r^{*3}}{4}\Gamma-\frac{r^{*5}}{4}\Gamma+lb\left[\frac{r^{*3}}{4}\Gamma-\frac{r^{*5}}{4}\Gamma\right]+\frac{r^{*3}}{4}\Gamma^2-\frac{r^{*5}}{4}\Gamma^2\right.$$

$$\left.-\frac{r^{*5}}{16}\Gamma^2+\frac{r^{*7}}{16}\Gamma^2-\frac{\Gamma}{K^2 I_0(K)}(r^* I_0(Kr^*)-r^{*3}I_0(Kr^*))\right\}dr^*$$

$$-\frac{a}{I_0(K)}\left\{\int_0^1\frac{r^{*3}}{4}I_0(Kr^*)dr^*+\int_0^1\frac{lb}{4}r^{*3}I_0(Kr^*)dr^*+\int_0^1\frac{\Gamma}{4}r^{*3}I_0(Kr^*)dr^*\right.$$

$$\left.-\int_0^1\frac{\Gamma}{16}r^{*5}I_0(Kr^*)dr^*-\int_0^1\frac{1}{K^2 I_0(K)}r^* I_0^2(Kr^*)dr^*\right\}$$

$$+\int_0^1\left(\frac{r^{*3}}{4}d+dlb\frac{r^{*3}}{4}+d\Gamma(\frac{r^{*3}}{4}-\frac{r^{*5}}{4})-\frac{d}{4I_0(K)}r^{*3}I_0(Kr^*)\right)dr^*$$

$$+C_4\int_0^1\left(r^*+lbr^*+\Gamma(r^*-r^{*3})-\frac{1}{I_0(K)}r^* I_0(Kr^*)\right)dr^*=0,$$

and

$$(a+bal)\left[\frac{r^{*4}}{16}+lb\frac{r^{*4}}{16}+\Gamma\frac{r^{*4}}{16}-\frac{r^{*6}}{96}\Gamma-\frac{1}{K^3 I_0(K)}r^* I_1(Kr^*)\right]_0^1+$$

$$a\left[\frac{r^{*4}}{16}\Gamma-\frac{r^{*6}}{24}\Gamma+lb\Gamma\frac{r^{*4}}{16}-lb\Gamma\frac{r^{*6}}{24}+\frac{r^{*4}}{16}\Gamma^2-\frac{r^{*6}}{24}\Gamma^2-\frac{r^{*6}}{96}\Gamma^2+\right.$$

$$\left.\frac{r^{*8}}{128}\Gamma^2-\frac{\Gamma}{K^3 I_0(K)}r^* I_1(Kr^*)+\frac{\Gamma}{K^2 I_0(K)}\int_0^1 r^{*3}I_0(Kr^*)dr^*\right]$$

$$-\frac{a}{I_0(K)}\left\{\int_0^1 r^{*3}I_0(Kr^*)dr^*\left(\frac{1}{4}+\frac{lb}{4}+\frac{\Gamma}{4}\right)-\int_0^1\frac{\Gamma}{16}r^{*5}I_0(Kr^*)dr^*-\right.$$

$$\left.\int_0^1\frac{1}{K^2 I_0(K)}r^* I_0^2(Kr^*)dr^*\right\}+\frac{r^{*4}}{16}d+dlb\frac{r^{*4}}{16}+d\Gamma\frac{r^{*4}}{16}-\frac{r^{*6}}{24}d\Gamma$$

$$-\frac{d}{4I_0(K)}\int_0^1 r^{*3}I_0(Kr^*)dr^*+C_4\left[\frac{r^{*2}}{2}+lb\frac{r^{*2}}{2}+\Gamma\frac{r^{*2}}{2}-\Gamma\frac{r^{*4}}{4}-\frac{1}{I_0(K)}\frac{1}{K}r^* I_1(Kr^*)\right]=0.$$

(4.36)

The above formula involves the integrals of $r^{*3}I_0(Kr^*), r^{*5}I_0(Kr^*)$ and $r^* I_0^2(Kr^*)$.

68

We first evaluate these integrals below.

$$(i) \quad \int r^{*3} I_0(Kr^*) dr^* = \int r^{*2} r^* I_0(Kr^*) dr^*$$

$$= r^{*2} \frac{1}{K} r^* I_1(Kr^*) - \int \frac{1}{K} r^* I_1(Kr^*) 2r^* dr^*$$

$$= r^{*3} \frac{1}{K} I_1(Kr^*) - \frac{2}{K} \int r^{*2} I_1(Kr^*) dr^*$$

$$= r^{*3} \frac{1}{K} I_1(Kr^*) - \frac{2}{K} \frac{1}{K} r^{*2} I_2(Kr^*)$$

$$= r^{*3} \frac{1}{K} I_1(Kr^*) + \frac{2r^*}{K^3} \Big(2I_1(Kr^*) - Kr^* I_0(Kr^*) \Big),$$

where we have used the following Modified Bessel function properties in the above formulation,

$$\int r^{*2} I_1(Kr^*) dr^* = \frac{1}{K} r^{*2} I_2(Kr^*),$$

$$Kr^* I_2(Kr^*) = -2I_1(Kr^*) + Kr^* I_0(Kr^*),$$

(ii) $\displaystyle\int r^{*5}I_0(Kr^*)dr^*$

$\displaystyle = \int r^{*4}r^*I_0(Kr^*)dr^*$

$\displaystyle = r^{*4}\frac{1}{K}r^*I_1(Kr^*) - \int \frac{1}{K}r^*I_1(Kr^*)4r^{*3}dr^*$

$\displaystyle = \frac{r^{*5}}{K}I_1(Kr^*) - \frac{4}{K}\int r^{*4}I_1(Kr^*)dr^*,$

where $\displaystyle\int r^{*4}I_1(Kr^*)dr^*$

$\displaystyle = \int r^{*2}r^{*2}I_1(Kr^*)dr^*$

$\displaystyle = r^{*2}\frac{1}{K^3}K^2r^{*2}I_2(Kr^*) - \int \frac{1}{K}r^{*2}I_2(Kr^*)2r^*dr^*$

$\displaystyle = \frac{1}{K}r^{*4}I_2(Kr^*) - \frac{2}{K}\int r^{*3}I_2(Kr^*)dr^*$

$\displaystyle = \frac{1}{K}r^{*4}I_2(Kr^*) - \frac{2}{K}\frac{1}{K}r^{*3}I_3(Kr^*)$

$\displaystyle = \frac{1}{K}r^{*4}I_2(Kr^*) - \frac{2}{K^2}r^{*3}I_3(Kr^*)$

$\displaystyle = \frac{1}{K^2}r^{*3}Kr^*I_2(Kr^*) - \frac{2}{K^3}r^{*2}Kr^*I_3(Kr^*)$

$\displaystyle = -\frac{1}{K^2}r^{*3}\left(2I_1(Kr^*) - Kr^*I_0(Kr^*)\right) + \frac{2}{K^3}r^{*2}\left(4I_2(Kr^*) - Kr^*I_1(Kr^*)\right)$

$\displaystyle = -\frac{2}{K^2}r^{*3}I_1(Kr^*) + \frac{1}{K}r^{*4}I_0(Kr^*) + \frac{8}{K^3}r^{*2}I_2(Kr^*) - \frac{2}{K^2}r^{*3}I_1(Kr^*)$

$\displaystyle = -\frac{4}{K^2}r^{*3}I_1(Kr^*) + \frac{1}{K}r^{*4}I_0(Kr^*) - \frac{8}{K^4}r^*\left(2I_1(Kr^*) - Kr^*I_0(Kr^*)\right).$

(iii) $\int r^*I_0^2(Kr^*)dr^*$. To evaluate this integral, we use the following integral relation

$$\int_0^a r^*I_n^2(Kr^*)dr^* = \frac{a^2}{2}\left[-\{I_n'(Ka)\}^2 + \left(1 + \frac{n^2}{K^2a^2}\right)\{I_n(Ka)\}^2\right].$$

That is,

$$\int_0^1 r^*I_0^2(Kr^*)dr^* = \frac{1}{2}[I_0^2(K)] - \frac{1}{2}[I_0'^2(K)].$$

70

By using the properties of Modified Bessel functions, we have

$$\int_0^1 r^* I_0^2(Kr^*)dr^* = \frac{1}{2}[I_0^2(K)] - \frac{1}{2}[I_1^2(K)].$$

Substituting the results of the above integrals into (4.36) yields

$$(a+bal)\left[\frac{r^{*4}}{16}+lb\frac{r^{*4}}{16}+\frac{r^{*4}}{16}\Gamma-\frac{r^{*6}}{96}\Gamma-\frac{1}{K^3 I_0(K)}r^* I_1(Kr^*)\right]_0^1$$

$$+a\left[\frac{r^{*4}}{16}\Gamma-\frac{r^{*6}}{24}\Gamma+\frac{r^{*4}}{16}lb\Gamma-\frac{r^{*6}}{24}lb\Gamma+\frac{r^{*4}}{16}\Gamma^2-\frac{r^{*6}}{24}\Gamma^2-\frac{r^{*6}}{96}\Gamma^2+\frac{r^{*8}}{128}\Gamma^2\right.$$

$$\left.-\frac{\Gamma}{K^3 I_0(K)}r^* I_1(Kr^*)+\frac{\Gamma}{K^2 I_0(K)}\left[\left(r^{*3}\frac{1}{K}I_1(Kr^*)+\frac{4}{K^3}r^* I_1(Kr^*)-\frac{2}{K^2}r^{*2}I_0(Kr^*)\right)\right]\right]_0^1$$

$$-\frac{a}{I_0(K)}\left\{\left(\frac{1}{4}+\frac{lb}{4}+\frac{\Gamma}{4}\right)\left[r^{*3}\frac{1}{K}I_1(Kr^*)+\frac{4}{K^3}r^* I_1(Kr^*)-\frac{2}{K^2}r^{*2}I_0(Kr^*)\right]_0^1\right.$$

$$-\Gamma\left[\frac{r^{*5}}{16K}I_1(Kr^*)+\frac{1}{K^3}r^{*3}I_1(Kr^*)-\frac{1}{4K^2}r^{*4}I_0(Kr^*)+\frac{4}{K^5}r^* I_1(Kr^*)-\frac{2}{K^4}r^{*2}I_0(Kr^*)\right]_0^1$$

$$\left.-\frac{1}{K^2 I_0(K)}\left(\frac{1}{2}I_0^2(K)-\frac{1}{2}I_1^2(K)\right)\right\}+\left[\frac{r^{*4}}{16}d+\frac{r^{*4}}{16}dlb+\frac{r^{*4}}{16}d\Gamma-\frac{r^{*6}}{24}d\Gamma\right.$$

$$-\frac{d}{4I_0(K)}\left(r^{*3}\frac{1}{K}I_1(Kr^*)+\frac{4}{K^3}r^* I_1(Kr^*)-\frac{2}{K^2}r^{*2}I_0(Kr^*)\right)$$

$$+C_4\left[\frac{r^{*2}}{2}+\frac{r^{*2}}{2}lb+\frac{r^{*2}}{2}\Gamma-\frac{r^{*4}}{4}\Gamma-\frac{1}{I_0(K)}\frac{1}{K}r^* I_1(Kr^*)\right]_0^1=0.$$

Now we substitute the limits of integration to yield

$$(a+bal)\left[\frac{1}{16}+\frac{1}{16}lb+\frac{1}{16}\Gamma-\frac{1}{96}\Gamma-\frac{1}{K^3 I_0(K)}I_1(K)\right]$$

$$+a\left[\frac{1}{16}\Gamma-\frac{1}{24}\Gamma+\frac{1}{16}lb\Gamma-\frac{1}{24}lb\Gamma+\frac{1}{16}\Gamma^2-\frac{1}{24}\Gamma^2-\frac{1}{96}\Gamma^2\right.$$

$$\left.+\frac{1}{128}\Gamma^2-\frac{\Gamma}{K^3 I_0(K)}I_1(K)+\frac{\Gamma}{K^2 I_0(K)}\left[\left(\frac{1}{K}I_1(K)+\frac{4}{K^3}I_1(K)-\frac{2}{K^2}I_0(K)\right)\right]\right]$$

$$-\frac{a}{I_0(K)}\left\{\left(\frac{1}{4}+\frac{lb}{4}+\frac{\Gamma}{4}\right)\left(\frac{1}{K}I_1(K)+\frac{4}{K^3}I_1(K)-\frac{2}{K^2}I_0(K)\right)\right.$$

$$-\Gamma\left[\frac{1}{16K}I_1(K)+\frac{1}{K^3}I_1(K)-\frac{1}{4K^2}I_0(K)+\frac{4}{K^5}I_1(K)-\frac{2}{K^4}I_0(K)\right]$$

$$\left.-\frac{1}{K^2 I_0(K)}\left(\frac{1}{2}I_0^2(K)-\frac{1}{2}I_1^2(K)\right)\right\}+\frac{1}{16}d+\frac{1}{16}dlb+\frac{1}{16}d\Gamma-\frac{1}{24}d\Gamma$$

$$-\frac{d}{4I_0(K)}\left(\frac{1}{K}I_1(K)+\frac{4}{K^3}I_1(K)-\frac{2}{K^2}I_0(K)\right)+C_4\left[\frac{1}{2}+\frac{1}{2}lb+\frac{1}{2}\Gamma-\frac{1}{4}\Gamma\right.$$

$$\left.-\frac{1}{I_0(K)}\frac{1}{K}I_1(K)\right]=0.$$

Then, we have

$$C_4 = \frac{-2}{1+lb+\frac{\Gamma}{2}-\frac{2I_1(K)}{KI_0(K)}}\left\{(a+bal)\left[\frac{1}{16}+\frac{1}{16}lb+\frac{1}{16}\Gamma-\frac{1}{96}\Gamma-\frac{1}{K^2I_0(K)}\frac{1}{K}I_1(K)\right]\right.$$

$$+a\left[\frac{1}{16}\Gamma-\frac{1}{24}\Gamma+\frac{1}{16}lb\Gamma-\frac{1}{24}lb\Gamma+\frac{1}{16}\Gamma^2-\frac{1}{24}\Gamma^2-\frac{1}{96}\Gamma^2\right.$$

$$+\frac{1}{128}\Gamma^2-\frac{\Gamma}{K^3I_0(K)}I_1(K)+\frac{\Gamma}{K^2I_0(K)}\left[\left(\frac{1}{K}I_1(K)+\frac{4}{K^3}I_1(K)-\frac{2}{K^2}I_0(K)\right)\right]\Big]$$

$$-\frac{a}{I_0(K)}\left\{\left(\frac{1}{4}+\frac{lb}{4}+\frac{\Gamma}{4}\right)\left(\frac{1}{K}I_1(K)+\frac{4}{K^3}I_1(K)-\frac{2}{K^2}I_0(K)\right)\right.$$

$$-\Gamma\left[\frac{1}{16K}I_1(K)+\frac{1}{K^3}I_1(K)-\frac{1}{4K^2}I_0(K)+\frac{4}{K^5}I_1(K)-\frac{2}{K^4}I_0(K)\right]$$

$$\left.-\frac{1}{K^2I_0(K)}\left(\frac{1}{2}I_0^2(K)-\frac{1}{2}I_1^2(K)\right)\right\}+\frac{1}{16}d+\frac{1}{16}dlb+\frac{1}{16}d\Gamma-\frac{1}{24}d\Gamma$$

$$\left.-\frac{d}{4I_0(K)}\left(\frac{1}{K}I_1(K)+\frac{4}{K^3}I_1(K)-\frac{2}{K^2}I_0(K)\right)\right\},$$

that is,

$$C_4 = \frac{-2}{u_m^*}\left\{(a+bal)\left[\frac{1}{16}+\frac{1}{16}lb+\frac{1}{16}\Gamma-\frac{1}{96}\Gamma-\frac{1}{K^2I_0(K)}\frac{1}{K}I_1(K)\right]\right.$$

$$+a\left[\frac{1}{16}\Gamma-\frac{1}{24}\Gamma+\frac{1}{16}lb\Gamma-\frac{1}{24}lb\Gamma+\frac{1}{16}\Gamma^2-\frac{1}{24}\Gamma^2-\frac{1}{96}\Gamma^2\right.$$

$$+\frac{1}{128}\Gamma^2-\frac{\Gamma}{K^3I_0(K)}I_1(K)+\frac{\Gamma}{K^2I_0(K)}\left[\left(\frac{1}{K}I_1(K)+\frac{4}{K^3}I_1(K)-\frac{2}{K^2}I_0(K)\right)\right]\Big]$$

$$-\frac{a}{I_0(K)}\left\{\left(\frac{1}{4}+\frac{lb}{4}+\frac{\Gamma}{4}\right)\left(\frac{1}{K}I_1(K)+\frac{4}{K^3}I_1(K)-\frac{2}{K^2}I_0(K)\right)\right.$$

$$-\Gamma\left[\frac{1}{16K}I_1(K)+\frac{1}{K^3}I_1(K)-\frac{1}{4K^2}I_0(K)+\frac{4}{K^5}I_1(K)-\frac{2}{K^4}I_0(K)\right]$$

$$\left.-\frac{1}{K^2I_0(K)}\left(\frac{1}{2}I_0^2(K)-\frac{1}{2}I_1^2(K)\right)\right\}+\frac{1}{16}d+\frac{1}{16}dlb+\frac{1}{16}d\Gamma-\frac{1}{24}d\Gamma$$

$$\left.-\frac{d}{4I_0(K)}\left(\frac{1}{K}I_1(K)+\frac{4}{K^3}I_1(K)-\frac{2}{K^2}I_0(K)\right)\right\},$$

which can be written as

$$-C_4 = \frac{a}{u_m^*}E+\frac{d}{u_m^*}F, \tag{4.37}$$

72

where

$$E = \frac{1}{8} + \frac{lb}{4} + \frac{b^2 l^2}{8} + \frac{7}{48}\Gamma + \frac{7lb}{48}\Gamma + \frac{lb}{K^2} + \frac{7}{192}\Gamma^2$$
$$- \frac{8\Gamma}{K^4} + \frac{\Gamma}{2K^2} + \frac{2}{K^2} + \frac{I_1(K)}{I_0(K)}\left\{ \frac{16\Gamma}{K^5} - \frac{4}{K^3} - \frac{4bl}{K^3} \right.$$
$$\left. - \frac{1}{2K} - \frac{lb}{2K} - \frac{3\Gamma}{8K} \right\} - \left[\frac{I_1(K)}{KI_0(K)} \right]^2,$$
$$F = \frac{1}{8} + \frac{1}{8}lb + \frac{1}{24}\Gamma + \frac{1}{K^2} - \frac{I_1(K)}{I_0(K)}\left[\frac{1}{2K} + \frac{2}{K^3} \right].$$

By substituting (4.37) into (4.32), we have

$$\phi = \left[2\frac{Pe}{\alpha}f(x^*) + \frac{S}{u_m^*} \right]\left[A(r^*) - \frac{E}{u_m^*} \right] + \left[2\mathcal{Q}_w(x^*) - 2u_m^*\frac{Pe}{\alpha}f(x^*) - S \right]\left[\frac{r^{*2}}{4} - \frac{F}{u_m^*} \right].$$
$$(4.38)$$

Remark 4.3.3 *In comparison with the work for the no-slip case in [83], the solution for the slip case can be expressed in the same form. However, the formulae for $A(r^*)$, E and F are different to those for the no-slip case. All of the $A(r^*)$, E and F have some additional terms for the slip case. In addition, u_m^* and $f(x^*)$ are also different to those for the no-slip case. A careful examination indicates that the solutions for the slip case include the no-slip case as a special case.*

4.4   Investigation of Temperature field

In this section, we first investigate the distributions of $\theta_b(x^*)$, $\theta_w(x^*)$ and the Nusselt number $Nu(x^*)$ along the axial direction for the slip case, where θ_b is the dimensionless bulk temperature as defined before, $\theta_w(x^*) = \theta(x^*, 1)$ denotes the dimensionless temperature on the wall $r^* = 1$, $Nu(x^*) = \frac{2\mathcal{Q}_w(x^*)}{\theta_w(x^*) - \theta_b(x^*)}$ is the local Nusselt number evaluating the heat transfer rate. Three different forms of heat flux from the wall are considered for the investigation, namely, $\mathcal{Q}_w = 2x^*$, $(4e^{4x^*} - 1)/(e^4 - 2)$ and $\frac{\pi}{2}\sin(\pi x^*)$ respectively.

The axial distributions of θ_b and θ_w for various Pe values and different form of $q_w(x^*)$ for the slip case are shown in Fig.4.2 and Fig.4.3 respectively. It can be noted from the figures that the fluid temperature decreases as the value of *Pe* increases. This is as expected and is consistent with the results for the no-slip case in literature because a higher *Pe* indicates a higher flow rate and, as a result, the energy storage capacity becomes larger.

Figure 4.4 shows the distribution of the local Nusselt number $Nu(x^*)$ along the axial direction for two different *Pe* values, 0.01 and 40, for the slip case. As illustrated in the figure, the distribution of the local Nusselt number along the axial direction is similar to that of $q_w(x^*)$. For example, for the linear case $q_w(x^*) = 2x^*$, $Nu(x^*)$ is zero at $q_w(x^*) = 0$ and increases as $q_w(x^*)$ increases. For the $q_w(x^*) = \frac{\pi}{2}\sin(x^*)$, the axial distribution of $Nu(x^*)$ is very close to the shape of a sine function in the interval $x^* \in [0,1]$. Although qualitatively, the axial distributions of $\theta_b(x^*), \theta_w(x^*)$ for the slip case are similar to those for the no-slip case, the values are different for the two cases. As the fluid flow velocity is affected by the slip parameter l, we will investigate the influence of l on $\theta_b(x^*)$ and $\theta_w(x^*)$.

Figures 4.5 and 4.6 show the influences of the variation of the slip parameter l on θ_b and θ_w at three different locations $x^* = -0.5, 0.5$ and 1.5. It is clear from the figures that, the slip parameter l has significant effects on both $\theta_b(x^*)$ and $\theta_w(x^*)$. As l increases, both $\theta_b(x^*)$ and $\theta_w(x^*)$ decrease as shown in the figures.
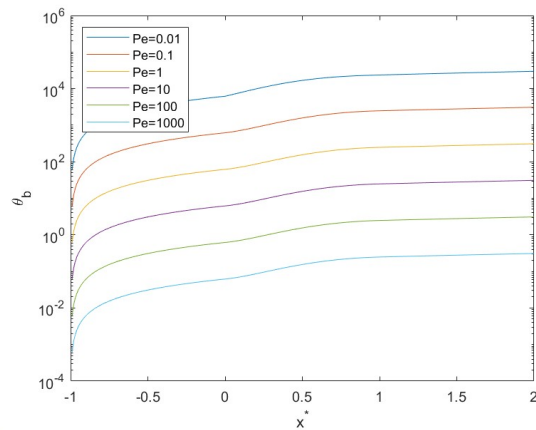
4.5   Concluding Remarks

The properties and features of heat transfer in a mixed electroosmotic and pressure-driven flow are analyzed in this chapter. By considering the Navier slip boundary condition, new analytical solutions for the velocity and temperature fields have been obtained based on previous work in the field for the no-slip
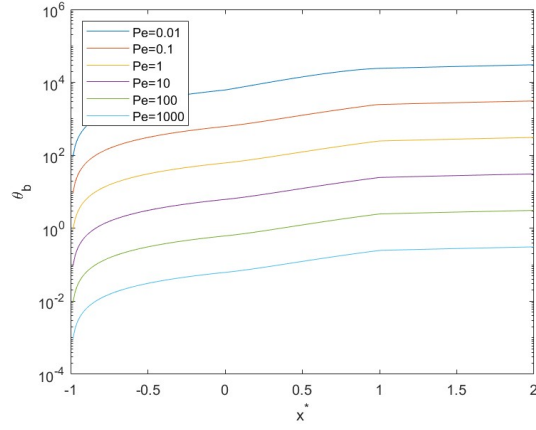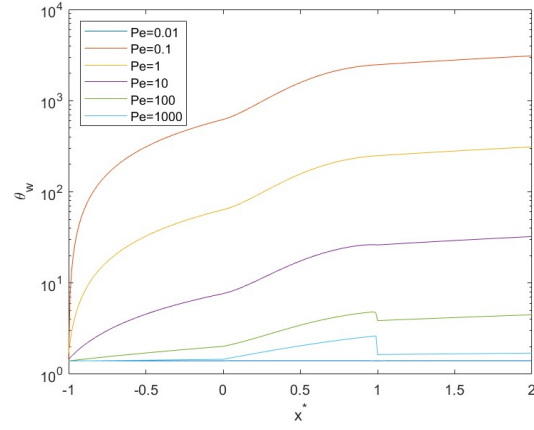
(a) $q_w = 2x^*$
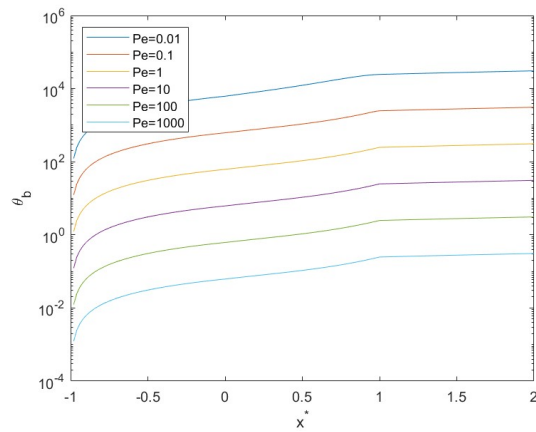
(b) $q_w = (4e^{4x^*} - 1)/(e^4 - 2)$

(c) $q_w = \pi/2\sin(\pi x^*)$

Figure 4.2: Distribution of θ_b along the axial direction for different *Pe* values for three different wall heat flux q_w

(a) $\mathfrak{q}_w = 2x^*$

(b) $\mathfrak{q}_w = (4e^{4x^*} - 1)/(e^4 - 2)$
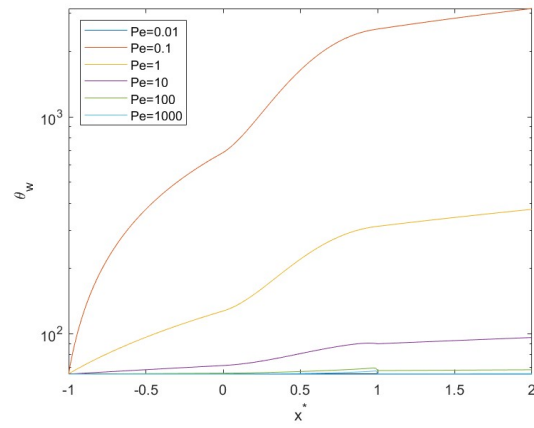

(c) $\mathfrak{q}_w = \pi/2 \sin(\pi x^*)$
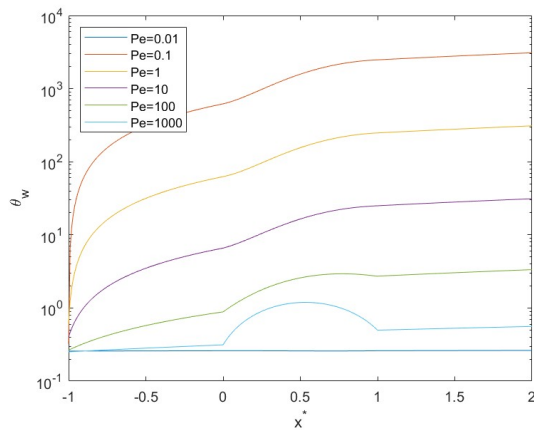
Figure 4.3: Distribution of θ_w along the axial direction at different Pe values for three different wall heat flux q_w
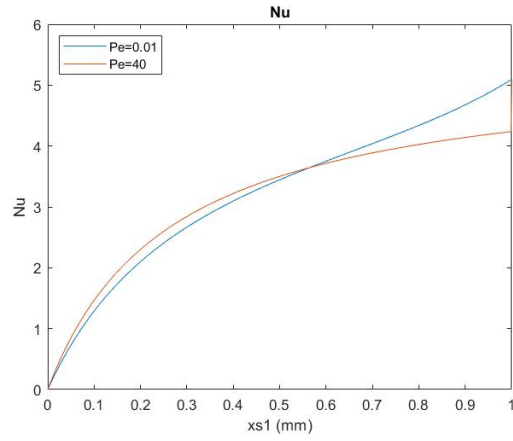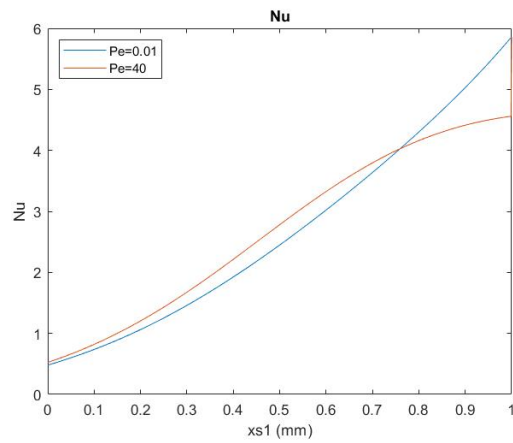
(a) $q_w = 2x^*$

(b) $q_w = (4e^{4x^*} - 1)/(e^4 - 2)$

(c) $q_w = \pi/2\sin(\pi x^*)$

Figure 4.4: Axial distributions of the local Nusselt number at different *Pe* values for three different wall heat flux q_w
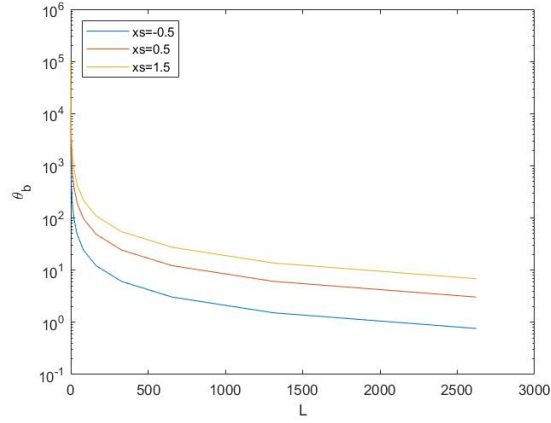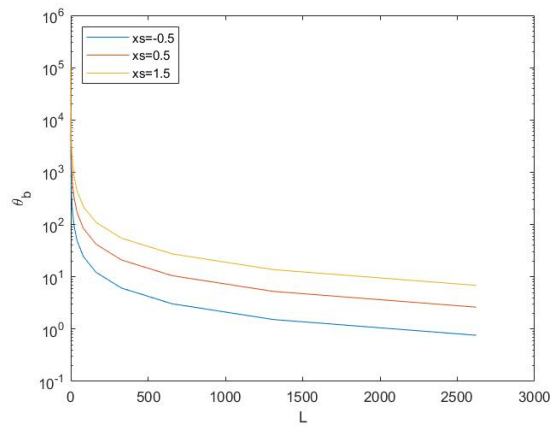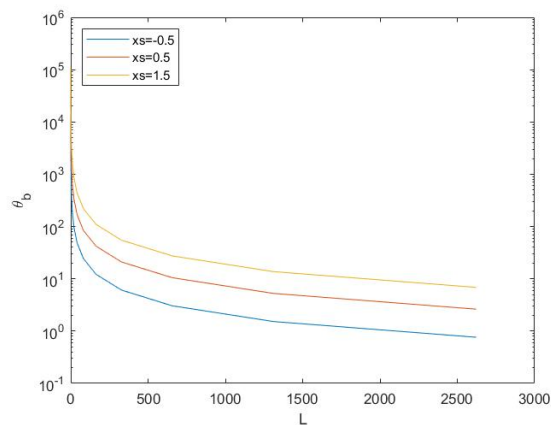
(a) $q_w = 2x^*$

(b) $q_w = (4e^{4x^*} - 1)/(e^4 - 2)$

(c) $q_w = \pi/2 \sin(\pi x^*)$

Figure 4.5: Influence of the slip parameter l on θ_b for three different wall heat flux q_w
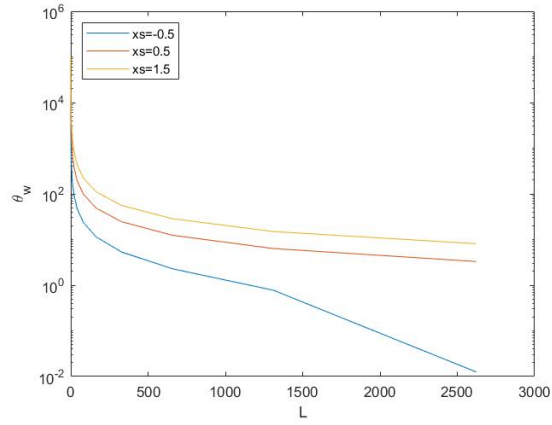
(a) $q_w = 2x^*$
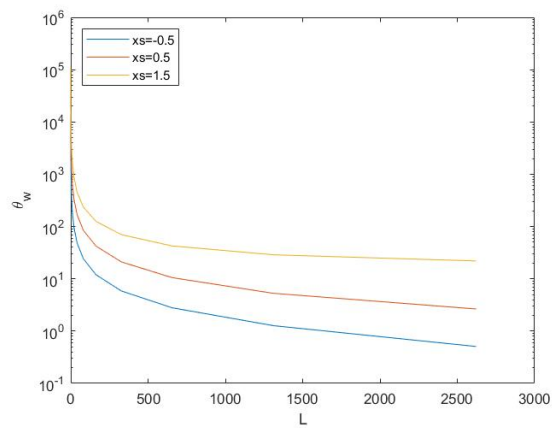
(b) $q_w = (4e^{4x^*} - 1)/(e^4 - 2)$
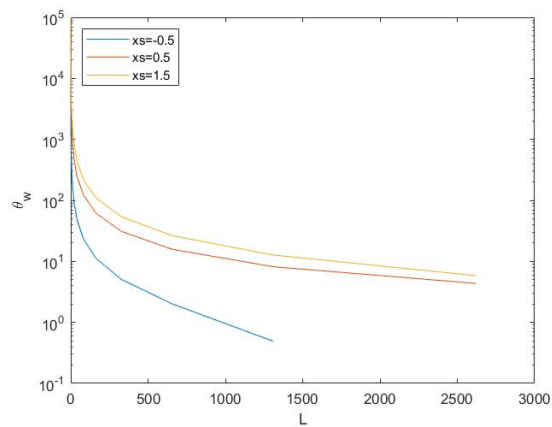
(c) $q_w = \pi/2 \sin(\pi x^*)$

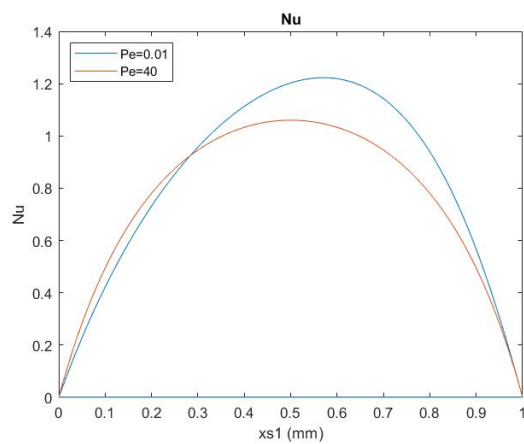Figure 4.6: Influence of the slip parameter l on θ_w for three different wall heat flux q_w

case. The results are more general than those in the literature and include the no-slip case as a special case. The axial dependence of the dimensionless bulk temperature and the dimensionless wall temperature that are involved in our solutions have been derived and shown graphically in this chapter. They have been demonstrated for three different types of wall heat flux and different values of Péclet number. The results obtained for the axial dependence in the slip case are consistent with the previous study for the non-slip case. The influence of the slip parameter l on the temperature field has been investigated. The numerical results show that the slip parameter l has a significant influence on the temperature field. As l increases, the temperature decreases as shown graphically in the chapter.

Chapter 5

Unsteady slip flow of fluids in rectangular microchannels

5.1 Introduction

Over the past couple of decades, micro-fluidic devices have been developed and used in many engineering applications, including micro-electrical systems (MEMS), integrated micro-electric system cooler, digital microprocessors, micro-reactors, and hot heating devices. Hence, scientists have been attracted to the study of fluid flow through microchannels due to its usage in developing microde-vices. For both commercial and scientific objectives, microchannels with various cross-sectional geometries have been manufactured recently.

In recent years, a lot of work was conducted to study fluid flow in microchannels under slip conditions, and many results, both analytical and numerical, have been achieved. The slip coefficient in slip conditions was predicted by obtaining an analytical slip flow solution in [8]. Colin et al. [86] proposed a slip-flow model to study gaseous flow in rectangular microchannels and developed experiment device for measuring gaseous microflow rates. Slip flow via parabolic microchannels was investigated in 2014 [87]. With thermal radiation heat transfer, the

effects of slip on unsteady flow over a stretching surface were explored in [88]. Slip flow in rectangular microchannels was also studied in [89]. The problem of slip flow and heat transfer in rectangular microchannels was studied in 2001 [45]. The temperature field was developed by solving the heat transfer equation using a modified generalized integral transform method. Many other investigations on slip flow have also been carried as reviewed in chapter two.

Based on previous work and results achieved, this chapter focuses on the study of unsteady flow of incompressible Newtonian fluids through rectangular microchannels under slip conditions. The rest of the chapter is organized as follows. Section 5.2 presents the mathematical model. Section 5.3 focuses on the derivation of a new analytical solution for the problem. Section 5.4 applies the developed analytical solution to investigate the flow characteristics of fluids through rectangular channels under slip conditions and the influences of boundary slip, followed by a concluding remark in section 5.5.

5.2   Mathematical Model

In this chapter, we consider the slip flow of an incompressible Newtonian fluid through a rectangular microchannel. The geometry of the channel together with the coordinate system used is as shown in Fig. 5.1. The velocity vector $\mathbf{v}$ is given by $\mathbf{v} = v_x i + v_y j + u k$. The Navier-Stokes equation in z direction can be expressed as

$$\rho \left(\frac{\partial u}{\partial t} + v_x \frac{\partial u}{\partial x} + v_y \frac{\partial u}{\partial y} + u \frac{\partial u}{\partial z} \right) = \rho g_z - \frac{\partial p}{\partial z} + \mu \left(\frac{\partial^2 u}{\partial x^2} + \frac{\partial^2 u}{\partial y^2} + \frac{\partial^2 u}{\partial z^2} \right). \quad (5.1)$$

Since we assume that the flow is parallel to the z axis, v_x and v_y both vanish.

To satisfy the standard continuity equation for incompressible fluids, namely

$$\frac{\partial v_x}{\partial x} + \frac{\partial v_y}{\partial y} + \frac{\partial u}{\partial z} = 0,$$
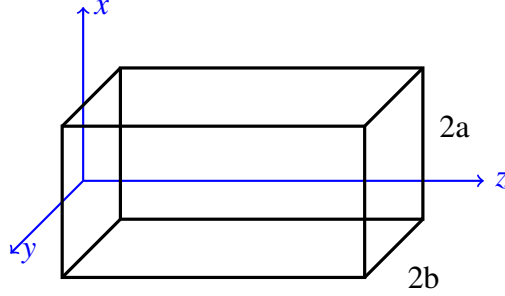
Figure 5.1: The coordinate system for the rectangular microchannel

we get $u = u(t, x, y)$. Furthermore, since the flow is horizontal, $g_z = 0$. In our case, it is assumed that the flow is unsteady. Hence, the governing equation (5.1) for the axial velocity $u(t, x, y)$ is simplified to

$$\left(\frac{\partial^2 u}{\partial x^2} + \frac{\partial^2 u}{\partial y^2} \right) - \frac{\rho}{\mu} \left(\frac{\partial u}{\partial t} \right) = \frac{1}{\mu} \frac{\partial p}{\partial z}. \tag{5.2}$$

As the problem is symmetric about the xz-plane and the yz-plane, the velocity field must satisfy the symmetrical conditions,

$$\frac{\partial u}{\partial x}(t, 0, y) = 0, \quad \frac{\partial u}{\partial y}(t, x, 0) = 0. \tag{5.3}$$

As boundary slip occurs at microscale, the Navier slip boundary condition is used for the problem, namely

$$u(t, a, y) = -l \frac{\partial u}{\partial x}(t, a, y), \tag{5.4}$$

$$u(t, x, b) = -l \frac{\partial u}{\partial y}(t, x, b). \tag{5.5}$$

Hence, the axial velocity of the fluid flow in the rectangular microchannel is governed by Eq. (5.2) subject to the symmetrical condition (5.3) and boundary conditions (5.4) and (5.5).

83

5.3　Derivation of New Analytical solutions

To solve the problem in section (5.2), firstly, the pressure gradient is expressed as a Fourier series in exponential form

$$\frac{\partial p}{\partial z} = \sum_{n=0}^{\infty} [a_n \cos(n\omega t) + b_n \sin(n\omega t)] = Re\left(\sum_{n=0}^{\infty} c_n e^{in\omega t}\right), \qquad (5.6)$$

where $c_n = a_n - b_n i$, $e^{in\omega t} = \cos(n\omega t) + i\sin(n\omega t)$.

As many functions can be written in Fourier series form, the above formula can be used to approximate the general pressure field. As the underlying boundary value problem is linear, we can let

$$u = \sum_{n=0}^{\infty} Re(u_n), \qquad (5.7)$$

where u_n is governed by

$$\left(\frac{\partial^2 u_n}{\partial x^2} + \frac{\partial^2 u_n}{\partial y^2}\right) - \frac{\rho}{\mu}\frac{\partial u_n}{\partial t} = \frac{c_n}{\mu} e^{in\omega t}. \qquad (5.8)$$

From the symmetrical condition (5.3) and the boundary conditions (5.4) and (5.5), we have

$$\frac{\partial u_n}{\partial x}(t,0,y) = 0, \quad \frac{\partial u_n}{\partial y}(t,x,0) = 0, \qquad (5.9)$$

$$u_n(t,a,y) = -l\frac{\partial u_n}{\partial x}(t,a,y), \qquad (5.10)$$

$$u_n(t,x,b) = -l\frac{\partial u_n}{\partial y}(t,x,b). \qquad (5.11)$$

To solve Eq. (5.8) subject to (5.9)-(5.11), let

$$u_n = f_n e^{in\omega t}, \qquad (5.12)$$

where $f_n = f_n(x,y)$. Then Eq. (5.8) becomes

$$\left(\frac{\partial^2 f_n}{\partial x^2} + \frac{\partial^2 f_n}{\partial y^2}\right) - \frac{in\omega\rho}{\mu} f_n = \frac{c_n}{\mu}, \qquad (5.13)$$

which is a non-homogeneous equation. To solve the equation, first, consider the homogeneous equation

$$\left(\frac{\partial^2 f_n}{\partial x^2}+\frac{\partial^2 f_n}{\partial y^2}\right)-\frac{in\omega\rho}{\mu}f_n=0. \tag{5.14}$$

Let

$$f_n=X(x)Y(y), \tag{5.15}$$

then, one gets from Eq. (5.14) that

$$X''Y+XY''-\frac{in\omega\rho}{\mu}XY=0,$$

which gives

$$\frac{X''}{X}=-\frac{Y''}{Y}+\frac{in\omega\rho}{\mu}=-\delta_n^2. \tag{5.16}$$

Then, we have two ordinary differential equations.

$$X''+\delta_n^2 X=0,$$
$$Y''-(\delta_n^2+\frac{in\omega\rho}{\mu})Y=0.$$

Hence,

$$X=A\cos(\delta_n x)+B\sin(\delta_n x). \tag{5.17}$$

From $(5.9)_1$, (5.12), and (5.15), we have

$$X'(0)=[-A\delta_n\sin(\delta_n x)+B\delta_n\cos(\delta_n x)]_{x=0}=B\delta_n=0.$$

Hence,

$$X=A\cos(\delta_n x). \tag{5.18}$$

From (5.10), (5.12), and (5.15), we get

$$[X(a)+lX'(a)]Y(y)=0$$

and so

$$X(a)+lX'(a)=0.$$

85

Further from (5.18), we get

$$A\cos(\delta_n a) - Al\delta_n \sin(\delta_n a) = 0.$$

Hence,

$$\delta_n - \frac{\cot(\delta_n a)}{l} = 0, \tag{5.19}$$

which is a nonlinear equation for δ_n and can be solved to get a series of solutions $\delta_{nj}(j = 1, 2, 3, \dots)$.

Now, we consider the non-homogeneous equation (5.13), and try a solution of the following form

$$f_n = \sum_{j=1}^{\infty} Y_{nj}(y)\cos(\delta_{nj}x), \tag{5.20}$$

with the δ_{nj} determined by Eq. (5.19). With this solution form, the boundary conditions of $(5.9)_1$ and (5.10) have been satisfied. Hence, $Y(y)$ needs to be determined to satisfy the nonhomogeneous equation (5.13), the symmetrical condition $(5.9)_2$, and the slip boundary condition (5.11). Substituting (5.20) into Eq. (5.13) yields

$$\sum_{j=1}^{\infty} \left[-\delta_{nj}^2 Y_{nj}(y)\cos(\delta_{nj}x) + Y_{nj}''(y)\cos(\delta_{nj}x) - \frac{in\omega\rho}{\mu} Y_{nj}(y)\cos(\delta_{nj}x) \right] = \frac{c_n}{\mu},$$

that is

$$\sum_{j=1}^{\infty} \left[Y_{nj}''(y) - (\delta_{nj}^2 + \frac{in\omega\rho}{\mu})Y_{nj} \right] \cos(\delta_{nj}x) = \frac{c_n}{\mu}. \tag{5.21}$$

Multiplying both sides by $\cos(\delta_{nm}x)$, one gets

$$\sum_{j=1}^{\infty} \left[Y_{nj}'' - (\delta_{nj}^2 + \frac{in\omega\rho}{\mu})Y_{nj} \right] \cos(\delta_{nj}x)\cos(\delta_{nm}x) = \frac{c_n}{\mu}\cos(\delta_{nm}x). \tag{5.22}$$

It can be proved that the family of $\cos(\delta_{nj}x)_{j=1}^{\infty}$ is orthogonal, that is

$$\int_0^a \cos(\delta_{nj}x)\cos(\delta_{nm}x)dx = \begin{cases} 0 & \text{if } j \neq m \\ \neq 0 & \text{if } j = m \end{cases}$$

86

By integrating Eq. (5.22) with respect to x on both sides from 0 to a, one gets

$$Y_{nm}'' - (\delta_{nm}^2 + \frac{in\omega\rho}{\mu})Y_{nm} = \frac{\frac{c_n}{\mu}\int_0^a \cos(\delta_{nm}x)dx}{\int_0^a \cos^2(\delta_{nm}x)dx},$$

which gives

$$Y_{nm} = C_{nm}e^{\sqrt{\gamma_{nm}}y} + D_{nm}e^{-\sqrt{\gamma_{nm}}y} - \frac{\theta_{nm}(\delta_{nm},a)}{\gamma_{nm}},$$

where

$$\gamma_{nm} = \delta_{nm}^2 + \frac{in\omega\rho}{\mu}, \tag{5.23}$$

$$\theta_{nm} = \frac{\frac{c_n}{\mu}\int_0^a \cos(\delta_{nm}x)dx}{\int_0^a \cos^2(\delta_{nm}x)dx} = \frac{\frac{c_n}{\mu}\sin(\delta_{nm}a)}{\frac{1}{2}\delta_{nm}a + \frac{1}{4}\sin(2\delta_{nm}a)}. \tag{5.24}$$

Now consider the boundary condition $(5.9)_2$,

$$\sum_{m=1}^{\infty} Y_{nm}'(0)\cos(\delta_{nm}x) = 0.$$

That is

$$\sum_{m=1}^{\infty} \left[C_{nm} - D_{nm} \right]\sqrt{\gamma_{nm}}\cos(\delta_{nm}x) = 0,$$

which gives

$$C_{nm} = D_{nm}.$$

Hence,

$$Y_{nm} = C_{nm}\left[e^{\sqrt{\gamma_{nm}}y} + e^{-\sqrt{\gamma_{nm}}y} \right] - \frac{\theta_{nm}(\delta_{nm},a)}{\gamma_{nm}} = C_{nm}\cosh(\sqrt{\gamma_{nm}}y) - \frac{\theta_{nm}}{\gamma_{nm}}. \tag{5.25}$$

Substituting Eq. (5.25) into Eq. (5.20), we have

$$f_n = \sum_{m=1}^{\infty} [C_{nm}\cosh(\sqrt{\gamma_{nm}}y) - \frac{\theta_{nm}}{\gamma_{nm}}]\cos(\delta_{nm}x), \tag{5.26}$$

$$\frac{\partial f_n}{\partial y} = \sum_{m=1}^{\infty} C_{nm}\sqrt{\gamma_{nm}}\sinh(\sqrt{\gamma_{nm}}y)\cos(\delta_{nm}x).$$

Now from boundary condition (5.11), we get

$$\sum_{m=1}^{\infty} [C_{nm}\cosh(\sqrt{\gamma_{nm}}b) - \frac{\theta_{nm}}{\gamma_{nm}}]\cos(\delta_{nm}x) = -l\sum_{m=1}^{\infty} C_{nm}\sqrt{\gamma_{nm}}\sinh(\sqrt{\gamma_{nm}}b)\cos(\delta_{nm}x),$$

87

that is

$$\sum_{m=1}^{\infty}\left\{C_{nm}[\cosh(\sqrt{\gamma_{nm}}b)+l\sqrt{\gamma_{nm}}\sinh(\sqrt{\gamma_{nm}}b)]-\frac{\theta_{nm}}{\gamma_{nm}}\right\}\cos(\delta_{nm}x)=0,$$

Hence,

$$C_{nm}=\frac{\theta_{nm}(\delta_{nm},a)}{\gamma_{nm}\left[\cosh(\sqrt{\gamma_{nm}}b)+l\sqrt{\gamma_{nm}}\sinh(\sqrt{\gamma_{nm}}b)\right]}. \tag{5.27}$$

Substituting (5.26) into (5.12) and (5.7) gives the solution for the axial velocity as follows

$$u(t,x,y)=\sum_{n=0}^{\infty}Re\left\{\left[\sum_{m=1}^{\infty}[C_{nm}\cosh(\sqrt{\gamma_{nm}}y)-\frac{\theta_{nm}}{\gamma_{nm}}]\cos(\delta_{nm}x)\right]e^{in\omega t}\right\}. \tag{5.28}$$

Now the flow rate and the stress field need to be determined. The flow rate can be calculated by

$$Q(t)=4\int_{0}^{b}\int_{0}^{a}u(x,y,t)dxdy=Q_{0}+\sum_{n=1}^{\infty}Q_{n}, \tag{5.29}$$

where Q_0 and Q_n respectively are the flow rate corresponding to the constant pressure gradient and the nth harmonic component. They are given as follows

$$Q_{0}=4\left[Re\left\{\sum_{m=1}^{\infty}\left[\frac{C_{0m}\sinh(\delta_{0m}b)\sin(\delta_{0m}a)}{\delta_{0m}^{2}}-\frac{b\theta_{0m}\sin(\delta_{0m}a)}{\delta_{0m}^{3}}\right]\right\}\right], \tag{5.30}$$

$$Q_{n}=4\left[Re\left\{\sum_{m=1}^{\infty}\left[\frac{C_{nm}\sinh(\sqrt{\gamma_{nm}}b)\sin(\delta_{nm}a)}{\delta_{nm}\sqrt{\gamma_{nm}}}-\frac{b\theta_{nm}\sin(\delta_{nm}a)}{\delta_{nm}\gamma_{nm}}\right]\right\}e^{in\omega t}\right]. \tag{5.31}$$

The stress in the fluid can be determined by the standard constitutive equation for incompressible Newtonian fluid, namely

$$\sigma=-pI+2\mu d, \tag{5.32}$$

where d is the rate of deformation which can be determined by the geometric equations

$$d=\frac{1}{2}(\nabla v+(\nabla v)^{T}), \tag{5.33}$$

In what follows, we will evaluate the stress field in the fluid. From $v = (0, 0, u(t, x, y))$, we can get

$$d = \frac{1}{2} \begin{pmatrix} 0 & 0 & \frac{\partial u}{\partial x} \\ 0 & 0 & \frac{\partial u}{\partial y} \\ \frac{\partial u}{\partial x} & \frac{\partial u}{\partial y} & 0 \end{pmatrix}. \tag{5.34}$$

From the above formula and using Eq. (5.33) and Eq. (5.28), we achieve $d_{xx} = d_{yy} = d_{zz} = d_{xy} = 0$ and

$$d_{xz} = \frac{1}{2} \sum_{n=0}^{\infty} Re \left\{ \left[\sum_{m=1}^{\infty} (\frac{\theta_{nm}}{\gamma_{nm}} - C_{nm} \cosh(\sqrt{\gamma_{nm}}y)) \delta_{nm} \sin(\delta_{nm}x) \right] e^{in\omega t} \right\}, \tag{5.35}$$

$$d_{yz} = \frac{1}{2} \sum_{n=0}^{\infty} Re \left\{ \left[\sum_{m=1}^{\infty} (C_{nm} \sqrt{\gamma_{nm}} \sinh(\sqrt{\gamma_{nm}}y) \cos(\delta_{nm}x) \right] e^{in\omega t} \right\}. \tag{5.36}$$

Therefore, from Eq. (5.32) we have

$$\sigma_{xx} = \sigma_{yy} = \sigma_{zz} = -p = q(t)z + p_0(t), \sigma_{xz} = 2\mu d_{xz}, \sigma_{yz} = 2\mu d_{yz}, \tag{5.37}$$

where $q(t)$ represents the pressure gradient $\frac{\partial p}{\partial z}$, whilst $p_0(t)$ is a constant based on the pressure condition.

5.4 Investigation of flow characteristics and influence of boundary slip

This section investigates the flow characteristics and the influence of boundary slip. Without losing generality, in this discussion, we consider two different forms of pressure gradient which drive the flow of fluids through the microchannel.

5.4.1 Case 1: $\frac{\partial p}{\partial z} = a_0$

Since

$$\frac{\partial p}{\partial z} = Re(\sum_{n=0}^{\infty} c_n e^{in\omega t}),$$

(a) $l = 0.01$ (b) $l = 0.1$ (c) $l = 0.5$
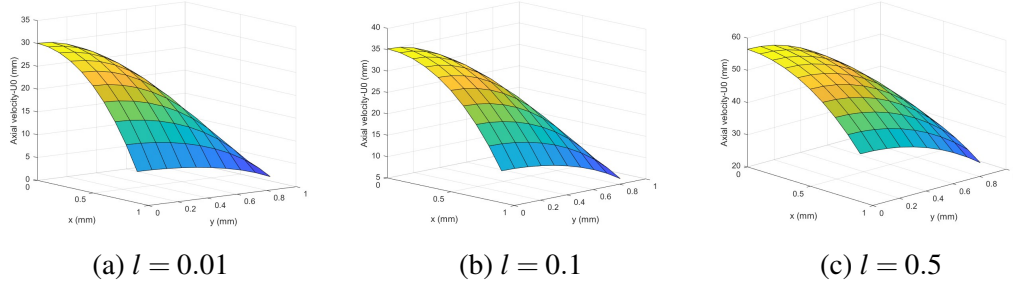
Figure 5.2: Axial velocity profiles on the cross-section $z = L/2$ of the channel for various different values of l

in this condition we have $c_0 = a_0, c_n = 0$ for all $n \neq 0$. As the pressure gradient is constant, the corresponding u function can be assumed to be time independent, and so for $n = 0$, following the same procedure as for finding $u_n(x,y,t)$, we achieve

$$u_0(x,y) = \sum_{m=1}^{\infty} \left[C_{0m} \cosh(\delta_{0m}y) - \frac{\theta_{0m}}{\delta_{0m}^2} \right] \cos(\delta_{0m}x), \quad (5.38)$$

where $\delta_{0m}, \theta_{0m}, C_{0m}$ are determined by (5.19), (5.24), and (5.27) with $n = 0$. The flow rate in this condition is defined above by (5.30). The axial velocity, the flow rate, and shear stress are time independent.

By taking different values of the slip parameter l, we demonstrate the solutions graphically and investigate the influence of the slip parameter l on the velocity profiles. Fig.5.2 and Fig.5.3 show respectively 3D graphs and 2D graphs of the axial velocity profiles for different values of slip parameters. The influence of the slip parameters l on the flow rate Q is shown in Fig.5.4. It can be realized from these graphs that the slip parameter has a significant influence on the velocity and flow rate. As l increases, the magnitudes of velocity and flow rate increase.

(a) Along the $x-$axis
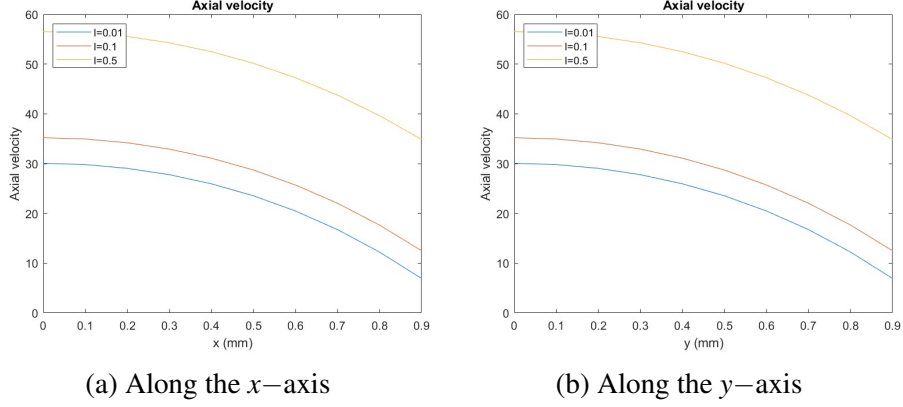
(b) Along the $y-$axis

Figure 5.3: Axial velocity profiles along the $x-$axis and $y-$axis at $z = L/2$ for different l values

5.4.2 Case 2: $\frac{\partial p}{\partial z} = b_1 \sin(\omega t)$

For this case, $c_1 = -b_1 i, c_n = 0$ for $n \neq 1$. The pressure gradient then becomes sinusoidal with amplitude b_1. In this case, the axial velocity becomes

$$u_1(t,x,y) = Re\left\{ e^{i\omega t} \left[\sum_{m=1}^{\infty} [C_{1m} \cosh(\sqrt{\gamma_{1m}}y) - \frac{\theta_{1m}}{\gamma_{1m}}] \cos(\delta_{1m}x) \right] \right\}, \qquad (5.39)$$

where

$$C_{1m} = \frac{\theta_{1m}}{\gamma_{1m}[\cosh(\sqrt{\gamma_{1m}}b) + l\sqrt{\gamma_{1m}}\sinh(\sqrt{\gamma_{1m}}b)]},$$

$$\gamma_{1m} = \delta_{1m}^2 + \frac{i\omega\rho}{\mu},$$

$$\theta_{1m} = \frac{\frac{-b_1 i}{\mu}\sin(\delta_{1m}a)}{\frac{1}{2}\delta_{1m}a + \frac{1}{4}\sin(2a\delta_{1m})} = A_{1m}i, \quad \text{where} \quad A_{1m} = \frac{\frac{-b_1}{\mu}\sin(\delta_{1m}a)}{\frac{1}{2}\delta_{1m}a + \frac{1}{4}\sin(2a\delta_{1m})}.$$

Let

$$\sqrt{\gamma_{1m}} = \sqrt{\delta_{1m}^2 + i\frac{\omega\rho}{\mu}} = \alpha_{1m} + i\beta_{1m}.$$

By using imaginary number properties, we have

$$\sqrt{\delta_{1m}^4 + (\frac{\omega\rho}{\mu})^2}\cos\theta = \delta_{1m}^2, \qquad \sqrt{\delta_{1m}^4 + (\frac{\omega\rho}{\mu})^2}\sin\theta = \frac{\omega\rho}{\mu},$$

91
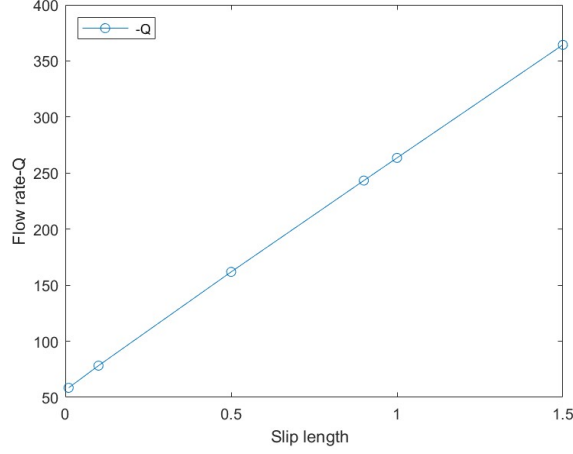
Figure 5.4: Variation of flow rate with slip parameter l

thus, we have

$$\alpha_{1m} = \left(\delta_{1m}^4 + (\frac{\omega\rho}{\mu})^2\right)^{\frac{1}{4}} \cos\frac{\theta}{2}, \qquad \beta_{1m} = \left(\delta_{1m}^4 + (\frac{\omega\rho}{\mu})^2\right)^{\frac{1}{4}} \sin\frac{\theta}{2},$$
$$\theta = arc\tan\left(\frac{\rho\omega}{\mu\delta_{1m}^2}\right).$$

Hence, we have the following properties

$$\cosh\left(\sqrt{\gamma_{1m}}b\right) = \cosh\left(b\alpha_{1m}\right)\cos\left(b\beta_{1m}\right) + i\sinh\left(b\alpha_{1m}\right)\sin\left(b\beta_{1m}\right),$$

$$\sinh\left(\sqrt{\gamma_{1m}}b\right) = \sinh\left(b\alpha_{1m}\right)\cos\left(b\beta_{1m}\right) + i\cosh\left(b\alpha_{1m}\right)\sin\left(b\beta_{1m}\right).$$

By an extensive derivation and using the above properties, we get

$$C_{1m} = \theta_{1m}\Big\{(\delta_{1m}^2 + \frac{i\omega\rho}{\mu})\Big[\cosh(b\alpha_{1m})\cos(b\beta_{1m}) + i\sinh(b\alpha_{1m})\sin(b\beta_{1m}) +$$
$$(l\alpha_{1m} + il\beta_{1m})\sinh(b\alpha_{1m})\cos(b\beta_{1m}) + (l\alpha_{1m} + li\beta_{1m})i\cosh(b\alpha_{1m})\sin(b\beta_{1m})\Big]\Big\}^{-1}.$$

Then, we obtain

$$C_{1m} = \frac{iAd_{1m} + Ad_{2m}}{d_{1m}^2 + d_{2m}^2}, \tag{5.40}$$

92

where

$$d_{1m} = \delta_{1m}^2 \cosh(b\alpha_{1m})\cos(b\beta_{1m}) - \frac{\omega\rho}{\mu}\sinh(b\alpha_{1m})\sin(b\beta_{1m}) +$$

$$l\delta_{1m}^2\alpha_{1m}\sinh(b\alpha_{1m})\cos(b\beta_{1m}) - l\frac{\omega\rho}{\mu}\beta_{1m}\sinh(b\alpha_{1m})\cos(b\beta_{1m}) -$$

$$l\delta_{1m}^2\beta_{1m}\cosh(b\alpha_{1m})\sin(b\beta_{1m}) - l\alpha_{1m}\frac{\omega\rho}{\mu}\cosh(b\alpha_{1m})\sin(b\beta_{1m}),$$

$$d_{2m} = \delta_{1m}^2 \sinh(b\alpha_{1m})\sin(b\beta_{1m}) + \frac{\omega\rho}{\mu}\cosh(b\alpha_{1m})\cos(b\beta_{1m}) +$$

$$l\delta_{1m}^2\beta_{1m}\sinh(b\alpha_{1m})\cos(b\beta_{1m}) + \frac{\omega\rho}{\mu}l\alpha_{1m}\sinh(b\alpha_{1m})\cos(b\beta_{1m}) +$$

$$l\delta_{1m}^2\alpha_{1m}\cosh(b\alpha_{1m})\sin(b\beta_{1m}) - l\beta_{1m}\frac{\omega\rho}{\mu}\cosh(b\alpha_{1m})\sin(b\beta_{1m}).$$

The flow rate is

$$Q_1 = 4Re\left\{ e^{i\omega t}\sum_{m=1}^{\infty}\left[\frac{C_{1m}}{\delta_{1m}\sqrt{\gamma_{1m}}}\sin(\delta_{1m}a)\sinh(\sqrt{\gamma_{1m}}b) - \frac{b\theta_{1m}}{\gamma_{1m}\delta_{1m}}\sin(\delta_{1m}a) \right] \right\}.$$
(5.41)

By the above results, through extensive calculation, we get

$$\frac{C_{1m}}{\sqrt{\gamma_{1m}}}\sinh(\sqrt{\gamma_{1m}}b) = \frac{C_{1m}}{\alpha_{1m}+i\beta_{1m}}\left[\sinh(b\alpha_{1m})\cos(b\beta_{1m}) + i\cosh(b\alpha_{1m})\sin(b\beta_{1m}) \right]$$

$$= \frac{1}{(d_{1m}^2+d_{2m}^2)(\alpha_{1m}+i\beta_{1m})}\left[iAd_{1m}\sinh(b\alpha_{1m})\cos(b\beta_{1m}) - Ad_{1m}\cosh(b\alpha_{1m})\sin(b\beta_{1m}) + Ad_{2m}\sinh(b\alpha_{1m})\cos(b\beta_{1m}) + iAd_{2m}\cosh(b\alpha_{1m})\sin(b\beta_{1m}) \right].$$

Then,

$$\frac{C_{1m}}{\sqrt{\gamma_{1m}}}\sinh\left(\sqrt{\gamma_{1m}}b\right) = \frac{\alpha_{1m}d_{3m}+\beta_{1m}d_{4m}}{(d_{1m}^2+d_{2m}^2)(\alpha_{1m}^2+\beta_{1m}^2)} + i\frac{(\alpha_{1m}d_{4m}-d_{3m}\beta_{1m})}{(d_{1m}^2+d_{2m}^2)(\alpha_{1m}^2+\beta_{1m}^2)},$$

where

$$d_{3m} = -Ad_{1m}\cosh(b\alpha_{1m})\sin(b\beta_{1m}) + Ad_{2m}\sinh(b\alpha_{1m})\cos(b\beta_{1m}),$$

$$d_{4m} = Ad_{1m}\sinh(b\alpha_{1m})\cos(b\beta_{1m}) + Ad_{2m}\cosh(b\alpha_{1m})\sin(b\beta_{1m}),$$

$$\frac{\theta_{1m}}{\gamma_{1m}}\left[\frac{b}{\delta_{1m}}\sin(\delta_{1m}a)\right] = iF+G,$$

where

$$F = \frac{A\delta_{1m}^2 b \sin(\delta_{1m}a)}{\delta_{1m}(\delta_{1m}^4 + (\frac{\omega\rho}{\mu})^2)},$$

$$G = \frac{A\frac{\omega\rho}{\mu} b \sin(\delta_{1m}a)}{\delta_{1m}(\delta_{1m}^4 + (\frac{\omega\rho}{\mu})^2)},$$

$$\frac{C_{1m}}{\sqrt{\gamma_{1m}}} \sinh(\sqrt{\gamma_{1m}}b)\frac{\sin(\delta_{1m}a)}{\delta_{1m}} = D + iE,$$

where

$$D = \frac{(\alpha_{1m}d_{3m} + \beta_{1m}d_{4m})\sin(\delta_{1m}a)}{\delta_{1m}(d_{1m}^2 + d_{2m}^2)(\alpha_{1m}^2 + \beta_{1m}^2)},$$

$$E = \frac{(\alpha_{1m}d_{4m} - d_{3m}\beta_{1m})\sin(\delta_{1m}a)}{(d_{1m}^2 + d_{2m}^2)(\alpha_{1m}^2 + \beta_{1m}^2)\delta_{1m}}.$$

Substituting these values into Eq. (5.41), we have

$$
\begin{aligned}
Q_1 &= 4Re\left\{ [\cos(\omega t) + i\sin(\omega t)] \sum_{m=1}^{\infty} [D + iE - G - iF] \right\} \\
&= 4\sum_{m=1}^{\infty} \left[(D-G)\cos(\omega t) + (F-E)\sin(\omega t) \right] \\
&= \left[4\sum_{m=1}^{\infty}(D-G) \right]\cos(\omega t) + \left[4\sum_{m=1}^{\infty}(F-E) \right]\sin(\omega t) \\
&= Q_m\cos(\omega t)\cos(\phi) + Q_m\sin(\omega t)\sin(\phi) \\
&= Q_m\cos(\omega t - \phi),
\end{aligned}
$$

where $\quad Q_m\cos(\phi) = 4\sum_{m=1}^{\infty}(D-G),$

$$Q_m\sin(\phi) = 4\sum_{m=1}^{\infty}(F-E),$$

Thus,

$$Q_m = 4\left[\left(\sum_{m=1}^{\infty}(D-G) \right)^2 + \left(\sum_{m=1}^{\infty}(F-E) \right)^2 \right]^{\frac{1}{2}} \qquad (5.42)$$

is the amplitude of the flow rate, and

$$\phi = \tan^{-1}\left[\frac{\left(\sum_{m=1}^{\infty}(F-E) \right)}{\left(\sum_{m=1}^{\infty}(D-G) \right)} \right].$$

94
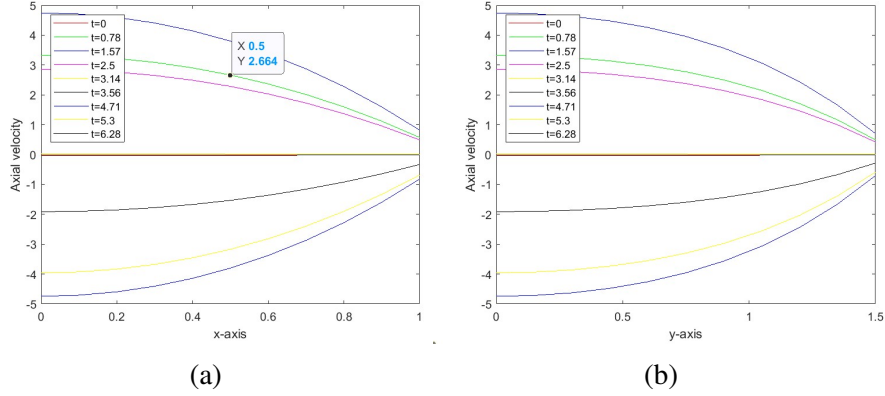
Figure 5.5: Axial Velocity profile along the $x-$axis and $y-$axis at different instants of time

Hence, the flow rate is in the form of a cosine wave function and the amplitude of the wave is influenced by the slip length.

The following figures show how the axial velocity is influenced by the slip length and time. Fig.5.5 shows 2D graphs of the axial velocity at various instants of time. 3D graphs of the axial velocity are shown in Fig.5.6 at different instants of time whilst Fig.5.7 shows 3D graphs of the axial velocity profiles at various values of slip parameters l. Significant changes occur on the axial velocity when l and t change as shown in Fig.5.8. The influence of slip parameter l on flow rate is demonstrated at various instants of time in Fig.5.9.

5.5 Concluding remarks

In summary, this chapter concerns the slip flow of fluids in rectangular microchannels. New analytical solutions for the axial velocity and the flow rate have been obtained. The influence of slip parameters on axial velocity and flow rate has been investigated. The investigation shows that the slip parameter l has a substantial influence on the velocity field. However, the characteristics of the influence for flow driven by different types of pressure gradients are different.

(a) $t = 0$ (b) $t = 0.78$ (c) $t = 1.57$

(d) $t = 2.5$ (e) $t = 3.14$ (f) $t = 3.56$

(g) $t = 4.71$ (h) $t = 5.3$ (i) $t = 6.28$
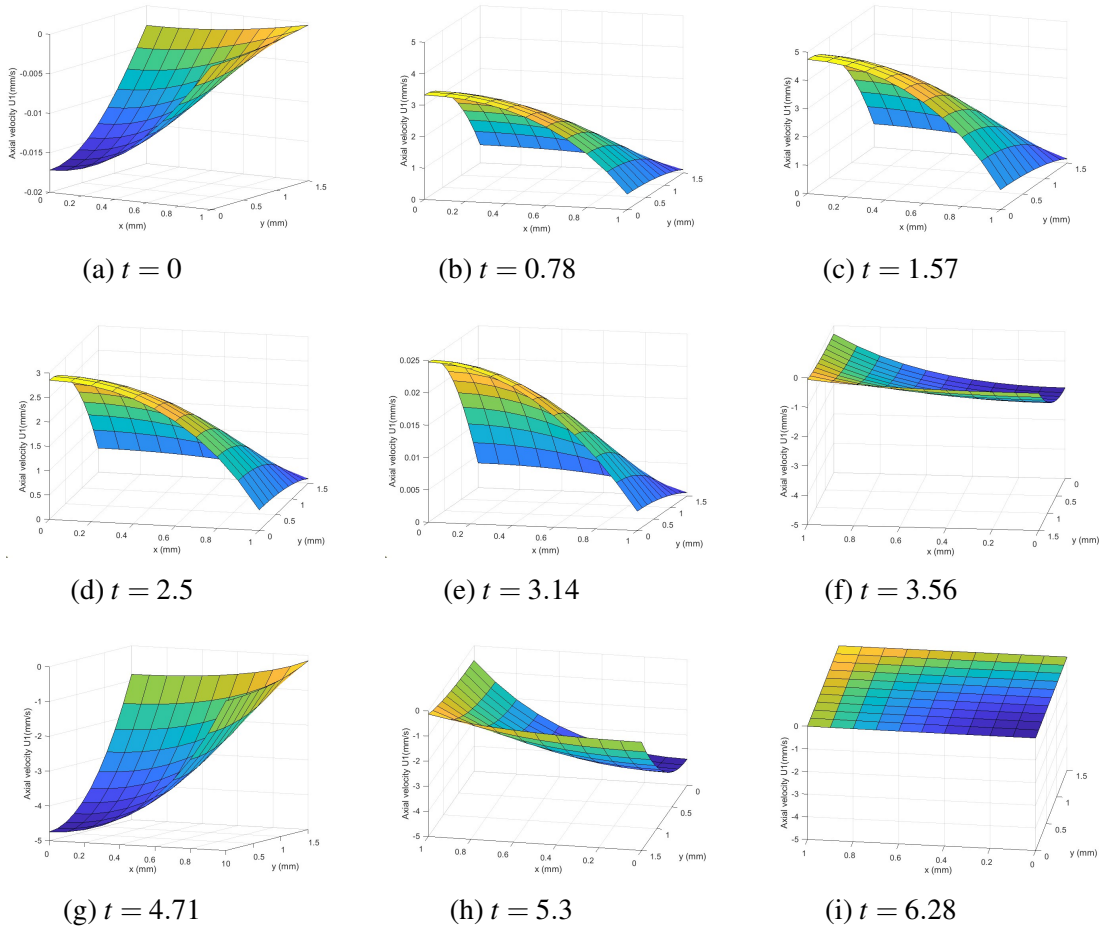
Figure 5.6: 3D graphs demonstrating the axial velocity profiles on the cross-section $z = L/2$ of the channel at various instants of time

(a) $l = 0.01$ (b) $l = 0.1$ (c) $l = 0.5$
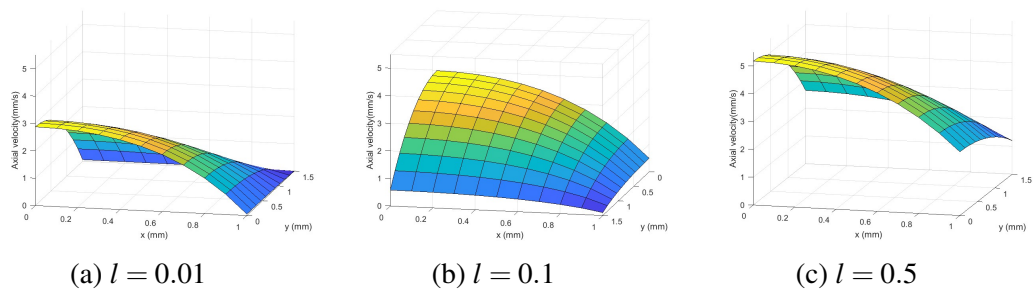
Figure 5.7: 3D graphs showing the axial velocity profiles on the cross-section $z = L/2$ of the channel for different values of slip parameter l

96

(a) $t = 0$ (b) $t = 0.78$ (c) $t = 3.14$
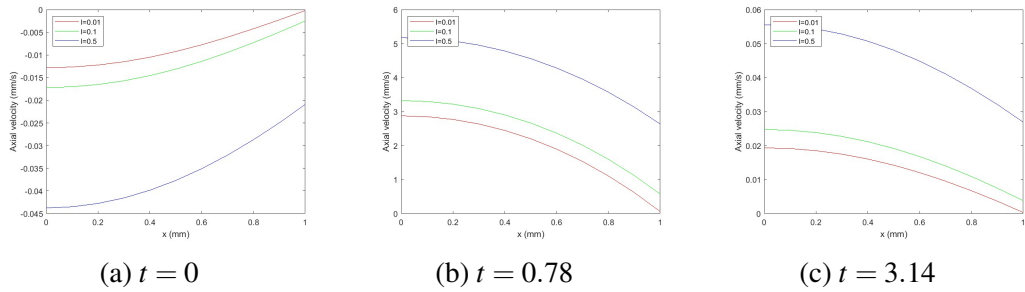
Figure 5.8: Influence of slip parameter l on velocity profile at different time

For flow driven by a constant pressure gradient, the velocity in the central part of the channel cross-section increases much faster than on the edge as l increases as shown graphically by the figures in this chapter.

Chapter 6

Summary and Further Research

6.1   Summary

In this thesis, we examined various slip flow and heat transfer problems in microchannels in the slip regime, including heat transfer in fluids in circular microchannels, mixed electroosmotic and pressure-driven flow, and unsteady flow of fluids in rectangular microchannels. Based on previous work in the field, various new results have been derived, including analytical and numerical results as well as investigation results. The main results from this study are summarized as follows.

(i) A mathematical model has been constructed for the transient temperature of an incompressible Newtonian fluid flowing through a microchannel with boundary slip. The governing field equation is the energy equation with the velocity field determined by the Navier-Stokes equations subject to the slip boundary condition. Numerical solutions for the temperature field have been developed based on the finite difference method. The algorithm has then been applied to investigate the influences of boundary slip and convection heat transfer due to axial fluid flow on the temperature field. The

numerical results obtained show that the convection heat transfer affects the temperature field significantly. As the fluid axial velocity increases, the temperature in the microchannel decreases significantly, as shown graphically in Chapter 3. It has also been found that as the slip parameter increases, the temperature decreases.

(ii) A mathematical model for slip flow and heat transfer in a mixed electroosmotic and pressure-driven flow of Newtonian fluid through a circular microchannel has been formulated based on the Navier-Stokes equation, continuity equation and the energy equation. The entire set of boundary conditions imposed to the field equations are developed based on the Navier slip condition. Based on previous work for the no-slip case, analytical solutions of velocity and temperature fields for the slip case have been derived. The new analytical results have some additional terms in comparison with results for the no-slip case, and include the results for the no-slip case as a special case. Numerical investigation of the temperature field under slip conditions and the influence of the slip parameter have been conducted. It has been found that (i) the fluid temperature decreases as the value of the Péclet number Pe increases; (ii) the axial distribution of the local Nusselt number is similar to that of the heat flux on the wall; (iii) As the slip parameter l increases, both the bulk average temperature on cross-section and the temperature on the wall decrease as shown graphically in Chapter 4.

(iii) The governing partial differential equations for incompressible Newtonian fluid flow through rectangular microchannels have been formulated based on some assumptions. It is complemented by symmetrical condition and Navier slip condition. A new analytical solution in series form for the problem has been derived and applied to study the flow characteristics of fluid through rectangular channels under slip conditions as well as the influences of boundary slip. It has been found from the investigation that

(i) For the case where the fluid is driven by a constant pressure gradient, as the slip parameter increases, the amplitude of velocity and flow rate increase. (ii) For the case where the fluid is driven by a wave from pressure gradient, the flow rate is also in wave form with the amplitude influenced by the slip parameter. (iii) The influences of the slip parameter on flow driven by different forms of pressure gradient are different. For flow driven by a constant pressure gradient, the axial velocity in the central part of the channel cross-section increases much faster than on the edge as the slip parameter l increases, while for wave form pressure gradient, the increase of axial velocity is relatively more uniform across the channel cross-section.

6.2   Further research

In this thesis, various fluid flow and heat transfer problems in the slip regime have been investigated. However, numerous problems in the field still need to be studied. Further work from this thesis is to extend the work to non-Newtonian fluids. Another possible further work is to extend the results to microchannels with other types of cross-section, such as elliptic cross-section.

Bibliography

[1] Seyed Ali Sajadifar, Arash Karimipour, and Davood Toghraie. Fluid flow and heat transfer of non-newtonian nanofluid in a microtube considering slip velocity and temperature jump boundary conditions. *European Journal of Mechanics-B/Fluids*, 61:25–32, 2017.

[2] Tim A Ameel, Xianming Wang, Randall F Barron, and Robert O Warrington. Laminar forced convection in a circular tube with constant heat flux and slip flow. *Microscale Thermophysical Engineering*, 1(4):303–320, 1997.

[3] A Barletta and E Zanchini. On the laminar forced convection with axial conduction in a circular tube with exponential wall heat flux. *Heat and mass transfer*, 30(5):283–290, 1995.

[4] L De Vargas and O Manero. On the slip phenomenon of polymeric solutions through capillaries. *Polymer Engineering & Science*, 29(18):1232–1236, 1989.

[5] John Randolph Sellars, Myron Tribus, and John Klein. Heat transfer to laminar flow in a round tube or flat conduit: the graetz probem extended. Technical report, 1954.

[6] Yingxi Zhu and Steve Granick. Rate-dependent slip of newtonian liquid at smooth surfaces. *Physical review letters*, 87(9):096105, 2001.

[7] Metin Renksizbulut, H Niazmand, and G Tercan. Slip-flow and heat transfer in rectangular microchannels with constant wall temperature. *International Journal of Thermal Sciences*, 45(9):870–881, 2006.

[8] Gokturk Tunc and Yildiz Bayazitoglu. Heat transfer in rectangular microchannels. *International Journal of Heat and Mass Transfer*, 45(4):765–773, 2002.

[9] Mostafa Shojaeian, Mehmet Yildiz, and Ali Koşar. Convective heat transfer and second law analysis of non-newtonian fluid flows with variable thermophysical properties in circular channels. *International Communications in Heat and Mass Transfer*, 60:21–31, 2015.

[10] M Barkhordari and S Gh Etemad. Numerical study of slip flow heat transfer of non-newtonian fluids in circular microchannels. *International Journal of Heat and Fluid Flow*, 28(5):1027–1033, 2007.

[11] A Raisi, B Ghasemi, and SM Aminossadati. A numerical study on the forced convection of laminar nanofluid in a microchannel with both slip and no-slip conditions. *Numerical Heat Transfer, Part A: Applications*, 59(2):114–129, 2011.

[12] Luc Bousse, Claudia Cohen, Theo Nikiforov, Andrea Chow, Anne R Kopf-Sill, Robert Dubrow, and J Wallace Parce. Electrokinetically controlled microfluidic analysis systems. *Annual Review of Biophysics and Biomolecular Structure*, 29(1):155–181, 2000.

[13] C Ll Rice and R‿ Whitehead. Electrokinetic flow in a narrow cylindrical capillary. *The Journal of Physical Chemistry*, 69(11):4017–4024, 1965.

[14] S Levine, JR Marriott, G Neale, and N Epstein. Theory of electrokinetic flow in fine cylindrical capillaries at high zeta-potentials. *Journal of Colloid and Interface Science*, 52(1):136–149, 1975.

[15] Chun Yang, Dongqing Li, and Jacob H Masliyah. Modeling forced liquid convection in rectangular microchannels with electrokinetic effects. *International journal of heat and mass transfer*, 41(24):4229–4249, 1998.

[16] G Mohiuddin Mala, Dongqing Li, and JD Dale. Heat transfer and fluid flow in microchannels. *International journal of heat and mass transfer*, 40(13):3079–3088, 1997.

[17] Eric Lauga and Howard A. Stone. Effective slip in pressure-driven Stokes flow. *Journal of Fluid Mechanics*, (489):55–77, 8 2003.

[18] C. Y. Wang. Slip flow in a curved tube. *Journal of Fluids Engineering, Transactions of the ASME*, 125(3):443–446, 5 2003.

[19] Zhipeng Duan and YS Muzychka. Slip flow in the hydrodynamic entrance region of circular and noncircular microchannels. *Journal of Fluids Engineering*, 132(1), 2010.

[20] C. Y. Wang. Ritz method for slip flow in curved micro-ducts and application to the elliptic duct. *Meccanica*, 51(5):1069–1076, 5 2016.

[21] Yong Hong Wu, B. Wiwatanapataphee, and Maobin Hu. Pressure-driven transient flows of Newtonian fluids through microtubes with slip boundary. *Physica A: Statistical Mechanics and its Applications*, 387(24):5979–5990, 10 2008.

[22] Benchawan Wiwatanapataphee, Yong Hong Wu, Maobin Hu, and Kittisak Chayantrakom. A study of transient flows of newtonian fluids through micro-annuals with a slip boundary. *Journal of Physics A: Mathematical and Theoretical*, 42(6):065206, 2009.

[23] Zhipeng Duan and YS Muzychka. Slip flow in elliptic microchannels. *International Journal of Thermal Sciences*, 46(11):1104–1111, 2007.

[24] Sumeet Gupta, Dimos Poulikakos, and Vartan Kurtcuoglu. Analytical solution for pulsatile viscous flow in a straight elliptic annulus and application to the motion of the cerebrospinal fluid. *Physics of Fluids*, 20(9):093607, 2008.

[25] Samir K Das and F Tahmouresi. Analytical solution of fully developed gaseous slip flow in elliptic microchannel. *Int. J. Adv. Appl. Math. Mech*, 3(3):1–15, 2016.

[26] Zhipeng Duan and Yuri S. Muzychka. Slip flow in non-circular microchannels. *Microfluidics and Nanofluidics*, 3(4):473–484, 8 2007.

[27] Z. M. Wilmott, C. J.W. Breward, and S. J. Chapman. Slip flow through channels with varying elliptic cross section. *IMA Journal of Applied Mathematics (Institute of Mathematics and Its Applications)*, 83(5):874–893, 9 2018.

[28] Suharsono Suharsono. A study slip flow through elliptic microchannels. *Sci. Int (Lahore)), 30 (3), 423-426, 2018*, 30(3):423–426, 2018.

[29] Pearanat Chuchard, Somsak Orankitjaroen, and Benchawan Wiwatanapataphee. Study of pulsatile pressure-driven electroosmotic flows through an elliptic cylindrical microchannel with the Navier slip condition. *Advances in Difference Equations*, 2017(1), 12 2017.

[30] C. Y. Wang. Discussion: "Slip-flow pressure drop in microchannels of general cross section". *Journal of Fluids Engineering, Transactions of the ASME*, 134(5), 2012.

[31] Namgyun Jeong, Ching Long Lin, and Do Hyung Choi. Lattice Boltzmann study of three-dimensional gas microchannel flows. *Journal of Micromechanics and Microengineering*, 16(9):1749–1759, 9 2006.

[32] Suharsono Suharsono, Yong Hong Wu, and B Wiwatanapataphee. Mathematical analysis of fluid flow through channels with slip boundary. *Australian Journal of Basic and Applied Sciences*, 5:35–40, 2011.

[33] C Y Wang. Heat transfer and flow through a super-elliptic duct – Effect of corner rounding. *Mechanics Research Communications*, 36:509–514, 2009.

[34] C Y Wang. Ritz method for slip flow in super-elliptic ducts. *European Journal of Mechanics B/Fluids*, 43:85–89, 2014.

[35] Akand Islam and Tad Patzek. Slip in natural gas flow through nanoporous shale reservoirs. *Journal of Unconventional Oil and Gas Resources*, 7:49–54, 2014.

[36] Subrata Roy, Reni Raju, Helen F. Chuang, Brett A. Cruden, and M. Meyyappan. Modeling gas flow through microchannels and nanopores. *Journal of Applied Physics*, 93(8):4870–4879, 4 2003.

[37] T. Hayat, Masood Khan, and M. Ayub. The effect of the slip condition on flows of an Oldroyd 6-constant fluid. *Journal of Computational and Applied Mathematics*, 202(2):402–413, 5 2007.

[38] Kerim Yapici, Bulent Karasozen, and Yusuf Uludag. Numerical analysis of viscoelastic fluids in steady pressure-driven channel flow. *Journal of Fluids Engineering, Transactions of the ASME*, 134(5), 2012.

[39] M. Bahrami, A. Tamayol, and P. Taheri. Slip-flow pressure drop in microchannels of general cross section. *Journal of Fluids Engineering, Transactions of the ASME*, 131(3):0312011–0312018, 3 2009.

[40] Qian Sun, Yonghong Wu, Lishan Liu, and B Wiwatanapataphee. Solution of Time Periodic Electroosmosis Flow with Slip Boundary. 2014.

[41] A-RA Khaled and K Vafai. The effect of the slip condition on stokes and couette flows due to an oscillating wall: exact solutions. *International Journal of Non-Linear Mechanics*, 39(5):795–809, 2004.

[42] Zhipeng Duan and Y. S. Muzychka. Slip flow heat transfer in annular microchannels with constant heat flux. *Journal of Heat Transfer*, 130(9), 9 2008.

[43] Stéphane Colin. Gas microflows in the slip flow regime: a critical review on convective heat transfer. *Journal of heat transfer*, 134(2), 2012.

[44] E Mo Sparrow and SH Lin. Laminar heat transfer in tubes under slip-flow conditions. 1962.

[45] Shiping Yu and Timothy A Ameel. Slip-flow heat transfer in rectangular microchannels. *International Journal of Heat and Mass Transfer*, 44(22):4225–4234, 2001.

[46] Bo Yu, Wen-Quan Tao, Jin-Jia Wei, Yasuo Kawaguchi, Toshio Tagawa, and Hiroyuki Ozoe. Discussion on momentum interpolation method for collocated grids of incompressible flow. *Numerical Heat Transfer: Part B: Fundamentals*, 42(2):141–166, 2002.

[47] Marco Spiga and Pamela Vocale. Slip flow in elliptic microducts with constant heat flux. *Advances in Mechanical Engineering*, 4:481280, 2012.

[48] Oluwole Daniel Makinde and Tiri Chinyoka. Mhd transient flows and heat transfer of dusty fluid in a channel with variable physical properties and navier slip condition. *Computers & Mathematics with Applications*, 60(3):660–669, 2010.

[49] Mohamed Gad-El-Hak. The fluid mechanics of microdevices—the freeman scholar lecture. *Journal of Fluids Engineering, Transactions of the ASME*, 121(1):5–33, 1999.

[50] H Herwig and O Hausner. Critical view on "new results in micro-fluid mechanics": an example. *International Journal of Heat and Mass Transfer*, 46(5):935–937, 2003.

[51] Yu-Chuan Su and Liwei Lin. A water-powered micro drug delivery system. *Journal of Microelectromechanical Systems*, 13(1):75–82, 2004.

[52] Chih-Ming Ho and Yu-Chong Tai. Micro-electro-mechanical-systems (mems) and fluid flows. *Annual review of fluid mechanics*, 30(1):579–612, 1998.

[53] R Pit, H Hervet, and L Leger. Direct experimental evidence of slip in hexadecane: solid interfaces. *Physical review letters*, 85(5):980, 2000.

[54] Bing-Yang Cao, Min Chen, and Zeng-Yuan Guo. Liquid flow in surface-nanostructured channels studied by molecular dynamics simulation. *Physical Review E*, 74(6):066311, 2006.

[55] Remco Tuinier and Takashi Taniguchi. Polymer depletion-induced slip near an interface. *Journal of Physics: Condensed Matter*, 17(2):L9, 2004.

[56] Cao Bing-Yang, Chen Min, and GUO Zeng-Yuan. Velocity slip of liquid flow in nanochannels. *Acta Physica Sinica*, 10(55):5305–5310, 2006.

[57] Lajos Szalmás. Slip-flow boundary condition for straight walls in the lattice boltzmann model. *Physical Review E*, 73(6):066710, 2006.

[58] Jinliang Xu and Yuxiu Li. Boundary conditions at the solid–liquid surface over the multiscale channel size from nanometer to micron. *International Journal of Heat and Mass Transfer*, 50(13-14):2571–2581, 2007.

[59] MT Matthews and JM Hill. Newtonian flow with nonlinear navier boundary condition. *Acta Mechanica*, 191(3):195–217, 2007.

[60] Shi-Pu Yang and Ke-Qin Zhu. Analytical solutions for squeeze flow of bingham fluid with navier slip condition. *Journal of non-newtonian fluid mechanics*, 138(2-3):173–180, 2006.

[61] Bertrand Bourlon, Joyce Wong, Csilla Mikó, László Forró, and Marc Bockrath. A nanoscale probe for fluidic and ionic transport. *Nature Nanotechnology*, 2(2):104–107, 2007.

[62] Richard L Burden, J Douglas Faires, and Annette M Burden. *Numerical analysis*. Cengage learning, 2015.

[63] Prashanta Dutta and Ali Beskok. Analytical solution of combined electroosmotic/pressure driven flows in two-dimensional straight channels: finite debye layer effects. *Analytical chemistry*, 73(9):1979–1986, 2001.

[64] Da Yong Yang. Analytical solution of mixed electroosmotic and pressure-driven flow in rectangular microchannels. In *Key Engineering Materials*, volume 483, pages 679–683. Trans Tech Publ, 2011.

[65] Keisuke Horiuchi, Prashanta Dutta, and Cecilia D Richards. Experiment and simulation of mixed flows in a trapezoidal microchannel. *Microfluidics and Nanofluidics*, 3(3):347–358, 2007.

[66] Reza Monazami and Mehrdad T Manzari. Analysis of combined pressure-driven electroosmotic flow through square microchannels. *Microfluidics and Nanofluidics*, 3(1):123–126, 2007.

[67] Liqing Ren, Weilin Qu, and Dongqing Li. Interfacial electrokinetic effects on liquid flow in microchannels. *International journal of heat and mass transfer*, 44(16):3125–3134, 2001.

[68] Heng Ban, Bochuan Lin, and Zhuorui Song. Effect of electrical double layer on electric conductivity and pressure drop in a pressure-driven microchannel flow. *Biomicrofluidics*, 4(1):014104, 2010.

[69] Hsin-Fu Huang and Pao-Wen Yang. Electrokinetic streaming power generation using squeezing liquid flows in slit channels with wall slip. *Colloids and Surfaces A: Physicochemical and Engineering Aspects*, 514:192–208, 2017.

[70] Sung Il Kim and Sung Jin Kim. Analysis of the electroviscous effects on pressure-driven flow in nanochannels using effective ionic concentrations. *Microfluidics and Nanofluidics*, 22(1):12, 2018.

[71] D Maynes and BW Webb. Fully developed electro-osmotic heat transfer in microchannels. *International journal of heat and mass transfer*, 46(8):1359–1369, 2003.

[72] D Maynes and BW Webb. The effect of viscous dissipation in thermally fully-developed electro-osmotic heat transfer in microchannels. *International journal of heat and mass transfer*, 47(5):987–999, 2004.

[73] BC Liechty, BW Webb, and RD Maynes. Convective heat transfer characteristics of electro-osmotically generated flow in microtubes at high wall potential. *International journal of heat and mass transfer*, 48(12):2360–2371, 2005.

[74] D Maynes and BW Webb. Fully-developed thermal transport in combined pressure and electro-osmotically driven flow in microchannels. *J. Heat Transfer*, 125(5):889–895, 2003.

[75] Heng-Kwong Tsao. Electroosmotic flow through an annulus. *Journal of colloid and interface science*, 225(1):247–250, 2000.

[76] Arun Sharma and Suman Chakraborty. Semi-analytical solution of the extended graetz problem for combined electroosmotically and pressure-driven microchannel flows with step-change in wall temperature. *International journal of heat and mass transfer*, 51(19-20):4875–4885, 2008.

[77] Keisuke Horiuchi and Prashanta Dutta. Joule heating effects in electroosmotically driven microchannel flows. *International journal of heat and mass transfer*, 47(14-16):3085–3095, 2004.

[78] L Graetz. Uber die warmeleitungsfahighevon von flussingkeiten. *Part 1, Annalen der Physik und Chemie*, 18:79–94, 1883.

[79] J Lahjomri and A Oubarra. Analytical solution of the graetz problem with axial conduction. 1999.

[80] Robert J Hunter. *Zeta potential in colloid science: principles and applications*, volume 2. Academic press, 2013.

[81] Peter Gravesen, Jens Branebjerg, and O Søndergård Jensen. Microfluidics-a review. *Journal of micromechanics and microengineering*, 3(4):168, 1993.

[82] FF Reuss. Charge-induced flow. *Proceedings of the Imperial Society of Naturalists of Moscow, 1809*, 3:327–344, 1809.

[83] Milad Azari, Arman Sadeghi, and Suman Chakraborty. Graetz problem for combined pressure-driven and electroosmotic flow in microchannels with distributed wall heat flux. *International Journal of Heat and Mass Transfer*, 128:150–160, 1 2019.

[84] Hadi Yavari, Arman Sadeghi, Mohammad Hassan Saidi, and Suman Chakraborty. Combined influences of viscous dissipation, non-uniform joule heating and variable thermophysical properties on convective heat transfer in microtubes. *International journal of heat and mass transfer*, 55(4):762–772, 2012.

[85] Hadi Yavari, Arman Sadeghi, Mohammad Hassan Saidi, and Suman Chakraborty. Temperature rise in electroosmotic flow of typical non-newtonian biofluids through rectangular microchannels. *Journal of Heat Transfer*, 136(3), 2014.

[86] Stéphane Colin, Pierre Lalonde, and Robert Caen. Validation of a second-order slip flow model in rectangular microchannels. *Heat transfer engineering*, 25(3):23–30, 2004.

[87] Farzad Tahmouresi and Samir K Das. Analytical modeling of gaseous slip flow in parabolic microchannels. *Journal of Fluids Engineering*, 136(7), 2014.

[88] SP Anjali Devi and D Vasantha Kumari. Numerical investigation of slip flow effects on unsteady hydromagnetic flow over a stretching surface with thermal radiation. 2014.

[89] Suharsono Suharsono. *Analytical study of fluid flows with slip boundary*. PhD thesis, Curtin University, 2012.